

Norwegian University of Life Sciences
Faculty of Environmental Science and
Technology
Department of Environmental Sciences
Centre for Environmental Radioactivity, CERAD

Master Thesis 2014
60 credits

Potential Mobility of Radionuclides and Trace Elements in Bedrock Materials and in the Deposition Area at a Tunnel Construction Site RV4 Gran, Hadeland

Stephanie Hernandez Santos

Preface

The present work represents the final stage of a two-year Masters in Sciences degree in Radioecology at the Plant and Environment Sciences Institute of the Norwegian University of Life Sciences, Ås, Norway.

It was done as a part of Task 2 of the project “Effects and Environmental Risk related to Interventions in zones with Sulfide-Rich Minerals” in collaboration with the Norwegian Public Roads Administration NPRA as a part of the NORWAT project. Task 2 aims at giving an overview of the natural levels of radionuclides and metals, as well as other important in the construction area. Moreover, within the main project, effects and consequences due to runoff to the environment, and countermeasures for its protection are considered.

The research consisted in fieldwork done in 2012 and 2013, literature review, planning the analytical strategy with my advisors, Ole Christian Lind, Lindis Skipperud and Brit Salbu from the Isotope Laboratory at NMBU and Sondre Meland and Per Hagelia from the NPRA. The experimental work and analysis and interpretation of the data were done in 2013 and 2014.

The two main objectives of the present work are to test if the Sequential Extraction Method can be applied to obtain representative extractability of radionuclides and metals from anoxic environmental samples under anaerobic extractions and compare these results with aerobic extractions. The second objective consists in the development of a combined leaching and imaging method to study weathering mechanisms in geological material.

Acknowledgments

I would like to express my gratitude to my advisors: Ole, Lindis, Brit from the Norwegian University of Life Sciences NMBU and Per and Sondre from Statens Vegvesen, for lending me their time and sharing their knowledge with me, it is truly inspiring and motivational to work with people with such passion for their areas of expertise. I deeply appreciate all your help, support and encouragement. Your commitment to education is an amazing example that I hope to follow in the future.

I acknowledge the people working at the Isotope and Analytical Chemistry Laboratory at NMBU. Marit, Tove, Lene, Merethe, Cato, Simone, Karl-Andreas, Solfrid, Øyvind and Emilio for helping me countless times with my experiments and patiently answering my many - many - questions. Thanks to Tari in whom I have also found a dear friend.

A special gratitude to Salahaldin Akvahan, Institute of Geology, the University of Oslo and Lars Kirkseter, Institute for Energy Technology for their cooperation and help with the preparation of samples. Thanks to Hans Jørgen from the Natural History Museum in Oslo for analyzing my samples in the XRD and nonetheless for showing me the original samples of Ellen Gleditsch!.

I also would like to thank Fredrik Vanmeert and Stijn Legrand from the University of Antwerp, Belgium for providing me with interesting new data for my thesis.

Last but never least, thanks to my friends and family - the Mexican and the Norwegian - for supporting and encouraging my dreams wherever they may take me. Thanks to my best friend and my companion in life, my husband Anders, for your patience and your love every day.

Abstract.

The present work focuses on the deposition of tunnel rock masses and the potential for pollution afterwards in connection with tunnel construction for the new express way at Gran – Hadeland, East Norway.

The geology of the zone includes alum shale, this sedimentary rock is of particular environmental interest due to its content of sulphide, metals, metalloids and radionuclides. During tunnel constructions these rocks, among others, are excavated and stored. Oxidation of sulphides to sulphates by atmospheric oxygen can eventually lead to acidifying conditions in water. Low pH have the potential to mobilize the elements present in the material by weathering processes, this phenomenon may lead to negative effects on the environment.

The main hypothesis of this work is that the mobility of radionuclides and other redox sensitive elements will be different under aerobic and anaerobic conditions.

The present work studies the potential for mobilization of selected elements and attempts to provide information about weathering processes using a combined method of imaging and micro-analytical techniques. This work was divided in to two experiments 1) Sequential Extractions to on the substrate media to test the if elements have different behaviors under oxic and anoxic conditions and Experiment 2) Weathering experiments on a thin-section of alum shale. Thin-section sample was characterized before and after leaching experiments with sulfuric acid pH 2. The techniques used were Digital Autoradiography, EDX-ESEM, micro-XRF and micro-XRD and LA ICP-MS.

The selected substrate media consisted in Alum Shale, Black Shale and Peat Moss from the planned deposition area. The elements that were studied are aluminum, sulfur, calcium, vanadium, chromium, manganese, iron, cobalt, nickel, copper, zinc, arsenic, molybdenum, cadmium, tin, thorium, uranium, silica and magnesium under aerobic and anaerobic conditions. Uranium will be in focus in this study due to 1) its ubiquitous distribution

the zone and its radiological and chemical toxicity and 2) due to its progenies during radioactive decay, radium and radon, which are highly radiotoxic.

Results for Alum and Black Shale demonstrated that there are no statistically significant differences between oxic and anoxic conditions for the extracted concentrations of uranium in the bioavailable fraction. However, the similarities in the redox potential suggest that anoxic conditions were not achieved for the experiment.

Uranium presented higher extraction percentages under anoxic conditions (22%) for the bioavailable fraction than under oxic conditions (16%). Paired t-test on Bioavailable Fraction for Peat Moss demonstrates statistically significant differences for the concentrations of uranium extracted in this fraction. However, 45% of the total concentration of extracted uranium in the sample was mobilized under oxic conditions, while a 28% was mobilized under anoxic conditions. These results suggest that uranium may be found in more stable forms under anoxic conditions than in oxic ones. This supports the main hypothesis of the present work. However, since the percentage of extraction presented the opposite behavior as for the total extractor percentage, this observation should be considered during risk assessment studies.

Moreover, principal component analysis in sequential extraction data demonstrated association among the studied metals, especially for those that are sensitive to redox potential and pH changes. Associations between uranium, iron and arsenic were observed in Peat Moss. Calcium , magnesium and manganese presented different patterns of leachability to those for metals. These observations were confirmed by leaching experiments and electron microscopy. Weathering processes were well characterized by the observations made before and after treatment showing significant changes on the thin-section sample.

Sammendrag

Denne oppgaven fokuserer på deponering av bergmasser fra tunellutgravning, og potensialet for forurensning etterpå i forbindelse med tunnelbyggingen på nye Riksvei 4 - Gran - Hadeland, Øst Norge.

Geologien i området omfatter alunskifer, denne sedimentære bergarten er av spesiell interesse med tanke på miljøet på grunn av dens innhold av sulfider, metaller, metalloider og radionukliser. Under tunnelutgravninger blir disse bergartene med fler gravd ut og lagret. Oksidasjon av sulfider til sulfater av atmosfærisk oksygen kan føre til forsurende forhold i vann. Lav pH har potensiale til å mobilisere de elementene som er tilstede i materialet ved forvitnings prosess, dette kan føre til negative virkninger på miljøet.

Hoved hypotesen for dette arbeidet er at mobiliteten av radionukliser og andre redoks-følsomme elementer vil være forskjellige under aerobic og anaerobic betingelser.

Dette arbeidet undersøker potensialet for mobilisering av utvalgte elementer og forsøker å gi informasjon om vitrings prosesser ved hjelp av en kombinert metode for bildebehandling og mikro-analytiske teknikker. Dermed ble dette arbeidet delt i to ulike eksperimenter som utfyller hverandre: sekvensielle ekstraksjoner og vitringsekspimenter på tynnslipp prøve av alunskifer. Eksperiment 1: Sekvensielle Ekstraksjoner under henholdsvis luftatmosfære (aerobt) og N₂ stmosfære (anaerob). Mer detalert informasjon om mekanismene for vitring ble det utført vitringsforsøk på en tynnsjiktprøve hvor endringene over tid ble undersøkt ved hjelp av en kombinasjon av mikroanalytiske teknikker og monitoering av utlekking, dette er Experiment 2. Tynnslipprøven ble karakterisert før og etter utvaskings forsøk med svovelsyre pH 2. Teknikkene som ble brukt var Digital Autoradiografi, EDX-ESEM, mikro-XRF og mikro-XRD og LA ICP-MS.

Grunnstoffer som ble studert er aluminium, svovel, kalsium, vanadium, krom, mangan, jern, kobolt, nikkel, kobber, sink, arsen, molybden, kadmium, tinn, thorium, kadmium, tinn, thorium, uran, magnesium under aerobe og anaerobe betingelser. Uran vil være i fokus i denne studien på grunn av 1) den allestedsnærværende fordeling av i område og dens radiologiske og kjemiske giftighet, og 2) på grunn av radium og radon.

Uran hadde høyere utlekkings prosenter under anokside betingelse (22 %) for den biotilgjengelige Fraksjon enn under oksisk betingelse (16 %) . Pared t - test på Biotilgjengelig Fraksjon for myrprøver viser statistisk signifikante forskjeller for de konsentrasjoner av uran i fraksjonen .Derimot, det ble ekstraheres 45% av den totale konsentrasjon av uran i prøven mobilisert under oksisk betingelse, mens en 28% ble mobilisert under anokside betingelse. Disse resultatene fører til at uran kan finnes i mer stabile former under anokside betingelser enn i oksiske. Dette støtter hovedhypotesen av dette oppgaven . Derimot , siden den prosentvise ekstraksjon av frem motsatt oppførsel som for den totale prosentvise ekstraksjon, denne observasjon bør vurderes ved risikovurdering studier.

Prinsipal komponent analyse i sekvensiell ekstraksjon data demonstrerte foreningen blant de studerte metaller , spesielt for de som er følsomme ved redokspotensial og pH-endringer . Sammenhenger mellom uran , jern og arsen ble observert i myrprøver . Kalsium , magnesium og mangan frem forskjellige mønstre av utlekkings for metaller. Disse observasjonene ble bekreftet ved utlekkingsforsøk og elektronmikroskopi. Forvitring prosesser var godt kjennetegnet av de observasjoner som ble gjort før og etter behandling som viser signifikante endringer på tynnslip prøven.

List of Abbreviations.

NORWAT: Nordic Road Water

RV4: Riksvei (National Highway)

NPRA: Norwegian Public Road Administration

NMBU: Norwegian University of Life Sciences

NORM: Naturally Occurring Radioactive Material

XRF: X-ray Fluorescence Spectrometry

XRD: X-ray Diffraction

ICP-MS: Inductively Coupled Plasma Mass Spectrometry

LA ICP-MS: Laser Ablation Inductively Coupled Plasma Mass Spectrometry

EDX -ESEM: Environmental Scanning Electron Microscope with Energy Dispersive X-ray Spectroscopy

SEI: Secondary Electron Image

BEI: Backscattered Electron Image

μ -XRD: Micro X-ray Diffraction

μ -XRF: Micro X-ray Fluorescence

PCA: Principal Component Analysis

PC1,2,3,4: Principal Component 1,2,3,4

ANOVA: Analysis Of Variance

TOC: Total Organic Carbon

TOM: Total Organic Matter

LD: Limit of Detection

LQ: Limit of Quantification

List of Figures.

Figure 1 Thorium Decay Series. (Tosaka, Decay chain 4n, Thorium series, 2008)

Figure 2 Uranium Decay Series. (Tosaka, Decay chain 4n+2, Uranium series, 2008)

Figure 3 Geology of Gran municipality. The map shows the distribution of alum shale, granite rhyolite, monzonite latite, syenite tachyte, sediment, mafic intrusive and gnesis. (Smethurst, 2008)

Figure 4 Drift geology of Gran shows highly permeable deposits in yellow and moderate permeability in orange. (Smethurst, 2008)

Figure 5 Distribution of uranium according to its concentration in ppm (parts per million) over the Gran area. (Mark A. Smethurst, 2008)

Figure 6 Classification of some of the Primary and Secondary ores of Uranium found in nature. (Agency for Toxic Substances and Disease Registry, 2013)

Figure 7 Classification of physicochemical forms by size in aquatic systems. (Salbu, 2013)

Figure 8 Speciation of dissolved uranium and a function of pH for $[U]_{TOT} = 5 \text{ M}$, $I = 0.1 \text{ M}$, and $P_{CO_2} = 10^{-3.5} \text{ atm}$. Calculations were made without considering the precipitation of any solid phases. (Giammar, 2001)

Figure 9 Difference between the uranium extracted by bicarbonate at varying concentrations under oxic and anaerobic conditions. This difference is attributed to the oxidation of U(IV) in the soil under oxic conditions.(Ping, 2005).

Figure 10 Sampling area. Gran municipality border with Jaren, blue marks illustrate sampling locations for the project. Locations marked with red squares represent the sampling areas for Alum Shale and Black Shale (top) and Peat Moss (bottom) (Skipperud, 2013).

Figure 11 Engineering Geological Profile of projected tunnel area. Marked areas highlight BH-5 (black shale), BH-4 (alum shale) and BH-6 (alum shale). Colors indicate different materials: Grey: loose material, blue: calcareous shales of blackish to grey color, pink: black shales, green: calcareous shales of dark to gray color, orange: alum shale. (Statens Vegvesen , 2013)

Figure 12 Thin-section sample. Alum shale glued on PMMA, measurements 4.2 x 2.3 cm.

Figure 13 Sample used for the identification of Depleted Uranium in Kosovo soil. Observed in Back scattered Electron Image BEI mode. Identification directly in SEM. (Lind, 2006).

Figure 14 Sample selection. Boxplot based on XRF data for uranium, the analyzed samples are BH-5 Prove 1, BH-5 Prove 2 for black shales and BH-6 Prove 1, BH-6 Prove 2 and BH-6 Prove 4 for alum shale. The boxplot shows mean, median, Q1, interquartile range, Q3 and whiskers for each sample.

Figure 15 Sequential Extraction. Percentages of extraction for Major Elements in Alum Shale samples. Oxic and Anoxic conditions. Error bars calculated as 2 times the standard deviation of the three parallels.

Figure 16 Sequential Extraction. Percentages of extraction for Minor Elements in Alum Shale samples. Oxic and Anoxic conditions. Error bars calculated as 2 times the standard deviation of the three parallels.

Figure 17 Sequential Extraction. Percentages of extraction for Trace Elements in Alum Shale samples. Oxic and Anoxic conditions. Error bars calculated as 2 times the standard deviation of the three parallels.

Figure 18 Sequential Extraction. Percentages of extraction for Radionuclides in Alum Shale samples. Oxic and Anoxic conditions. Error bars calculated as 2 times the standard deviation of the three parallels.

Figure 19 Sequential Extraction. Percentages of extraction for Major Elements in Black Shale samples. Oxic and Anoxic conditions. Error bars calculated as 2 times the standard deviation of the three parallels.

Figure 20 Sequential Extraction. Percentages of extraction for Minor Elements in Black Shale samples. Oxic and Anoxic conditions. Error bars calculated as 2 times the standard deviation of the three parallels.

Figure 21 Sequential Extraction. Percentages of extraction for Trace Elements in Black Shale samples. Oxic and Anoxic conditions. Error bars calculated as 2 times the standard deviation of the three parallels.

Figure 22 Sequential Extraction. Percentages of extraction for Radionuclides in Black Shale samples. Oxic and Anoxic conditions. Error bars calculated as 2 times the standard deviation of the three parallels.

Figure 23 Sequential Extraction. Percentages of extraction for Major Elements in Peat Moss samples. Oxic and Anoxic conditions. Error bars calculated as 2 times the standard deviation of the three parallels.

Figure 24 Sequential Extraction. Percentages of extraction for Minor Elements in Peat Moss samples. Oxic and Anoxic conditions. Error bars calculated as 2 times the standard deviation of the three parallels. Vanadium was not analyzed under oxic conditions for Peat Moss.

Figure 25 Sequential Extraction. Percentages of extraction for Trace Elements in Peat Moss samples. Oxic and Anoxic conditions. Error bars calculated as 2 times the standard deviation of the three parallels. Chromium and tin were not analyzed under oxic conditions.

Figure 26 Sequential Extraction. Percentages of extraction for Radionuclides in Peat Moss samples. Oxic and Anoxic conditions. Error bars calculated as 2 times the standard deviation of the three parallels.

Figure 27 PCA analysis for the complete data set. Score Plots by material, by condition and by step of the sequential extraction process and its correspondent Loading Plot are shown.

Figure 28 PCA analysis for Alum Shale. Score plot by step of the sequential extraction process and loading plot are shown.

Figure 29 PCA analysis for Black Shale. Score plot by step of the sequential extraction process and loading plot are show.

Figure 30 PCA analysis for Peat Moss. Score plot by step of the sequential extraction process and loading plot are show.

Figure 31 PCA analysis for Bioavailable Fraction of all materials. Score plot by material and corresponding loading plot are shown. Score Plot shows differences in each material under different conditions.

Figure 32 Boxplot of PC1. Boxplot shows the differences between Alum Shale, Black, Shale and Peat Moss under oxic and anoxic conditions. Boxplot shows mean, median, Q1, interquartile range, Q3 and connecting mean line.

Figure 33 Radiograph for thin-section sample showing two areas of interest: Area 1 and Area 2.

Figure 34 Electron Microscope Image using BEI mode of Area 2, magnification 105 X. (left). Electron Microscope Image using SEI mode of Area 2 (right). Magnification 105 X. Profiles for LA ICP-MS are visible.

Figure 35 Electron microscope general scan mapping image of Area 2, using BEI mode.

Figure 36 Electron microscope sum spectrum of Area 2, corresponding to Figure 35.

Figure 37 Electron microscope image of area 2 using BEI mode. The figure shows the position of the point spectra performed on the zone.

Figure 38 Spectrum corresponding to Spectrum 9 position in Figure 37. This spectrum shows the presence of uranium, thorium and zirconium in the sample.

Figure 39 Electron microscope image of area 2, using BEI mode. The image shows the position of different point spectra performed on the sample.

Figure 40 Spectrum corresponding to Spectrum 9 position in Figure 55. This spectrum shows the presence of uranium in the sample.

Figure 41 Micro-XRD. Diffractogram of the thin-section sample. The graph shows no mineral phases detected but rather an amorphous background.

Figure 42 Micro X-ray Flourescence analysis. The image shows the presence of K K-edge , Ca K-edge. Ti K-edge and V K-edge in the thin-section sample.

Figure 43. Electron Microscope ESEM image showing the location of the analyzed sites with LA ICP-MS, image taken in BEI mode. The circles represent the craters and the horizontal marks, the lines. From Left to right: Crater 1 corresponding to Depth Profile 1, Crater 2 corresponding to Depth Profile 2 and Crater 3 corresponding to Depth Profile 3 and top to bottom, Line 1 corresponding to Surface Profile 1, Line 2 corresponding to Surface Profile 2 and Line 3 corresponding to Surface Profile 3.

Figure 44. LA ICP-MS Depth Profile 1. General profile for all elements is displayed. The y-axis, refers to a logarithmic transformation of the normalized counts of these values.

Figure 45. LA ICP-MS Surface Profile 1. General profile for all elements is displayed. The y-axis, Normalized Counts* refers to a logarithmic transformation of these values.

Figure 46 Leaching Experiment. Time Series for Major Elements Al, S, Mn and Fe and Minor Elements V, Ni, Cu and Zn against leaching time.

Figure 47 Leaching Experiment. Leaching percentage for Major Elements Al, S, Mn and Fe and Minor Elements V, Ni, Cu and Zn against leaching time.

Figure 48 Leaching Experiment. Time Series for Trace Elements Pb, Sn, Cd, Mo, As, Co and Cr and Radionuclides Th and U concentrations in leaching solution.

Figure 49 Leaching Experiment. Leaching percentage for Trace Elements Pb, Sn, Cd, Mo, As, Co and Cr and Radionuclides U and Th against leaching time.

Figure 50 Elemental mapping and sum spectra for site of interest in Area 2. Image shows the elemental mapping for Al, Si, S, K, Fe, Ca. The last image was taken by the electron microscope in BEI mode.

Figure 51 After treatment characterization. Electron Image after 10 days of leaching time BEI mode, magnification 85x (left) and Electron Image after 22 days of leaching time BEI mode, magnification 85x (right). Weathering signs are visible as black “cracks” on the material.

Figure 52 Electron Image after 10 days of leaching time BEI mode, magnification 1200x (right) and Electron Image after 22 days of leaching time BEI mode, magnification 800x. Weathering signs are visible as black “cracks” on the material.

List of Tables.

Table 1 Experimental Parameters for Experiment one: Sequential Extractions.

Table 2 Material, name and number of measurements performed to select samples with the XRF instrument.

Table 3. Experiment 1. Sequential Extraction Model used under Oxic and Anoxic conditions(Lindis Skipperud D. O., 2004) (Salbu, Speciation of Radionuclides in the Environment , 2000).

Table 4 Quality analysis for precision. Coefficient of Variation of the total concentration values for 13 of the studied elements for each material.

Table 5 Quality analysis for accuracy. Observed and Expected values for elements in Reference Materials. The Eoor is calculated as the difference between the observed value and the expected value divided by the expected value.

Table 6 Quality analysis. Limit of Detection and Limit of Quantification for the ICP-MS analysis of the elemental concentration for total concentration analysis.

Table 7 Sample selection. Redox potential values for each material studied, oxic and anoxic conditions.

Table 8. Sample characterization. Values for pH, moisture content, organic matter and total organic carbon for the studied materials are presented.

Table 9 Total Concentration analysis for each element in mg/kg for Alum Shale, Black Shale and Peat Moss. Error is calculated as 2 times the standard deviation value for the samples and Average corresponds to the average value of three parallels.

Table 10 X-ray diffraction results. Minerals identified by the XRD in the studied materials. Sulfides less than 1-2% of the total may not be detected.

Table 11. Extraction percentages of elements under oxic and anoxic conditions compared to total concentration of extraction. Missing values are shown in yellow for V, Cr and Sn for the oxic date set in Peat Moss.

Table 12 Principal components with the variation proportion and the cumulative values of the variation they explain of the complete data set.

Table 13 Principal components 1 and 2 values for the variables for the complete data set.

Table 14 Principal components with the variation proportion and the cumulative values of the variation they explain for Alum Shale.

Table 15. Principal components 1 and 2 values for the variables for Alum Shale.

Table 16 Principal components with the variation proportion and the cumulative values of the variation they explain for Black Shale.

Table 17 Principal components 1 and 2 values for the variables for Alum Shale.

Table 18 Principal components with the variation proportion and the cumulative values of the variation they explain for Peat Moss.

Table 19 Principal components 1 and 2 values for the variables for Alum Shale.

Table 20 Summarized results for paired t-test.

Table 21. Summarized results for Tukey test.

Table of Contents

<i>1. Introduction</i>	17
<i>2. Theory</i>	18
<i>2.1 Metals and radionuclides in the environment.....</i>	18
<i>2.2 NORM and Technologically enhanced NORM</i>	22
<i>2.3 Geology of Gran, Hadeland</i>	24
<i>2.4 Wetlands: Deposition areas for extracted rock masses</i>	26
<i>2.5 Speciation</i>	29
<i>3. Materials and Methods</i>	35
<i>3.1 Quality analysis</i>	36
<i>3.2 Sampling and sample preparation</i>	37
<i>3.2.1 Sampling area.....</i>	37
<i>3.2.2 Sample selection and preparation.....</i>	39
<i>3.2.3 Sample characterization.....</i>	42
<i>3.3 Experiment one: Sequential extractions.....</i>	44
<i>3.3.1 Sequential extraction method</i>	44
<i>3.3.2 Inductively Coupled Plasma Mass Spectrometry ICP-MS</i>	45
<i>3.3.3 Microwave Digestion: Ultraclave</i>	46
<i>3.4 Experiment 2: Thin-section characterization and leaching experiment for weathering process analysis.....</i>	46
<i>3.4.1 Digital Autoradiography.....</i>	47
<i>3.4.2 Environmental Scanning Electron Microscope EDX- ESEM.....</i>	47
<i>3.4.3 Micro X-ray Diffraction (μ-XRD) and Micro X-ray Fluorescence Spectroscopy (μ-XRF)</i>	48
<i>3.4.4 Laser Ablation Inductively Coupled Plasma Mass Spectrometry (LA ICP-MS).....</i>	49
<i>3.5 Statistical Methods</i>	50
<i>3.5.1 Principal Component Analysis PCA</i>	50
<i>3.5.2 Paired t-test</i>	51
<i>3.5.3 One-way Analysis of Variance (ANOVA)</i>	52
<i>4. Result and Discussion</i>	52
<i>4.1 Quality Analysis: Precision and accuracy</i>	53
<i>4.2 Sample selection.....</i>	57
<i>4.2.1 X-Ray Fluorescence.....</i>	57
<i>4.3 Sample Characterization</i>	59
<i>4.3.1 Total Concentration Analysis.....</i>	60
<i>4.3.2 X-Ray Diffraction</i>	62
<i>4.4 Experiment one: Sequential Extractions.....</i>	63
<i>4.4.1 Alum Shale samples.....</i>	63
<i>4.4.2 Black Shale samples</i>	68
<i>4.4.3 Peat Moss samples</i>	72
<i>4.4.4 Statistical Analysis: Principal Component Analysis, Paired t-test and ANOVA</i>	77
<i>4.5 Experiment two: Leaching experiments on thin-section for weathering process analysis</i>	92
<i>4.5.1 Sample characterization: Before treatment.....</i>	93
<i>4.5.2 Leaching Solutions Analysis</i>	103
<i>4.5.3 Sample characterization: After treatment with EDX-ESEM</i>	106
<i>5 Conclusions</i>	110
<i>References</i>	112

1. Introduction

The project focuses on deposition of tunnel rock masses, and the potential for pollution afterwards in connection with tunnel construction for the new, RV4 highway at Gran – Hadeland, East Norway.

Alum shale is a sedimentary rock commonly found in the construction area; it contains sulfide and relatively high levels of metals, metalloids and radionuclides, especially uranium. During the tunnel construction, large amounts of rock masses are excavated and stored, this processes can change the original physical and chemical properties of elements in the alum shale (Project from NORWAT in cooperation with NMBU, 2012).

Oxidation of sulfide to sulfate has been observed to when the material is exposed to atmospheric oxygen and when sulfates come into contact with water, acidic conditions are created in the water by creation of sulfuric acid. The pH of the runoff water has been reported to be as low as 2. Weathering processes involving water at this level of acidity can lead to the mobilization of metals and other elements, such as uranium and arsenic that can have a negative effect on the environment.

In the present work, Alum Shale, Black Shale and Peat Moss from the deposition area for the masses will be studied. The main hypothesis is that the mobility of radionuclides and other redox sensitive elements will be different under oxic and anoxic conditions. Beside the main hypothesis, this work will attempt to answer the following specific scientific questions:

1. Hexavalent uranium is more commonly found under oxic conditions while tetravalent, in reducing conditions. How will the mobility be for bioavailable fractions under the two conditions?
2. Peat core samples will contain higher organic material than alum shale and black shale samples. How will the association of radionuclides and metals be for peat moss compared to the shales?

3. Redox sensitive metals are likely to behave differently under oxic and anoxic conditions. How will the distribution of these elements be during the sequential extractions?
4. How will the differences in the material be before and after treatment? Will the methods of characterization be able to identify these changes?

2. Theory

2.1 Metals and radionuclides in the environment.

Sources of metals and radionuclides are both, anthropogenic and natural, and in the case of radionuclides, cosmogenic as well (Chopin, 2002). Natural processes, like volcanic eruptions and natural disasters, affect the distribution and transport of these element, however these aspects have also been strongly influenced by human activity (Garrett, 2000).

Since the industrialization era started, the inputs of metals, metalloids and radionuclides have exceeded the ones from natural sources (Clemens, 2006). Mining activity, road construction, industrial activity and fossil fuel combustion have been important sources of contamination and proliferation of these elements. Water and soil contamination by arsenic has been observed in mining areas in Central Mexico (Armienta, 2012). When it comes to radionuclides, one if the most important sources of anthropogenic isotopes to the Arctic region in the 60's were the reprocessing facilities of Sellafield in England, La Hague in France and Dounreay in northeast Scotland. Among these the most important being the Sellafield facility due to the size of the discharges. (AMAP Secretariat , 2002). Nowadays, according to the Marina Report II, the oil and gas industry is the major contributor to the collective dose to the European Union population from industrial activities not related to the production of atomic energy production (Betti, 2004), which suggests that the focus is now turning towards Naturally Occurring Radioactive Material NORM.

Metals and semi-metals constitute approximately 75% of the elements in the periodic table and they are of great importance as they can interact with geological and organic material playing an important role in biological processes (Vanloon, 2010).

Calcium and potassium, for example, are essential elements for sustaining life and they are required in relatively large amounts by plants and animals. Copper and zinc are among the essential metals, these elements are needed in small amounts as they can become toxic for humans in higher concentrations (Appelo, 2005). However, concentrations in the range of 2-4 µg/L of copper are established as acute exposure in aquatic systems (Grosell, 2012).

The toxicity of a substance is not given only by its nature but also by the degree of exposure and by the ability of the organism to absorb, degrade and eliminate the toxicant (Donald, 1998).

Radionuclides have the potential for a dual toxicity: chemical and radiological due to its radioactive nature. The chemical toxicity of all isotopes of a radioactive element are equivalent, since their chemical behavior are similar, whilst their radiological toxicity is intrinsic to the particular isotope and its decay chain.

Thorium is a radioactive elements that consists mostly of the Th-232 isotope and it is the parent of the Thorium Decay Series, shown in Figure 1. This element has an average abundance of 10 ppm in Earth's crust and it occurs in minerals only as an oxide, it has a specific activity of 4.06 MBq/kg (Chopin, 2002). The most common of these minerals is monazite, however it can also be found in small amounts in granite and gneiss among others; this radionuclide may gain importance in the nuclear industry as it can be used as reactor fuel for the production of energy.

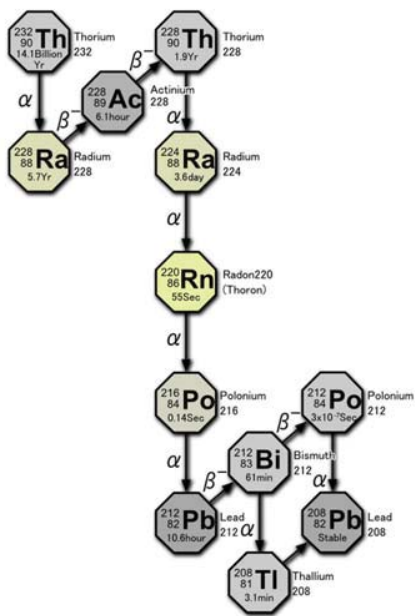


Figure 53 Thorium Decay Series. (Tosaka, 2008)

Uranium is a heavy metal that has a potential for targeting different organs in the body, specially liver, kidney and bone but it may also affect nervous system, reproductive system and respiratory tract. (Agency for Toxic Substances and Disease Registry, 2013)

It has been observed that damage to respiratory organs can occur by inhalation of insoluble compounds at levels of 1.5 mgU/ m^3 over a period of 3 and a half years, similar doses did not result on renal effects; this suggests that effects of target organs depends as well on the route of exposure and the chemical specie of uranium.

Insoluble species of uranium like particles may cause a greater effect on respiratory organs and soluble species in organs such as kidney. In general, it is possible to say that soluble species tend to be up to 5 times more toxic than insoluble ones due to absorption and uptake capacity. (Agency for Toxic Substances and Disease Registry, 2013). Uranium decay series is shown in Figure 2.

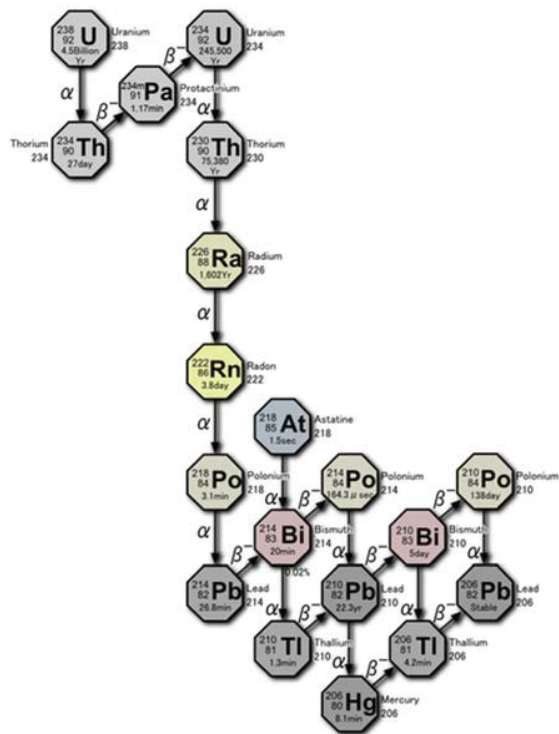


Figure 54 Uranium Decay Series. (Tosaka, 2008)

Radium and radon are formed during both the uranium and the thorium decay series. Both radionuclides, Ra and Rn are two of the most radio-toxic substances there are at relatively low concentrations (Chopin, 2002). Only in Norway, long-term exposure to radon and its progenies are accounted for 14% of the recent cases of lung cancer each year. Since uranium is naturally present in many minerals, during industrial processes these radionuclides may enter by-products or even final products, hence causing a radioactive contamination problem (Chopin, 2002), (Smethurst, 2008). According to Smethurst et al. (2008), the risk of exposure to radon for the population of Norway is increasing due to changes in the construction industry.

2.2 NORM and Technologically enhanced NORM

Sources of radionuclides can be classified according to its origin: anthropogenic and NORM.

The term NORM, naturally occurring radioactive material, refers to cosmic radiation in the form of tritium and C-14 and to natural resources containing natural radioactive material, U-238, U-235, Th-232 and K-40, commonly present in geological formations and water springs.

The term technologically enhanced NORM refers to naturally occurring radioactive material whose chemical, physical or radiological form has suffered alterations due to human activity. Such alterations have the potential to cause:

- Redistribution and contamination of air, water, and soil.
- Changes in speciation and increased environmental mobility.
- Incorporation of elevated levels of radioactivity in products and construction materials.
- Improper use of disposal methods that could result in unnecessary exposure to individuals and populations via environmental media.

Radioactivity from NORM did not use to be regulated in Norway even though the average world exposure, 2.4 mSv per year, is constituted in 91% of radiation from NORM materials according to MARINA II report (2003). Nowadays and since 2011 the materials extracted from industries that can produce radioactive contamination must be treated accordingly (Project from NORWAT in cooperation with NMBU, 2012).

On the other hand, technologically enhanced NORM is regulated only if the key product of the industry is a radioactive one, for example uranium mining industry. However, non-nuclear industries are a great contributor to radioactive contamination, oil and gas industry together with metal and coal mining and phosphate industry are among the most relevant ones.

The water produced in the extraction process of oil contains Ba²⁺, isotopes of Ra, ²¹⁰Pb and ²¹⁰Pb due to the presence of uranium in the bedrock. Radioactive isotopes of Ra are soluble and they are transported in the production system, while Ba²⁺ and SO₄²⁻ contribute to the precipitation of BaSO₄ in the form of scales inside the piping system. In order to prevent scales, barium binders are added and Ra, Pb, Po can form stable complexes with these binders and be directly discharged into the sea. These alpha emitters can replace calcium in bones and be stored in fat in the form of stable organic complexes and thus, have the potential for biomagnification in the food chain.

In Norway, the oil and gas industry had a release of 440 GBq of Ra-226 and 380 GBq of Ra-228 in 2003 according to the MARINA II report (2003) into the North Sea.

Another important case in Norway is the mining areas of Fen and Søve in the Telemark region. This area mainly consists of magmatic rocks, including iron minerals, niobium minerals related to carbonatite rocks with important levels of NORM, uranium and thorium, from which the most abundant is thorium (Mrdakovic, 2010). The mining activities on these areas were carried out between the 17th century and the 20th century and epidemiological and radiological impact of this period showed that the workers received an annual dose of 150 mSv in comparison to the occupational dose limit of 20 mSv per year for radiation workers. Researchers have found values of exposure doses from 0.15 to 9.20 µGy/h, which are above the world average terrestrial dose rate of 0.059 µGy/h (Skipperud, 2010)

High levels of NORM and technologically enhanced NORM represent a challenge in impact and risk assessment. The lack of regulations within the non-nuclear industries and the inventories of NORM, together with the lack of data on chemical and physical form of radionuclides can lead to inconsistencies in the analytical method and erratic conclusions, thus

affecting predictions for dispersion, transport in the environmental media and dose assessment (Lind, 2013).

2.3 Geology of Gran, Hadeland

This area is characterized by sedimentary rocks from mainly Ordovician to Lower Cambrian. These distributions are also similar to the ones found in some areas in Sweden (Tourtelot, 1979). Two of the most common minerals found in this area are chlorite and illite, these minerals are important clay mineral constituents of shales. The ratios of these minerals in rocks of the Røgsaker District, close to lake Mjösa are in the range of 0.2-3.55 for limestone and from 0.2 to 1.4 for black shales (Björlykke, 1974).

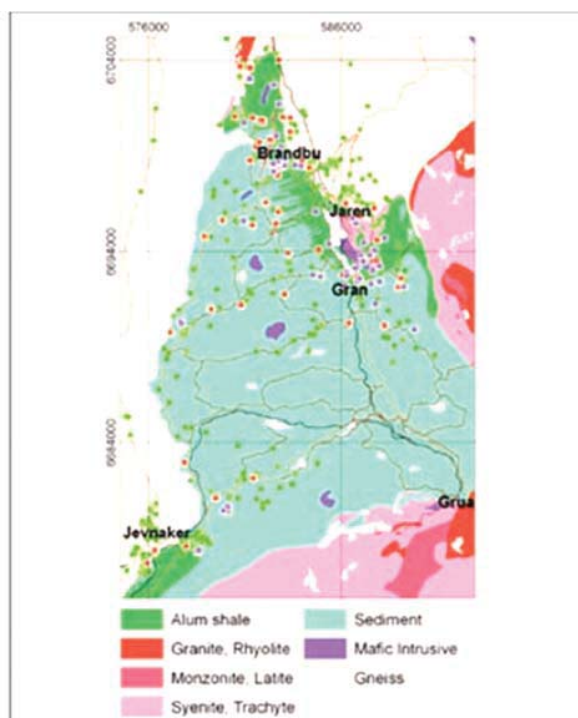


Figure 55 Geology of Gran municipality. The map shows the distribution of alum shale, granite rhyolite, monzonite latite, syenite tachyte, sediment, mafic intrusive and gneiss. (Smethurst, 2008)

The geology of this zone shows a great variety of rocks, from uranium and metal-rich alum shale, diverse black and calcareous shales to sedimentary

rocks with relatively low content of uranium (Smethurst, 2008) (Statens Vegvesen , 2013). In Figure 3, displays a map of the area illustrating the bedrock geology. Permeability of the superficial deposits is one key factor for the transport of radon gas in the ground. In Figure 4, a map of the drift geology is presented according to permeability level. In Figure 5, the distribution of uranium in Gran, according to its concentration, can be observed.



Figure 56 Drift geology of Gran shows highly permeable deposits in yellow and moderate permeability in orange. (Smethurst, 2008)

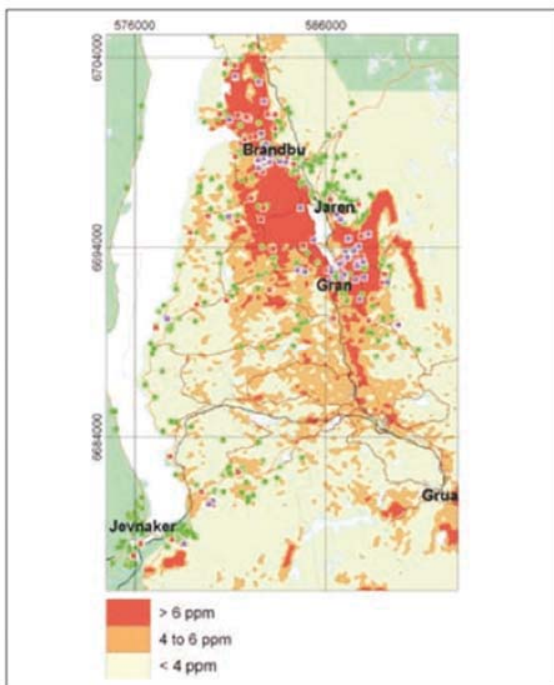


Figure 57 Distribution of uranium according to its concentration in ppm (parts per million) over the Gran area. (Smethurst, 2008)

2.4 Wetlands: Deposition areas for extracted rock masses

The Ramsar Convention, also known as the Convention for Wetlands of International Importance especially as Waterflow Habitat, has defined a wetland as "... areas of marsh, fen, peatland or water, whether natural or artificial, permanent or temporary, with water that is static or flowing, fresh, brackish or salt, including areas of marine water the depth of which at low tide does not exceed six metres, may incorporate riparian and coastal zones adjacent to the wetlands, and islands or bodies of marine water deeper than six metres at low tide lying within the wetlands" (Semeniuk V., 1997) and they are classified as follows:

- Marine and Coastal
- Inland
- Man-made

Inland wetlands can contain both saline or fresh water, and be seasonal or permanently flooded. The present work focuses on inland wetlands that are flooded by fresh water either seasonally or permanently; nonetheless, salinity will be commented as the pH is one of the main factors when it comes to speciation of metals and radionuclides (Semeniuk, 1997).

Regarding the Norwegian territory, one of the most interesting areas are the alpine wetlands since they depend greatly on ice and snow melting. Wetlands are usually very active zones: with water movement and circulation, vegetation and fauna. The deposition area in Gran is classified as bog, a type of wetland. This bog presents a various strata, the upper layers are rich in organic materials while at a depth of approximately 10 m, the composition is mainly marine silt clay materials with low content of organic matter.

Wetlands usually contain a high content of organic matter, either dissolved in the surface and ground water or as a part of the soil composition. Depending on the location, the mineral composition varies as well, crystalline bedrocks is a common characteristic in alpine zones and oxides, phosphate, calcium and silicate bearing minerals are associated with uranium (Regensprug, 2010), due to this complexity and different properties, these zones can enable the enrichment or even elimination of toxic elements and metals coming from different water sources, either anthropologically or naturally, containing uranium and other metals (Schöner, 2009). Speciation of metals in wetland soils, in this case uranium, is very difficult to describe without taking in consideration the ground and surface water chemistry. Therefore, even though this work will focus on soils and rocks, conditions and important parameters of water will be discussed. In Figure 6, some of the different uranium ores found in nature are presented and classified between primary ores and secondary ores.

Ore	Composition	Description
Primary ores		
Uraninite	$\text{UO}_2 + \text{UO}_3$	A steel-, velvet-, to brownish-black in color; major ore of uranium and radium
Pitchblende	$\text{UO}_2 + \text{UO}_3$	Essentially the same as uraninite
Brannerite	$\text{U}(\text{TiFe})_2\text{O}_2$	A black, brownish, olive greenish ore; primary mineral in granite, associated with uraninite
Coffinite	$\text{U}(\text{SiO}_4)_{1-x}(\text{OH})_{4x}$	A black or pale-to-dark brown mineral in sandstone, associated with uraninite
Davidite	$(\text{CeLa})\text{U}(\text{TiFe}^{3+})_{20}(\text{O},\text{OH})_{38}$	A black-brownish mineral in granite, associated with ilmenite and others
Thucholite	Mixture of petroleum hydrocarbons, uraninite, and sulfides	Black mixture, acronym stands for thorium, uranium, carbon, and hydrogen
Carnotite	$\text{K}_2\text{O} \cdot 2\text{U}_2\text{O}_3 \cdot \text{V}_2\text{O}_5 \cdot 3\text{H}_2\text{O}$ (uranium potassium vanadate)	Bright-, lemon-, or greenish-yellow mineral in sandstone associated with tyuyamunite and U-V oxides
Secondary ores		
Autunite	$\text{Ca} (\text{UO}_2)_2 (\text{PO}_4)_2 \cdot 10\text{H}_2\text{O}$	Yellow-to-greenish mineral produced under oxidizing conditions and associated with tormerlite
Torbernite	$\text{Cu} (\text{UO}_2)_2 (\text{PO}_4)_2 \cdot 10\text{H}_2\text{O}$	An emerald-, grassy-, to apple-green mineral formed in an oxidized zone and associated with uraninite and autunite
Tyuyamunite	$\text{Ca}(\text{UO}_2)_2 (\text{VO}_4)_2 \cdot 5-8\text{H}_2\text{O}$ (uranium calcium vanadate)	A canary-, lemon-, to greenish-yellow mineral associated with carnotite

Sources: Amethyst Galleries 1995; Mindat 2011; MSA 2011; Stockinger 1981; Uranium Institute 1996

Figure 58 Classification of some of the Primary and Secondary ores of Uranium found in nature. (Agency for Toxic Substances and Disease Registry, 2013)

Regarding Norway, crystalline bedrock containing traces of uranium is also commonly found in granites and pegmatites. One of the most important uranium-bearing rocks found in the Eastern region of the country and the Oslo area is alum shale (Smethurst, 2008), (Project from NORWAT in cooperation with NMBU, 2012).

2.5 Speciation

Elements, trace elements, heavy metals and radionuclides can be present in the environment in different physico-chemical forms and these factors have a direct influence on transport within the environmental media, mobility, bioavailability, uptake by organisms and accumulation and thus, effects on individuals and populations.

Speciation is defined as the distribution of an element amongst defined chemical species in a system (Tempelton, 2000).

The main physicochemical properties that influence speciation of radionuclides and metals are the following according to Salbu (2013),

- Nominal molecular mass
- Charge properties and Valence
- Oxidation state
- Structure and Morphology
- Density, Degree of Complexation

These properties give the chemical specie its identity in a defined system and it is basic to know these characteristics in order to understand their mobility through the environment. Two of the most important aspects for aquatic systems and water-sediment interaction systems are the size of the different species of trace elements and its charge. In Figure 7, it is possible to observe the classification of physicochemical forms by size.

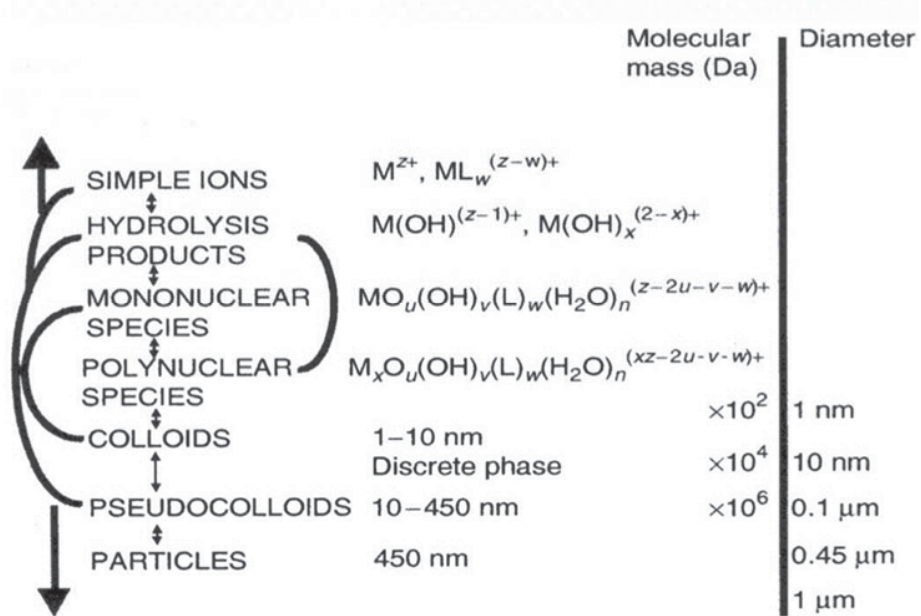


Figure 59 Classification of physicochemical forms by size in aquatic systems. (Salbu, 2013)

There are different mechanisms that contribute to size distribution. Increase in size can be achieved by hydrolysis, complexation, polymerization, colloid formation and aggregation; while decrease in size is influenced by desorption, dissolution and dispersion. These mechanisms will be discussed further since they play an important role in the speciation of elements, for example, uranium - U(IV) and U(VI) – behaves differently when it is in the presence of organic and inorganic ligands.

As mentioned in the description of the project, the area of study is rich in alum shale, which is also a sulphide-bearing rock. It has been observed that the oxidation of sulphide to sulphates by atmospheric oxygen produces H_2SO_4 , which promotes the acidification of water. This phenomenon has been observed and documented by several authors (Armienta, 2012), (Nordstrom, 2009). (Craw, 2005) and it has been reported pH values as low as 2 (Project from NORWAT in cooperation with NMBU, 2012). The pH value of the environmental media, soil and water, is a decisive factor on metals and radionuclide speciation.

Uranium is commonly present in nature in two oxidation states U(IV) and U(VI) and it can be found in different ores as oxides, phosphate, calcium and silicates (Regensprug, 2010) and dissolved in fresh and saline water. The geochemical processes that can influence the mobility of this metal in wetlands are precipitation and dissolution, sorption and desorption and complex formation with organic matter and other species. (Ping, 2005).

The factors that can influence uranium speciation in wetlands have been discussed by several authors, they concur that pH, organic matter, oxygen presence and redox potential are the ones that influence speciation the most. Furthermore, these factors have been observed to influence speciation not only uranium, but arsenic and selen as well (Ping, 2005), (Regensprug, 2010), (Schöner, 2009). The presence of anions and other compounds, such as carbonates and bicarbonates in water and soils are also very important to speciation metals and semi-metals. (Ping, 2005).

Under oxidative conditions, the dominant specie is U(VI) in the form of the uranyl cation UO_2^{2+} and regarding aqueous exposure, the hexavalent form is the main concern since it is highly soluble (Goulet, 2012). At pH lower than 5 and under oxic conditions the free uranyl cation can be found, while at higher pH it forms stable complexes with inorganic ligands like hydroxide. Carbonates, sulphates and fluorides, may also be important depending on their concentration. In presence of organic matter may also form stable complexes as acetates, oaxalates and humic and fulvic acids, these last two are of great importance since they are the main components of aqueous organic matter and they act as efficient proton exchangers with metals (Regensprug, 2010). The influence of pH on speciation can be observed in Figure 8.

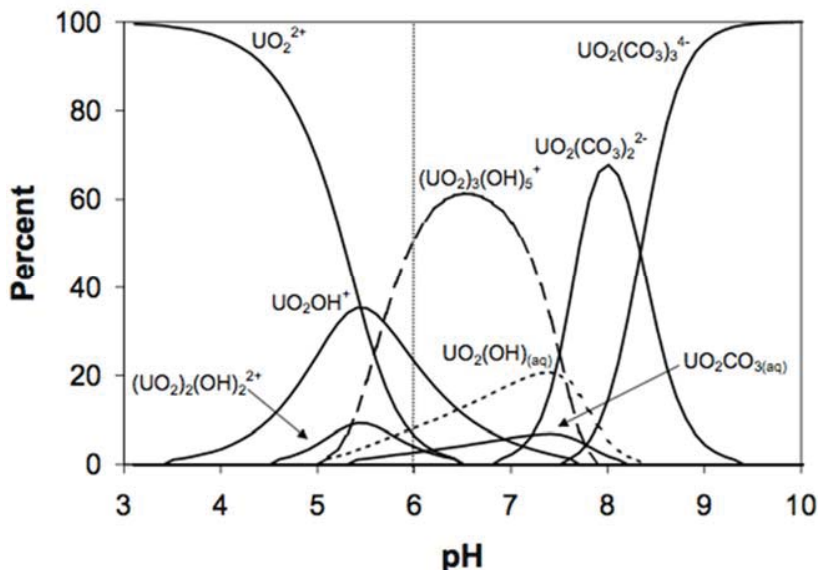


Figure 60 Speciation of dissolved uranium and a function of pH for $[U]_{TOT} = 5 \text{ M}$, $I = 0.1 \text{ M}$, and $P_{CO_2} = 10^{-3.5} \text{ atm}$. Calculations were made without considering the precipitation of any solid phases. (Giammar, 2001)

From the figure above, it is possible to observe that the dominant specie at pH around 8 are is a complex of uranium with carbonate, $UO_2(CO_3)_2^{2-}$, also that at low pH, below 5, the predominant specie is the free uranyl cation, thus supporting what was mentioned above. From this figure, it is possible to infer that water chemistry has a direct influence on speciation of uranium in soil-water systems. Analytical methods for water and soil characterization are of great importance when analyzing speciation characteristics.

Under reducing (anoxic) conditions, uranium (IV) complexes with hydroxide or fluoride are the only dissolved species. The precipitation of uranium (IV) under anaerobic conditions is the dominant process leading to naturally enriched zones of uranium in shallow layers of the ground (Giammar, 2001).

Tetravalent uranium is also a concern regarding benthic organisms since it is strongly bounded to sediments and mostly insoluble, however remobilization mechanisms include dissolution of iron oxyhydroxides and

upward and downward fluxes of water within the wetland (Goulet, 2012). Regarding reducing conditions, there is another special aspect to consider: the microbial reduction. Iron reducing bacteria are microorganisms that use metals as electron acceptors and humic substances as donors within their metabolism (Goulet, 2012), (Regensprug, 2010). These bacteria can accelerate the reduction of U(VI) to U(IV) at relatively fast rates.

The reason why the presence of oxygen is considered a key factor for the speciation of uranium is explained very clear by Ping (2005). The extraction of oxidized and reduced forms of uranium experiments by addition of carbonates, showed that most of the uranium present was extracted under aerobic conditions, 0.264 mg U per g of soil, while under anaerobic conditions 0.229 mg U per g of soil were recovered. This difference could be due to the presence of U(IV) which has been observed by Kohler (2004) to be highly insoluble under a N₂ atmosphere even when high concentrations of carbonate are found. (Ping, 2005). It is possible to observe this tendency in Figure 9.

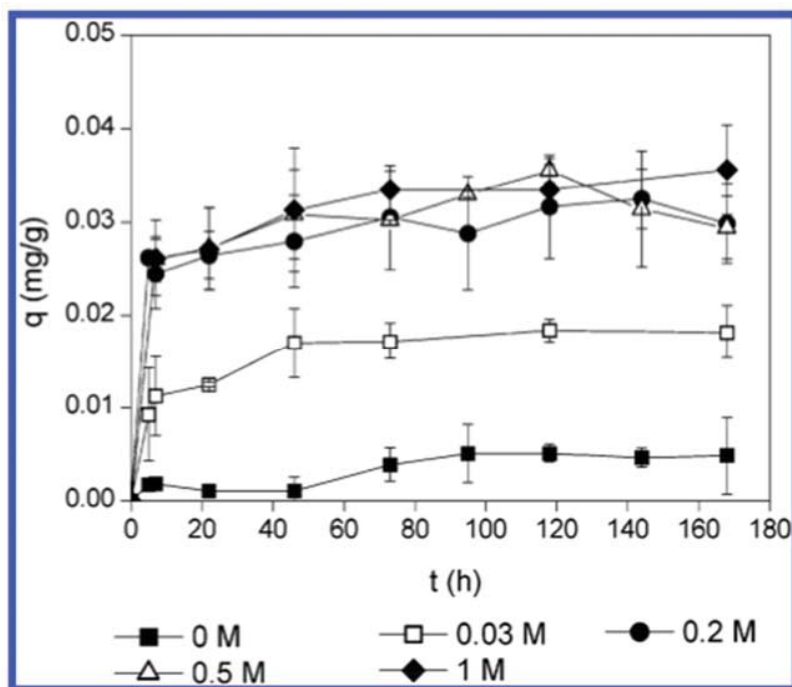


Figure 61 Difference between the uranium extracted by bicarbonate at varying concentrations under oxic and anaerobic conditions. This difference is attributed to the oxidation of U(IV) in the soil under oxic conditions. (Ping, 2005).

Metal content of enriched shales can be related to the amount of organic matter in the shales. Trace metal adsorption, sulfate reduction and sulfide precipitation are the some of the dominant processes for this phenomenon. Thus, content of organic matter does not necessarily identify metal-rich shales. The nature of the organic material and its original metal content, the nature of sediments, water chemistry in the source areas and ash content are factors that should be considered (Tourtelot, 1979).

The abundances of some elements are related to those of other constituents of black shales. For example, the contents of Si and Al may suggest a relation to the abundance minerals created by weathering processes; and the Sr content can be related to the abundance of carbonate minerals from rock transformation processes (Tourtelot, 1979).

3. Materials and Methods

This work was divided in two different experiments that complement each other. Experiment one, Sequential Extraction, gives information about the potential mobility and bioavailability of radionuclides and metals derived from alum shale and black shale rocks, as well as peat moss from the area selected for the permanent deposition of masses from the tunnel construction. Sequential Extractions were performed under both oxic and anoxic conditions in order to study the possible differences in mobility and speciation of the analyzed elements. . The elements that will be analyzed are aluminum Al, sulfur S, calcium Ca, vanadium V, chromium Cr, manganese Mn, iron Fe, cobalt Co, nickel Ni, copper Cu, zinc Zn, arsenic As, molybdenum Mo, cadmium Cd, tin Sn, thorium Th, uranium U in addition to silica Si and magnesium Mg in the leaching experiments.

Experiment two, Leaching Experiment on Thin-Section, provides information about weathering processes on alum shale, a sulfide-bearing rock, known for its high content of uranium and other metals. This experiment also attempts to contribute to the development of a new method for analysis of this phenomenon by using a combination of microanalytical techniques to characterize the sample before treatment and after the leaching experiments to determine the possible differences in concentrations of elements of interest and physical differences in the material itself.

Special attention will be directed to uranium among the studied elements. This element is of environmental importance due to 1) two of its daughter products during radioactive decay, Radium and Radon and 2) its ubiquitous nature and toxicity, both radiological and chemical.

3.1 Quality analysis

Quality analysis is an important part of the analytical result. Errors and uncertainties are common in analytical data and they must be explained and if possible, quantify in order to verify the reliability of the results. Unreliable data can lead to incorrect risk assessment and conclusions (Salbu, 2012).

The quality analysis of the ICP-MS analysis was studied by performing tests for precision and accuracy, in addition to determining the Limit of Detection (LD) and Limit of Quantification (LQ) for the analysis.

The precision of the analysis was based on the total concentration results for the samples. Three parallels from each material were used for this analysis; three blanks were also included for each material. The coefficient of variation was calculated by dividing the standard deviation by the mean. This value describes the relative variation observed for each element. Literature suggests that coefficients of variation less than 30 % are considered indicators of good to fair precision in a data set (Brown, 1998).

The accuracy of the ICP-MS analysis was determined by measuring total concentrations of two standard soil Reference Materials NCS DC 73324 and NCS DC 7335. The error percentage was calculated using the following equation:

$$\text{%Error} = \frac{(\text{Observed Concentration} - \text{Expected Concentration})}{\text{Expected Concentration}} \times 100$$

Values for Limit of Detection (LD) and Limit of Quantification (LQ), were calculated from the reactive blanks used in the experiment. The LD value represents the lowest concentration that can measure by the instrument, while the LQ represents the concentration that has a high enough

confidence level to be subjected to further statistical analysis. These values are calculated with the following equations:

$$\text{LD} = 3 \times \text{Standard Deviation (based on blanks concentration)}$$

$$\text{LQ} = 10 \times \text{Standard Deviation (based on blanks concentration)}$$

3.2 Sampling and sample preparation

3.2.1 Sampling area

The sampling area is located close to the border between Gran and Jaren municipalities in Easter Norway. This location is the building site of a tunnel along Highway RV 4, the NPRA plans to finish this construction by 2015. The area has a complicated geology and it has been previously studied for presenting elevated levels of radon gas emissions, as it was discussed in Section 2. Figure 10 illustrates the sampling locations within the field site.

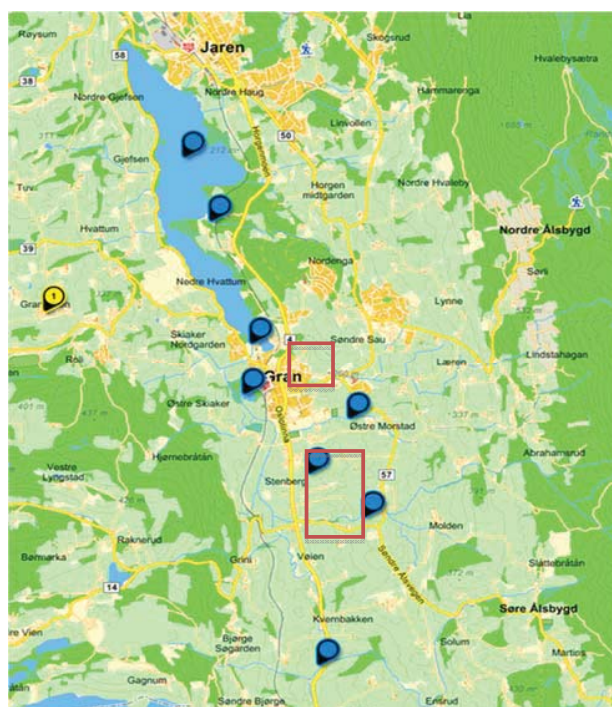


Figure 62 Sampling area. Gran municipality border with Jaren, blue marks illustrate sampling locations for the project. Locations marked with red squares represent the sampling areas for Alum Shale and Black Shale (top) and Peat Moss (bottom) (Skipperud, 2013).

Alum and Black Shale samples were collected from the area where the tunnel will be constructed, offering representative samples of the excavated material. Six rock cores boreholes were extracted from the tunnel area. Samples for the present study were collected from two different core samples by Frelsborg Drilling Company AB NUF personnel and stored in airtight bags filled with N₂ to prevent oxidation. In Figure 11, a profile of the geology over this zone is presented; in this profile three of the studied sites are shown.

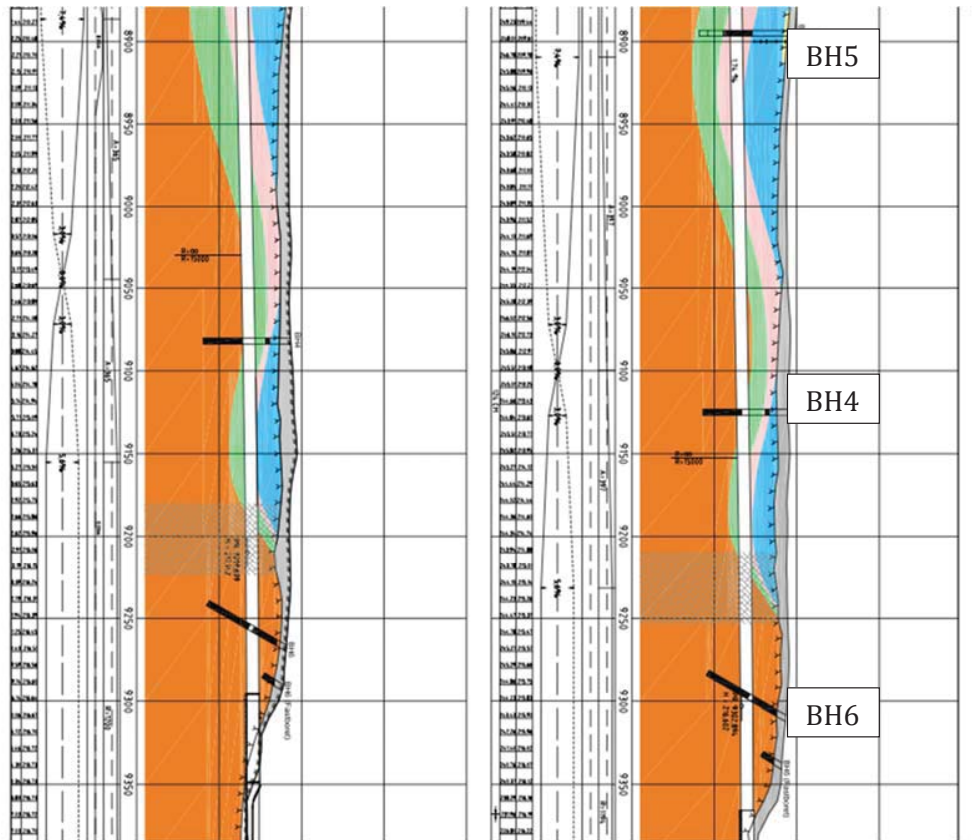


Figure 63 Engineering Geological Profile of projected tunnel area. Marked areas highlight BH-5 (black shale), BH-4 (alum shale) and BH-6 (alum shale). Colors indicate different materials: Grey: loose material, blue: calcareous shales of blackish to grey color, pink: black shales, green: calcareous shales of dark to gray color, orange: alum shale. (Statens Vegvesen , 2013)

Peat Moss samples were collected from the planned deposition area. Several cylinders were extracted from different locations within the bog zone; samples were collected by NPRA and NMBU personnel in February 2013 and placed into airtight bags filled with N₂. Samples were stored under these conditions and at cool temperatures to prevent oxidation.

Experiment one and Experiment two.

In order to make the following sections as clear as possible, a brief recapitulation of the two experiments is provided.

Experiment one consists in using the Sequential Extraction Procedure to test if there is a scientific need to perform leaching experiments of environmental samples under anoxic and oxic conditions.

Experiment two consists in the development of a combined method - imaging techniques and leaching experiment- to study the weathering process on rock samples observed in nature.

Together, these experiments complement each other to give information about the potential mobility of diverse elements in environmental samples.

3.2.2 Sample selection and preparation

3.2.2.1 Experiment one

The criteria for selecting BH-5 Prøve 1 and BH-6 Prøve 2 was based on XRF data, aiming to identify the fragments with the highest content of uranium.

After the selection process, both sample cores BH-6 Prøve 2 and BH-5 Prøve 1, Alum and Black Shale respectively, were cut lengthwise with a diamond saw with water as a coolant at the Geological Department of the University of Oslo. One piece was stored in N₂ atmosphere to prevent oxidation and the other section was divided into smaller pieces. A sub sample was taken from BH-5 Prøve 1 to be pulverized for the sequential extraction experiments; while for BH-6 Prøve 2, a sub sample was taken

for Experiment two and another one was taken to be pulverized for the sequential extraction experiments.

In order to select the Peat Moss number 15 sample for Experiment one, the redox potential value was measured on the collected samples from the deposition area in Gran. Sample number 15 Peat Moss was also characterized by NPRA and NMBU for moisture content, total organic carbon and mineral content by X-ray diffraction.

After the selection process, the peat moss sample was used in wet weight for the sequential extractions.

The samples used in Experiment 1: Sequential extractions are three:

1. Alum Shale BH-6 Prøve 2: Oxic samples OAS and Anoxic samples AAS
2. Black Shale BH-5 Prøve 1: Oxic samples OBS and Anoxic samples ABS
3. Peat Moss from the deposition area: Oxic samples OPM 15 and Anoxic samples APM 15.

Experimental parameters for the sequential extraction process are summarized in Table 1. Tari Helmers performed the sequential extractions under oxic conditions; the obtained data is used in the present work.

Table 22 Experimental Parameters for Experiment one: Sequential Extractions.

Material (approximately 2 g)	Conditions	Samples+ Blank	Parallels	Steps
Alum Shale	Anoxic	1+1	3	6
	Oxic	1+1	3	6
Black Shale	Anoxic	1+1	3	6
	Oxic	1+1	3	6
Peat Moss	Anoxic	1+1	3	6
	Oxic	1+1	3	6

3.2.2.2 Experiment two

As mentioned before, the sample for Experiment two is a sub sample from the alum shale sample BH-6 Prøve 2, used in Experiment one.

The thin-section sample was prepared by Lars Kirkseter from the Institute for Energy Technology (IFE). The sample of alum shale was glued onto a plate 4.2 x 2.3 cm of polymethylmethacrylate, (PMMA) also known as plexiglass, with Araldite 2020 in a two-component clear epoxy adhesive system by Ciba Specialty Chemicals. The alum shale sample was then cut to 15-30 μm thin-section and polished on the surface. Even though the standard thickness for thin-section samples is 30 μm , the material did pose difficulties during the process, hence the variation on its thickness. Since micro XRD was one of the selected characterization methods, small holes were drilled on the plexiglass surface to prevent interferences from it in the results. See Figure 12.



Figure 64 Thin-section sample. Alum shale glued on PMMA plate measurements 4.2 x 2.3 cm.

3.2.3 Sample characterization

NMBU personnel and myself did sample characterization of BH-5 and BH-6; the methods used are presented in detail in this section. On the other hand, Peat Moss sample was characterized by NMBU and NPRA personnel, this section does not include the methods used by the NPRA, although some results from this characterization is discussed.

3.2.3.1 X-Ray Florescence Spectrometry (XRF)

X-ray fluorescence spectrometry XRF is a non-destructive and non-invasive analytical method widely used for elemental quantitative analysis (Lind, 2006). Detection limits for high atomic mass elements is commonly in the range of ppm (Zawisza, 2012), making it a good tool for identifying metals and radionuclides.

The XRF uses short wavelength radiation, x-rays, to excite the atoms of the sample in order to produce ionization. An incident x-ray hits the sample with enough energy to displace an inner shell electron, since this creates instability within the atom; an outer shell electron replaces the ejected electron. This process releases energy, fluorescence radiation, which is a fixed value depending on the electron shells. This energy is detected and it can be used to quantify abundance of elements in the material (Shackley, 211).

Semi-quantitative X-ray fluorescence measurements were performed at Bioforsk Laboratory at NMBU, using a Spectro xSort XHH03 instrument manufactured by Ametek. The instrument uses an internal calibration performed after 3 measurements and was used in handheld mode. The materials measured can be found in Table 2 and the complete data set for the results can be found in Appendix A.

Table 23 Material, name and number of measurements performed to select samples with the XRF instrument.

Material	Name	No. of measurements
Black Shale	Prøv 1 BH-5	2
Black Shale	Prøv 2 BH-5	2
Alum Shale	Prøv 1 BH6	5
Alum Shale	Prøv 2 BH6	4
Alum Shale	Prøv 4 BH6	2

3.2.3.2 X-Ray Diffraction (XRD)

The X-ray diffraction is an analytical technique used to identify crystalline phases and atomic spacing in materials of environmental importance, like minerals. A monochromatic x-ray is produced and directed toward the mineral in a certain angle according to Bragg's Law; the interaction produces a constructive interference and a diffracted x-ray is produced. The x-ray signal leaving the material is detected counted. By comparing the characteristic diffraction spacing and relative intensities of reference materials to the signal detected from the sample, the mineral is identified. (Dutrow, 2012)

For the present work, a sub-sample of each material, Alum Shale, Black Shale and Peat Moss, were analyzed at the Museum of Natural History in Oslo. Small samples for the XRD, previously pulverized, were added ethanol and left to dry before being mounted on the sample holders and run in a Simens D 5005 Spectrometer, the instrument has a 0.02 degrees of uncertainty. All diffractograms were recorded from 2o to 70o in the 2-Theta scale 0.050o per second, and were set to 40 kV and 40 nA using Ni filtered CuK α radiation with wavelength $\lambda = 1.54178 \text{ \AA}$. The diffractograms were checked against the Power Diffraction Files database from the International Centre for Diffraction Data. Mineral proportions are regarded as semi-quantitative.

3.3 Experiment one: Sequential extractions

3.3.1 Sequential extraction method

The sequential extraction procedure that was used in the present work is a modified version of the original protocol designed by Tessier (1979) and adapted by the Isotope Laboratory at NMBU.

This is an analytical method that consists in extracting different chemical species using specific leaching solutions to the chemical composition of the soils (Tessier, 1979). The specificity of the extracting agents has been greatly discussed, however the general trend is to decrease the pH and to increase the redox power; by following this trend three general binding mechanisms can be identify:

- Reversible physical sorption: Step 1 and 2.
- Reversible electrostatic sorption: Step 3.
- Irreversible chemsorption: Step 4 (weak reducing), Step 5 (weak oxidizing) and Step 6 (Strong oxidizing).

Commonly the results from Step 1-3, represent the bioavailable fraction of the sample, Step 4 and 5 is associated with redox sensible metals and Step 6 is associated with strongly fixed elements (Salbu, 2000). For the present work, sequential extractions were performed under two different conditions, aerobic and anaerobic in order to identify possible differences in the concentration of elements in the different fractions and explore the implications for the overall project. In Table 3, the model of the sequential extraction used in the present work is presented.

Table 24. Experiment 1. Sequential Extraction Model used under Oxic and Anoxic conditions (Skipperud, 2004) (Salbu, 2000).

Model	Anoxic conditions	Oxic conditions
Consecutive layers, reversible reaction	Step 1. MiliQ water bubbled with N ₂ for 5 minutes. Room temperature.	Step 1. Mili Q water. Room temperature.
Consecutive layers, reversible reaction	Step 2. NH ₄ OAc pH 7 bubbled with N ₂ for 5 minutes. Room temperature.	Step 2. NH ₄ OAc pH 7. Room temperature.
Monolayer, reversible reaction	Step 3. NH ₄ OAc pH 5 bubbled with N ₂ for 5 minutes. Room temperature	Step 3. NH ₄ OAc pH 5. Room temperature.
Monolayer, reversible reaction	Step 4. NH ₂ OH·Cl pH 3 in 25% (v/v) acetic acid. At 80°C Weak reducing agent.	Step 4. NH ₂ OH·Cl pH 3 in 25% (v/v) acetic acid. At 80°C Weak reducing agent.
Monolayer, irreversible reaction	Step 5. H ₂ O ₂ adjusted to pH 2 with HNO ₃ . At 80°C Weak oxidizing agent.	Step 5. H ₂ O ₂ adjusted to pH 2 with HNO ₃ . At 80°C Weak oxidizing agent.
Monolayer, irreversible reaction	Step 6. 7M HNO ₃ , at 80°C Strong oxidizing agent.	Step 6. 7M HNO ₃ , at 80°C Strong oxidizing agent.

3.3.2 Inductively Coupled Plasma Mass Spectrometry ICP-MS

Inductively Coupled Plasma Mass Spectrometry ICP-MS, uses a high-temperature source combined with a mass spectrometer in order to analyze the elemental compositions of sample materials. The high-temperature section of the instrument, ICP, ionizes the atoms of the sample; these ions are send through the mass filter section of the Mass Spectrometer to be later on detected and counted to determinate the elemental composition of the sample (Wolf, 2013), (Salbu, 2000).

For the present work, the extracts from the sequential extraction procedure were diluted to 47.5 ml with MiliQ water and added 2.5 ml of concentrated ultrapure HNO₃, according to the instructions from the Environmental Chemistry Section at NMBU; this procedure is done in order to prevent formation of precipitate and maintain the elements of interest in solution.

3.3.3 Microwave Digestion: Ultraclave

Microwave digestion of samples is an analytical method that consists in using high temperature and high pressure to decompose a solid sample. It is used for Total Concentration Analysis. This technique requires minimal sample preparation, commonly mixing the sample with strong acids. Comparatively to other digestion techniques, is relatively fast. (Milestone Microwave Digestion Systems, 2008).

The instrument was an Ultraclave Digestion System III manufactured by MSL- Milestone Microwave Digestion Systems. The samples were weighted to approximately 250 mg and were added 5 mL of HNO₃ and 1mL of HF, they were placed in the Ultraclave along with two different Reference Materials, NCS DC 73324 and NCS DC 7335, for quality assurance, the time of processing was of approximately 30 minutes. Lene Valle and myself performed this sample preparation step at the Environmental Chemistry Section at NMBU.

3.4 Experiment 2: Thin-section characterization and leaching experiment for weathering process analysis

The thin section sample was subjected to a leaching experiment with 40 ml each time of H₂SO₄ with a pH=2. This pH value was selected to simulate the “worst case scenario”, since it has been found that pure sulphide rocks can give a acid run off as low as 2 and pH with a value as low as 4 has been measured in runoff water from alum shale.

The leaching experiment was performed over different period of time. The selected time intervals were after 1 hour, 24 hours, 1 week and 1 month of leaching.

ICP-MS analysis was performed on the extracts for all time intervals, however electron microscopy and stereomicroscopy was used on the thin section after time intervals of 1 week and 3 weeks as well.

3.4.1 Digital Autoradiography

Digital autoradiography is an analytical technique for mapping the radiation: x-ray, alpha, beta and gamma, present in a sample. This technique requires minimal sample preparation while providing important qualitative and even quantitative information about the radiation, however detailed study of the sample is needed to determine the nuclide producing it (Lind, 2006).

The thin-section sample was placed on the marked surface of the screening equipment in order to identify the orientation on the resulted radiograph. The autoradiography film (Molecular Dynamics) was placed on top of the sample; the exposure time for this characterization was of 5 days, this procedure was done at Isotope Laboratory at NMBU by Cato Wendel and myself.

3.4.2 Environmental Scanning Electron Microscope EDX- ESEM

There are two types of electron microscopes: Transmission Electron Microscope TEM and Scanning Electron Microscope SEM. The ESEM is a variation of the ordinary Scanning Electron Microscope in which only one section of the instrument is under vacuum and minimal pre-treatment of the samples is required, for example it can work with moisten samples. ESEM is a non-destructive analytical technique that uses a high-energy beam concentrated to a defined spot in the sample, where secondary electrons are ionized from the surface - penetration range of 1 to 5 microns of depth into the sample -. These electrons are detected and a signal is sent to an amplifier and transformed into a element spectrum. It is important to mention that not only secondary electrons are produced inside the detection chamber, back-scattered or reflected electrons, Auger electrons, x-rays, are also produced; these different particles are responsible for the variety of images the equipment can produce. For example, when using the BEI mode, back scattered electron mode, images with high contrast are obtained, where the lighter colored areas of the sample represent high atomic mass elements while dark areas represent light elements. See Figure 13.

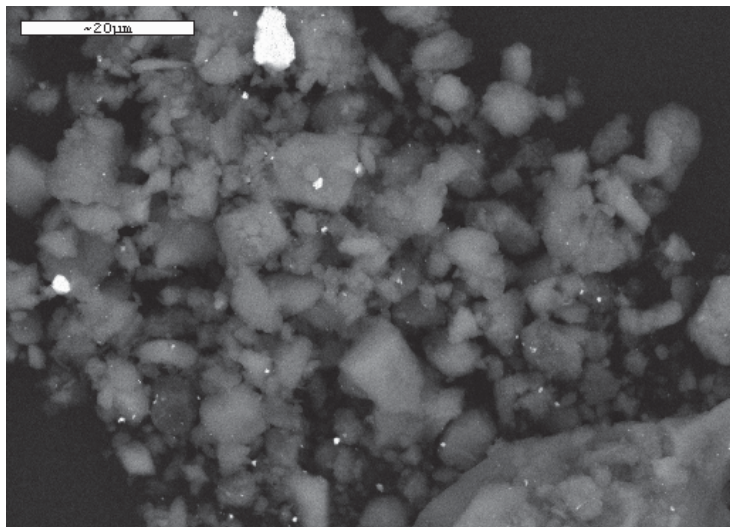


Figure 65 Sample used for the identification of Depleted Uranium in Kosovo soil. Observed in Back scattered Electron Image BEI mode. Identification directly in SEM. (Lind, 2006).

For the present work, the thin-section sample was characterized with EVO 50 Environmental Scanning Electron Microscope manufactured by Zeiss at the Imaging Centre at NMBU, this procedure was done by Simone Cagno, Ole Christian Lind and myself. Various image and mapping modes were used for the characterization, including back-scattered electron image BEI, secondary electron image mode SEI mode and sum spectra collected over time.

3.4.3 Micro X-ray Diffraction (μ -XRD) and Micro X-ray Fluorescence Spectroscopy (μ -XRF)

Micro X-ray diffraction (μ -XRD) is a synchrotron based x-ray microscopy technique that is used to characterize solid surfaces. By using monochromatic x-ray micro beams, μ -XRD can provide information on crystallographic structures in a micro scale. This technique is very useful to identify heterogeneous distributions in samples.

Micro X-ray Fluorescence Spectroscopy (μ - XRF) is also a synchrotron based x-ray microscopy technique that, similar to regular XRF, provides information about elemental composition but in a micro scale(Lind, 2006).

Experimental work was performed in the sample using $\text{I}\mu\text{S}$ - Ag^{HB} microfocus source and PILATUS 200K area detector. The analyzed stop size on the sample was of approximately 100 μm using 22.16 keV primary energy and 50 kV operating voltage. The operating current was set to 880 μA and each measurement had approximately 300 s of exposure time. This analysis was performed by Frederik Vanmeert and Stijn Legrand, from the Antwerp X-ray Analysis, Electrochemistry and Speciation Laboratory at University of Antwerp.

3.4.4 Laser Ablation Inductively Coupled Plasma Mass Spectrometry (LA ICP-MS)

In order to analyze samples on a regular ICP-MS, sample preparation is required to take the material to a solution, while the LA-ICP-MS can be used in the field and requires minimal sample preparation. Another difference between these two analytical method is that regular ICP-MS works on a “macro” scale since it uses a bulk sample and with LA-ICPMS, the area that is studied is in the “micro” level since the laser ablates rectangles of, for example, 0.1 microns of depth with length of 500 micro meters and width of 50 micro meters (Fallon, 2011).

Trace analysis was performed by means of Laser Ablation-Inductively Coupled Plasma Mass Spectrometry LA-ICPMS at the University of Antwerp, this analysis was done by Simone Cagno. It was performed directly on the thin-section with a New Wave NWR193 ArF excimer laser and a Varian 7700 quadrupole ICP-MS. The ablation of the sample was performed in He and transported to the plasma in Ar. The flow rate was set to 0.4 l/min for carrier gas and 0.7 l/min for make-up gas. The forward power was set to 1350 watt. The line scan was executed at the speed of 10 $\mu\text{m}/\text{s}$ with 3 mm length and 100 μm beam diameter. The repetition rate of scan was 20 Hz at 90% energy capacity. The depth scans were performed by repeatedly ablating a 100 μm crater at 10 Hz. The flow was maintained at approximately 8 J/cm². The laser warm up at the beginning of scan lasted till 20 s and washout begin after about 290 s lasting until 350 s.

3.5 Statistical Methods

3.5.1 Principal Component Analysis PCA

Principal Component Analysis is a multivariate statistical technique that is powerful tool when dealing with large sets of data. This method processes the data in a way that even values with different units can be compared to each other. It can be used to identify general trends and associations among the observations and the variable that would be difficult to observe in the original data set (Fallon, 2011).

The method uses the original data and transforms it into a new data set that has zero as a mean and 1 as a standard deviation, in other words it centralizes the data. After this data transformation, PCA creates new dimensions in which the variation of the data can be explained; these new dimensions are the principal components. The number of components is equal to the number of variables of the original data set and they are accounted for a proportion of the total variation of the data, these proportions do not overlap with each other. In other words, the percentage explained by PC1 does not overlap with the percentage explained by PC2 and so on.

The PCA analysis can show trends, correlations and differences but do not offer values for statistical significance of these observations. However, it can be complemented with further statistical analysis. Inferential statistics can be applied to the calculated values for PC1, PC2 and so on. As said before, the data transformations that the method does on the original data set, changes the mathematical values not the properties of this original data set.

In this work, for PCA on the complete data set, 3 variables were excluded due to missing data. Vanadium, chromium and tin were not analyzed in the Oxic Peat Moss extractions, thus 18 values are missing out of 108, which represents the 16.6% of the total observations. Same variables were excluded from the data set for Peat Moss. If those variables were to be taken in consideration, the PCA method may offer unreliable information

about the data set (Shaw, 2003). For Black Shale and Alum Shale, all variables were included on the analysis.

Concentrations below Limit of Detection LD were substitute by 0.5 times LD and were included on the data set. Values equal and below to Limit of Quantification LQ, were not included in the analysis. A logarithmic transformation, $\log(x+1)$, was applied to the concentrations of elements in the samples and Principal Component Analysis was then performed on these values.

ANOVA and paired t-test were applied on Johnson transformed values of score for PC1 of the bioavailable fraction. This was done in order to study the differences under the two different conditions studied and differences among materials. Tukey test was done for ANOVA results to further study the differences among the materials. Minitab 17 Software was used to perform all the statistical analysis.

3.5.2 Paired t-test

Paired t-test is a parametrical statistical analysis used to test the differences for two different observations done in the same subject or sample. The test assumes normality on the data sets and equal variances. Paired t-test hypothesizes that:

$$H_0: \mu_{\text{differences}} = \mu_1 - \mu_2$$

$$H_1: \mu_{\text{differences}} \neq \mu_1 - \mu_2$$

Where 1 and 2 represent condition 1 and condition 2.

This test is widely used in science, for example it is used in medical trials to test the efficiency of a treatment. The subject is tested before and after the treatment and the differences are tested for statistical significance.

For the present work, the values for PC1 were subjected to Johnson transformation in order to normalize the data. Paired t-test was applied

then for different conditions in each material and it was performed with a 95% confidence interval.

3.5.3 One-way Analysis of Variance (ANOVA)

One-way Analysis of Variance (ANOVA) is a parametric statistical analysis that can be used to test if the means of three or more samples differ from each other. The test assumes normality on the data sets and equal variances. ANOVA hypothesizes that:

$$H_0: \mu_1 = \mu_2 = \mu_3$$

$$H_1: \mu_1 \neq \mu_2 \neq \mu_3$$

Where 1,2,3 represent different samples.

The null hypothesis is that means from different samples are equal and the alternative hypothesis is that at least one of the means is different from the rest. Further analysis can be done to recognize which samples differ among each other. Tukey test is a *post hoc* of honestly significant difference, designed to test pairs of data sets for mean differences and it can be used with different confidence intervals (Muth, 2006).

In this work, Johnson transformation was applied to PC1 values to normalize the data. ANOVA was then performed along with Tukey test in order to observe which sample mean differs from the rest. Both tests were performed with a 95% confidence interval.

4. Result and Discussion

4.1 Quality Analysis: Precision and accuracy

The results for Quality Analysis for precision of the ICP-MS method are displayed in Table 4. In this table, it is possible to observe the mean concentration, standard deviation and coefficient of variation for 13 of the 18 elements studied. The values for the coefficient of variation displayed in Table 4, are in the range of 6-157%, this range suggests that these values differ greatly from one element to another, and for many elements is above the mentioned accepted value.

Table 25 Quality analysis for precision. Coefficient of Variation of the total concentration values for 13 of the studied elements for each material.

Sample	Value	V	Cr	Mn	Co	Ni	Cu	Zn
Alum Shale	Mean mg/kg	4700	156.67	476.67	35	693.33	266.67	1160
	Standard Deviation mg/kg	1928.73	92.38	317.70	17.44	360.19	161.66	771.49
	Coefficient of Variation %	41	59	67	50	52	61	67
Black Shale	Mean mg/kg	1166.67	95.33	230.00	41.67	213.33	246.67	393.33
	Standard Deviation mg/kg	115.47	9.02	69.28	30.62	30.55	387.99	90.18
	Coefficient of Variation %	10	9	30	73	14	157	23
Peat Moss	Mean mg/kg	183.33	85	756.67	18	76	47.33	107.67
	Standard Deviation mg/kg	83.27	46.52	402.16	10.58	40.45	25.72	57.49
	Coefficient of Variation %	45	55	53	59	53	54	53

Table 4. (Continued). Quality analysis for precision. Coefficient of Variation of the total concentration values for 13 of the studied elements for each material.

Sample	Value	As	Mo	Cd	Sn	Pb	U
Alum Shale	Average mg/kg	117.67	290	26.33	4.3	67.67	150
	Standard Deviation mg/kg	58.53	140.00	16.77	1.74	36.95	87.18
	Coefficient of Variation %	50	48	64	41	55	58
Black Shale	Average mg/kg	47.67	153.33	3.20	4.73	74.33	40.33
	Standard Deviation mg/kg	68.60	23.09	0.92	0.50	79.61	2.31
	Coefficient of Variation %	144	15	29	11	107	6
Peat Moss	Average mg/kg	8.23	4.5	0.63	1.8	21	7.13
	Standard Deviation mg/kg	3.14	1.93	0.28	0.53	9.17	3.58
	Coefficient of Variation %	38	43	44	29	44	50

The results of the accuracy test are displayed in Table 5. The expected values for the reference materials, the measure values, and the % error calculated for each measurement are shown. Reference Material NCS DC 73324 presented errors for 4 of the 13 elements analyzed, ranging from 3 to 51 %. From the elements with error, only copper were measured with fair accuracy, <10% of error, while vanadium, arsenic and chromium had poor accuracy. Reference Material NCS DC 73325 presented errors for 9 of the 13 elements analyzed, ranging from 4 to 68%. From the elements with error, manganese and arsenic were measured with fair accuracy, while the rest of these elements had poor accuracy.

Elements that present poor precision, see Table 4, and poor accuracy, see Table 5, may have been subjected to random errors, this is the case for chromium with 59% for coefficient of variation and 51% and 42% for accuracy with respect to RM NCS DC 73324 and RM NCS 73325 respectively. Poor precision in general may be due to random errors.

Random errors may be due unpredictable variations in the analysis, for example heterogeneous distribution in the material itself or in the sample preparation, e.g. large particles in the bulk sample, while poor accuracy may be due to systematic errors. This type of error may suggest miscalibration of the instrument, contamination of the samples, equipment or reagents. The later may be the case of vanadium, which shows coefficient of variation of 10% but its values for both Reference Materials are outside the certified range.

A possible explanation of why many of the elements measured in the Reference Materials are outside of its certified range is the use a mixture of HNO₃+HF, as the digestion solution. It has been observed that the combined use of these acids may give elevated values, for some element seven exceeding the upper range of certified values (Kassaye, 2012), (Güven, 2011).

Table 26 Quality analysis for accuracy. Observed and Expected values for elements in Reference Materials. The Eoor is calculated as the difference between the observed value and the expected value divided by the expected value.

Elements		V	Cr	Mn	Co	Ni	Cu	Zn
Reference Material		mg/kg	mg/kg	mg/kg	mg/kg	mg/kg	mg/kg	mg/kg
NCS DC 73324	Observed	110	39	1400	6.0	52	420	94
	Expected Range	130 ± 7	75 ± 6	1450 ± 82	7,6 ± 1,1	53 ± 4	390 ± 14	96 ± 6
	Error	10 %	51 %	0 %	0 %	0 %	3 %	0 %
NCS DC 73325	Observed	290	250	2100	120	360	130	190
	Expected Range	245 ± 21	410 ± 23	1780 ± 113	97 ± 6	276 ± 15	97 ± 6	142 ± 11
	Error	9 %	42 %	10%	16 %	23 %	26 %	24 %

Table 5 (Continued) Quality analysis for accuracy. Observed and Expected values for elements in Reference Materials. The Error is calculated as the difference between the observed value and the expected value divided by the expected value.

Elements		As	Mo	Cd	Sn	Pb	U
Reference Material		mg/kg	mg/kg	mg/kg	mg/kg	mg/kg	mg/kg
NCS DC 73324	Observed	200	19	0.0061	66	320	6.4
	Expected Range	220 ± 14	18 ± 2	0,13 ± 0,03	72 ± 7	314 ± 13	6,7 ± 0,7
	Error	14 %	0 %	0 %	0 %	0 %	0 %
NCS DC 73325	Observed	6.4	3.7	0.086	4.2	15	2.6
	Expected Range	4,8 ± 1,3	2,9 ± 0,3	0,08 ± 0,02	3,6 ± 0,7	14 ± 3	2,2 ± 0,4
	Error	4 %	68 %	0 %	0 %	0 %	0 %

The LD and LQ calculated for the elemental concentration of the studied materials are displayed in Table 6. Values below the LQ were not included in the any analysis of the materials.

Table 27 Quality analysis. Limit of Detection and Limit of Quantification for the ICP-MS analysis of the elemental concentration for total concentration analysis.

Element	V	Cr	Mn	Co	Ni	Cu	Zn
	mg/kg	mg/kg	mg/kg	mg/kg	mg/kg	mg/kg	mg/kg
Limit of detection, LD	0.015	0.096	0.068	0.0026	0.029	0.027	0.23
Limit of quantification, LQ	0.051	0.32	0.23	0.0088	0.098	0.090	0.77

Table 6 (Continued) Quality analysis. Limit of Detection and Limit of Quantification for the ICP-MS analysis of the elemental concentration for total concentration analysis.

Element	As	Mo	Cd	Sn	Pb	U
	mg/kg	mg/kg	mg/kg	mg/kg	mg/kg	mg/kg
Limit of detection, LD	0.23	0.0090	0.0061	0.12	0.0092	0.0037
Limit of quantification, LQ	0.76	0.030	0.020	0.39	0.031	0.012

4.2 Sample selection

4.2.1 X-Ray Fluorescence

X-ray fluorescence on hand-held mode was used on the black and alum shale cores to identify the one with the highest content of uranium. According to the data, BH-6 Prøve 2 for Alum Shale contained a mean concentration value ranging from 0.008 to 0.11 %, while the BH-5 Prøve 1 for black shale presented a mean value in the range of 0.004 to 0.005 %, these samples contained the highest concentrations of uranium and were selected as the samples for Experiments one and two. In Figure 14, a box plot for XRF data of U is displayed.

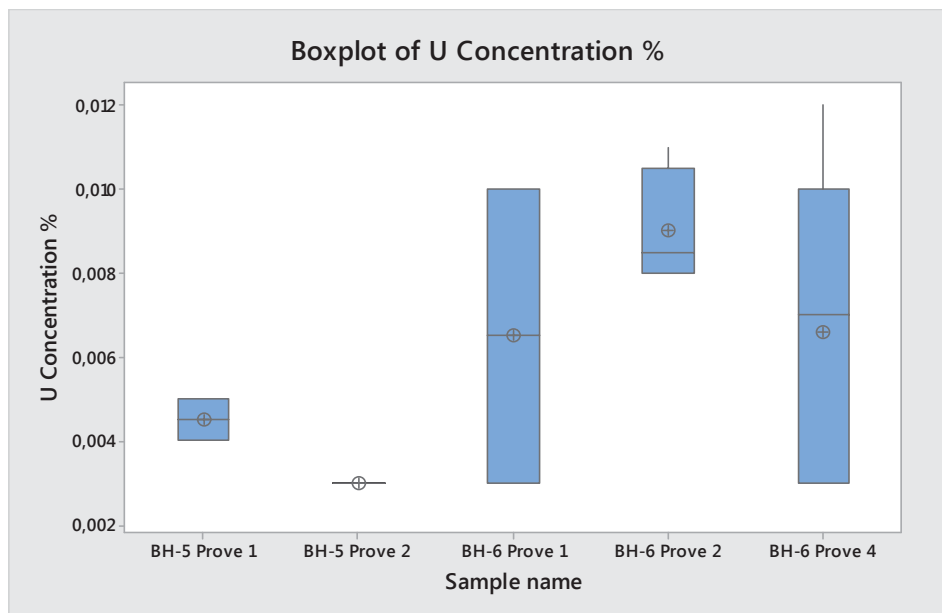


Figure 66 Sample selection. Boxplot based on XRF data for uranium, the analyzed samples are BH-5 Prove 1, BH-5 Prove 2 for black shales and BH-6 Prove 1, BH-6 Prove 2 and BH-6 Prove 4 for alum shale. The boxplot shows mean, median, Q1, interquartile range, Q3 and whiskers for each sample.

Values for redox potential for the studied materials and the dates in which they were obtained are listed in Table 7. For Alum Shale and Black Shale, the anoxic redox potentials were measured under the same conditions the first step of the anoxic extractions was performed. Approximately 2 g of Alum Shale and Black Shale were added 20 mL of MiliQ water bubbled with N₂ for five minutes. The samples were shaken and left inside the nitrogen tent for an hour; then Eh values were measured in the mixture while the samples were still inside the tent.

Table 28 Sample selection. Redox potential values for each material studied, oxic and anoxic conditions.

Material	Condition	Redox Potential mV	Date
Alum Shale	Oxic	118	29.04.2014
	Anoxic	110	29.04.2014
Black Shale	Oxic	65	29.04.2014
	Anoxic	31	29.04.2014
Peat Moss	Oxic	-3	15.10.2013
	Anoxic	-115	17.02.2014

It Table 7, it is possible to see that the redox potential for Alum and Black shale are similar under both conditions, this may suggest that the anaerobic conditions were not achieved completely, since positive values of redox potential are not typical for anoxic conditions. Possible explanations for it is 1) that the during the sample preparation process, the sample was in contact with oxygen and water or 2) iron reducing bacteria is not present in Alum and Black Shale as it is in the Peat Moss.

On the other hand, values of redox potential for Peat Moss are more different than for the other materials, this suggests that anaerobic conditions were achieved. The negative value for oxic conditions is not a concern since the first step of the extraction procedure involve MiliQ water and agitation, thus it is possible that the redox potential increased during this step.

4.3 Sample Characterization

Sample characterization general parameters for the studied materials are listed in Table 8.

Table 29. Sample characterization. Values for pH, moisture content, organic matter and total organic carbon for the studied materials are presented.

Material	pH	Eh at site	Moisture Content %	Organic Matter OM%	Total Organic Carbon TOC%
Alum Shale	7.9	-	-	-	-
Black Shale	8.3	-	-	-	-
Peat Moss	8.1	-103 mV	16	2.1	1.2

4.3.1 Total Concentration Analysis

The results for total concentrations were obtained by Ultraclave Digestion and ICP-MS analysis. Table 9, summarizes these results for the three materials analyzed.

Table 30 Total Concentration analysis for each element in mg/kg for Alum Shale, Black Shale and Peat Moss. Error is calculated as 2 times the standard deviation value for the samples and Average corresponds to the average value of three parallels.

Sample	Value	V	Cr	Mn	Co	Ni	Cu	Zn
		mg/kg	mg/kg	mg/kg	mg/kg	mg/kg	mg/kg	mg/kg
Alum Shale	Average	4700	156.67	476.6	35	693.3	266.6	1160
	Error	1928	92	317	17	360	161	771
Black Shale	Average	1166.6	95.3	230	41.6	213.3	246.6	393.3
	Error	115	9	69	30	30	387	90
Peat Moss	Average	183.3	85	756.6	18	76	47.3	107.6
	Error	83	46	402	10	40	25	57

Table 9 (Continued) Total Concentration analysis for each element in mg/kg for Alum Shale, Black Shale and Peat Moss. Error is calculated as 2 times the standard deviation value for the samples and Average corresponds to the average value of three parallels

Sample	Value	As	Mo	Cd	Sn	Pb	U
		mg/kg	mg/kg	mg/kg	mg/kg	mg/kg	mg/kg
Alum Shale	Average	117.6	290	26.3	4.3	67.6	150
	Error	58	140	16	1	36	87
Black Shale	Average	47.6	153.3	3.2	4.7	74.3	40.3
	Error	68	23	0.92	0.50	79	2.3
Peat Moss	Average	8.23	4.5	0.63	1.8	21	7.13
	Error	3.1	1.9	0.28	0.53	9.1	3.5

The value of 150 mg/kg observed for U in Alum Shale is exceeding the highest reported value for Alum Shale in the Oslo Rift (129 mg/kg.). For Black Shale, the value of 40.33 mg/kg is also higher than the reported average value of 29 mg/kg for Oslo Rift (Håvard, 2009). The value for Peat Moss of 7.13 mg/kg is comparable to those values found in contaminated soils in Eastern Germany by Schöner et. al (2009). Other elements which values are higher than the average value reported for this region are vanadium, chromium and nickel (Tourtelot, 1979).

In general, the errors (calculated as two times the standard deviation) for most of the elements are high. Alum Shale presents large errors all the elements except Sn with 1%, Black Shale has relatively lower values in comparison to those for Alum Shale. However, Peat Moss presents large errors for Major and Minor Elements (main components on the sample according to their abundance) while for Trace Elements, relatively low. This may be due to the large deviation of measured values from certified ranges for the Reference Materials presented in the Quality Analysis section. Other possible cause of these large errors in the results is that HF digestion is more effective to specific elements, like Mo and Sn, while HNO₃ is a better choice for elements like Mn, Fe and U.

4.3.2 X-Ray Diffraction

Mineral composition identified in Alum Shale, Black Shale and Peat Moss is summarized in Table 10. Diffractograms for these materials can be found in Appendix A.

Table 31 X-ray diffraction results. Minerals identified by the XRD in the studied materials. Sulfides less than 1-2% of the total may not be detected.

Material	Identified Minerals
Alum Shale	Quartz Muscovite 2M1 Alunite Titanomagnetite Andradite, titanium, aluminian
Black Shale	Quartz, syn Muscovite 3-T Dolomite ferroan Zircon, metamict Chlorite-serpentine Clinochlore Chamosite
Peat Moss	Quartz Albite, disordered Calcite, magnesian Chlorite-serpentine Clinochlore-1Mbllb ferroan Chamosite Clinochlore

The abundance of clay minerals in the Peat Moss sample may be related to the depth from which it was extracted. This sample was extracted from 9.2 to 10 m of depth, below the organic-rich layers of the bog and approximately 1 m above the bedrock.

4.4 Experiment one: Sequential Extractions

The terms “Major Elements”, “Minor Elements” and “Trace Elements” for this section follow the same criteria as in the Total Concentration Analysis. They refer to the abundance of these elements in the samples.

4.4.1 Alum Shale samples

Results of the sequential extraction process for Alum Shale are presented in Figure 15. The highest concentrations for Fe, S and Al are in Step 6 of the extraction, while for Ca and Mn are in Step 4, followed by Step 3, similar observations were done by Fjermstad (2013); this is consistent with literature for sequential extraction, which indicated that NH₄Ac pH 5 (Step 3) and NH₂OH·HCl pH 2 (Step 4) target carbonates and manganese oxides respectively.

It is also possible to observe that the percentages of extraction under oxic and anoxic conditions are similar for all the Major Elements.

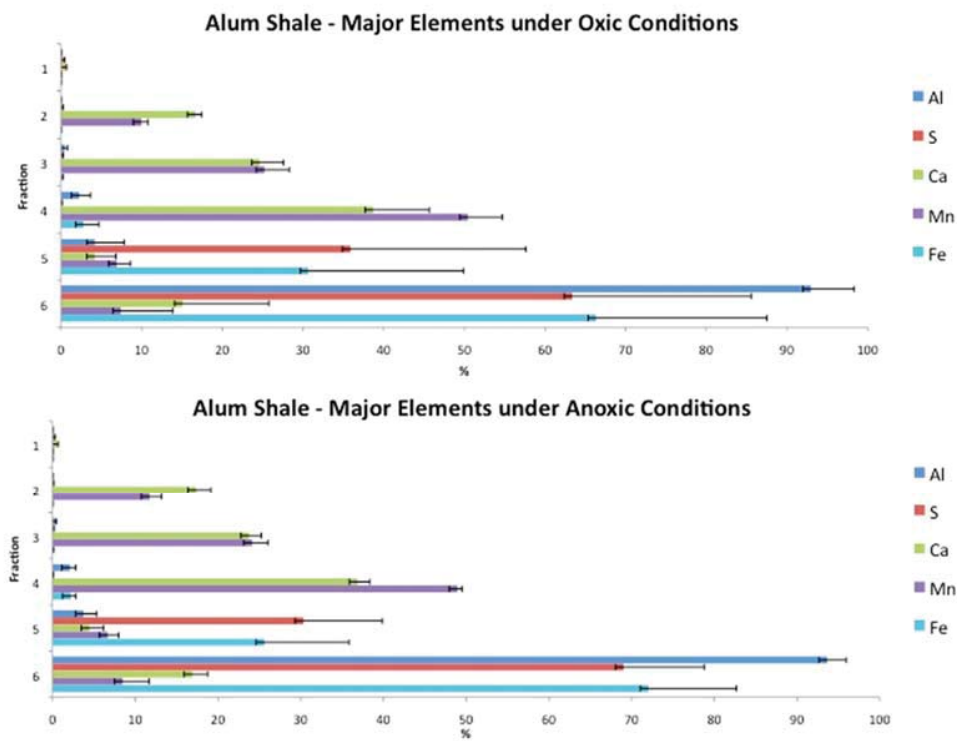


Figure 67 Sequential Extraction. Percentages of extraction for Major Elements in Alum Shale samples. Oxic and Anoxic conditions. Error bars calculated as 2 times the standard deviation of the three parallels.

In Figure 16, the percentages of extraction for Minor Elements in Alum Shale is displayed. There are similarities in the distribution of extraction for oxic and anoxic conditions.

Vanadium presents small percentages of extraction (less than 10%) in the first 5 steps. In general, all the Minor Elements had the largest extraction percentage with 7M HNO₃ (Step 6). However, nickel presents a visible percentage of extraction from Step 2.

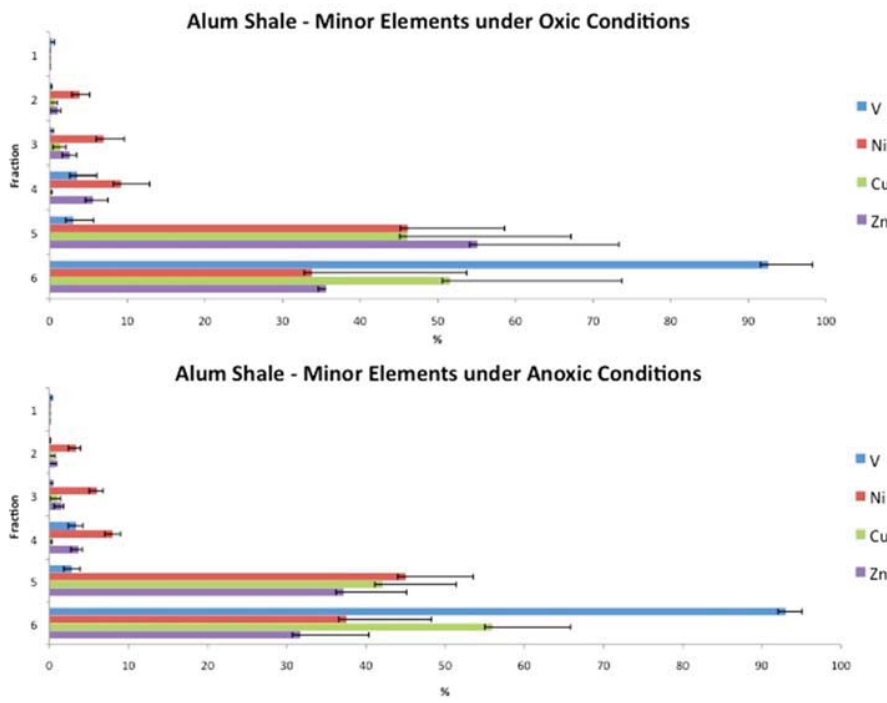


Figure 68 Sequential Extraction. Percentages of extraction for Minor Elements in Alum Shale samples. Oxic and Anoxic conditions. Error bars calculated as 2 times the standard deviation of the three parallels.

Percentages of extraction for Trace Elements can be observed in Figure 17. The most mobile element from these elements is molybdenum, which is present from the first step with MiliQ water with an extraction percentage of over 10%, (for oxic and anoxic conditions) this observation suggests that Mo may be present in the sample as free ions or associated with organic soluble matter (Tessier, 1979) (Filgueiras, 2002).

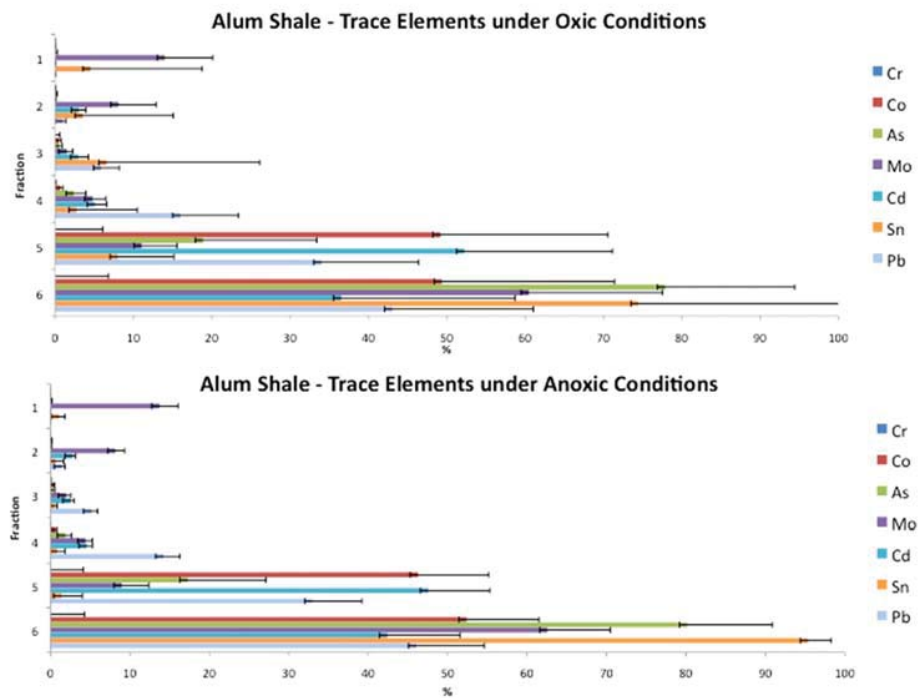


Figure 69 Sequential Extraction. Percentages of extraction for Trace Elements in Alum Shale samples. Oxic and Anoxic conditions. Error bars calculated as 2 times the standard deviation of the three parallels.

In Figure 18, the percentages of extraction for uranium and thorium are displayed. The largest percentages of both elements are in Step 6. These percentages are especially large for Th with over 90% under both conditions.

Uranium has visible percentages of extraction from Step 2 with NH₄Ac pH 7. However, the variation (two times the standard deviation) of U values are larger for extractions under oxic conditions than the ones for anoxic conditions.

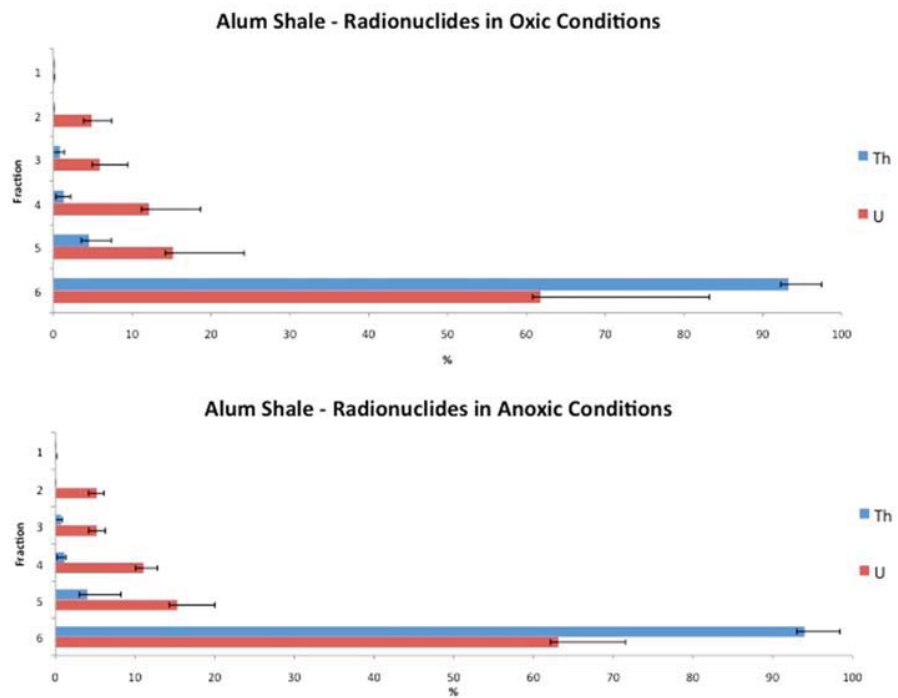


Figure 70 Sequential Extraction. Percentages of extraction for Radionuclides in Alum Shale samples. Oxic and Anoxic conditions. Error bars calculated as 2 times the standard deviation of the three parallels.

4.4.2 Black Shale samples

Figure 19, shows the distributions for Major Elements for Black Shale under both conditions. As it was observed for Alum Shale, iron, aluminum and sulfur are more abundant in the sixth step of the extraction.

By comparing Figure 15 and Figure 19, it is possible to observe that Major Elements follow similar distributions under both oxic and anoxic conditions for these two materials.

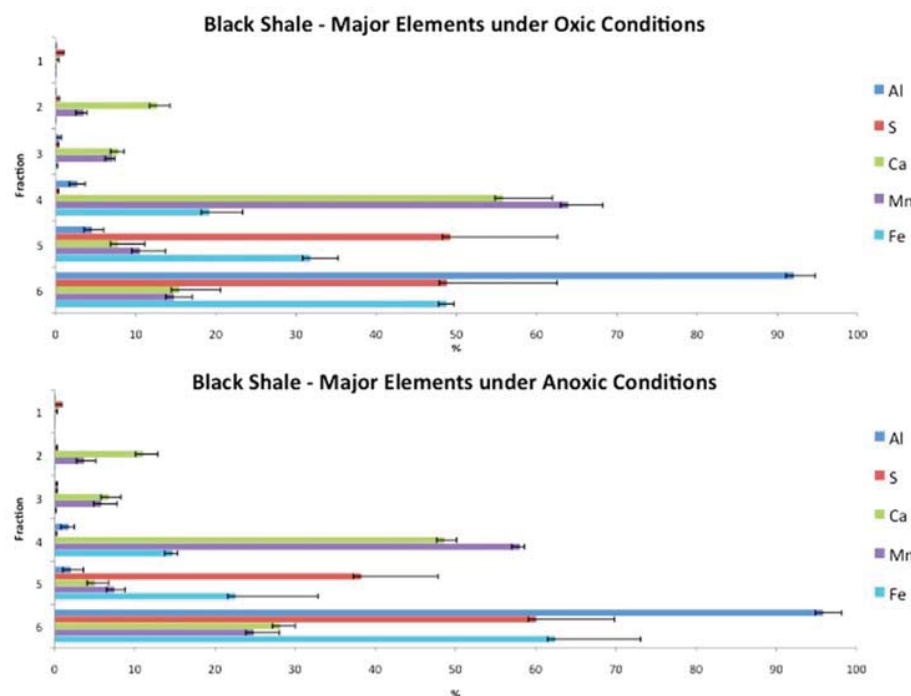


Figure 71 Sequential Extraction. Percentages of extraction for Major Elements in Black Shale samples. Oxic and Anoxic conditions. Error bars calculated as 2 times the standard deviation of the three parallels.

Percentages of extraction for Minor Elements are displayed in Figure 20. From these elements, Nickel seem to be the most relevant when it comes to the bioavailable fraction, since it is extracted from Step 2 with NH₄Ac pH 7.

It is also possible to observe that vanadium seem to be more resilient under anaerobic conditions than under aerobic ones. This observation is also true for copper that shows the largest extraction in Step 5 with H₂O₂ + NH₄Ac pH 2 under anoxic conditions.

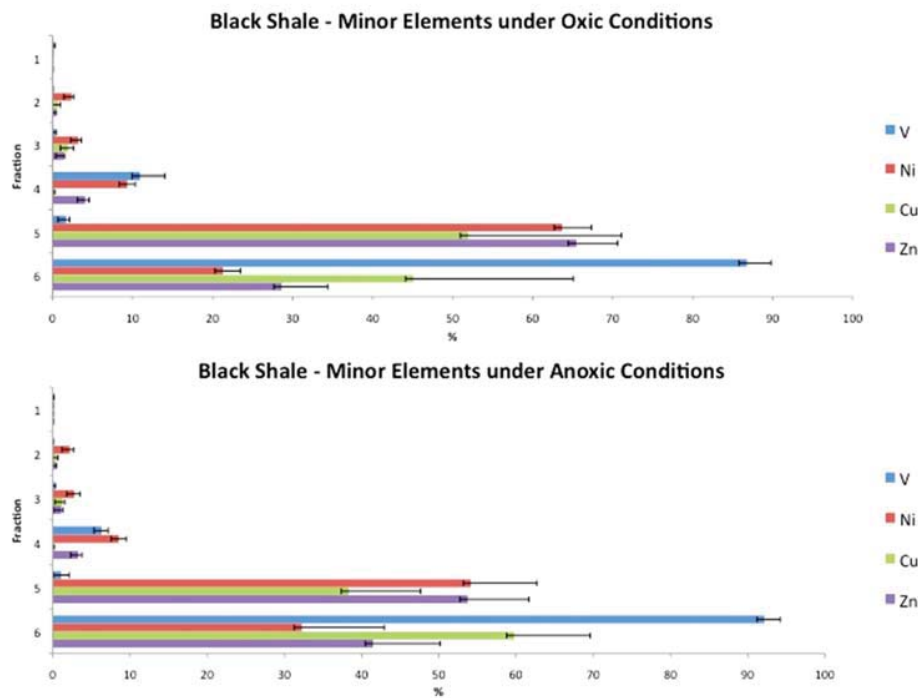


Figure 72 Sequential Extraction. Percentages of extraction for Minor Elements in Black Shale samples. Oxic and Anoxic conditions. Error bars calculated as 2 times the standard deviation of the three parallels.

For Trace Elements, Figure 21 illustrates its extraction distribution. The distribution of Tin under oxic conditions is the most notorious difference between the distributions for the two conditions.

Over 20% of the total concentration of Sn was extracted on the first step of the process under oxic conditions while less than 5% was extracted under anoxic conditions. However, the error bar for oxic Sn is larger than the one for anoxic Sn, this observation suggest the presence of an indeterminate error during the process. Literature on the mobility of Trace Elements, resemble the distribution under anoxic conditions rather than the oxic one (Kassaye, 2012).

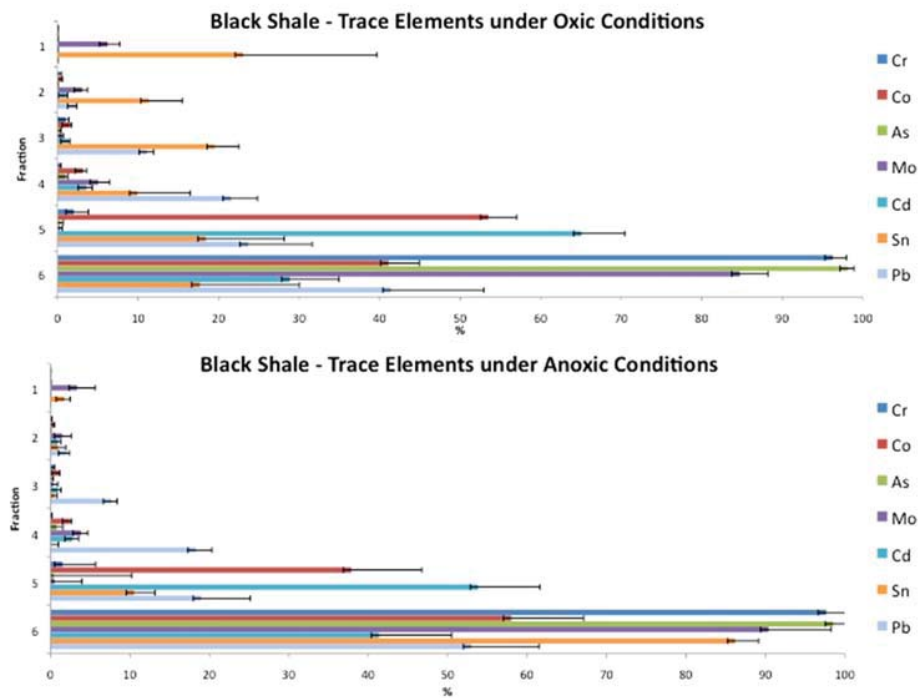


Figure 73 Sequential Extraction. Percentages of extraction for Trace Elements in Black Shale samples. Oxic and Anoxic conditions. Error bars calculated as 2 times the standard deviation of the three parallels.

Regarding radionuclides, Figure 22 shows that the distribution of these elements is similar to the one observed for Alum Shale: the largest extraction percentages are in the acid step. Thorium appears to be more resilient to mobilization than uranium; these observations are consistent with literature (Mrdakovic, 2010). One of the main differences between these distributions is that under oxic conditions approximately 20% of U was extracted compared to 12% under anoxic conditions. This observation suggests that U may be present in more stable forms under anoxic conditions.

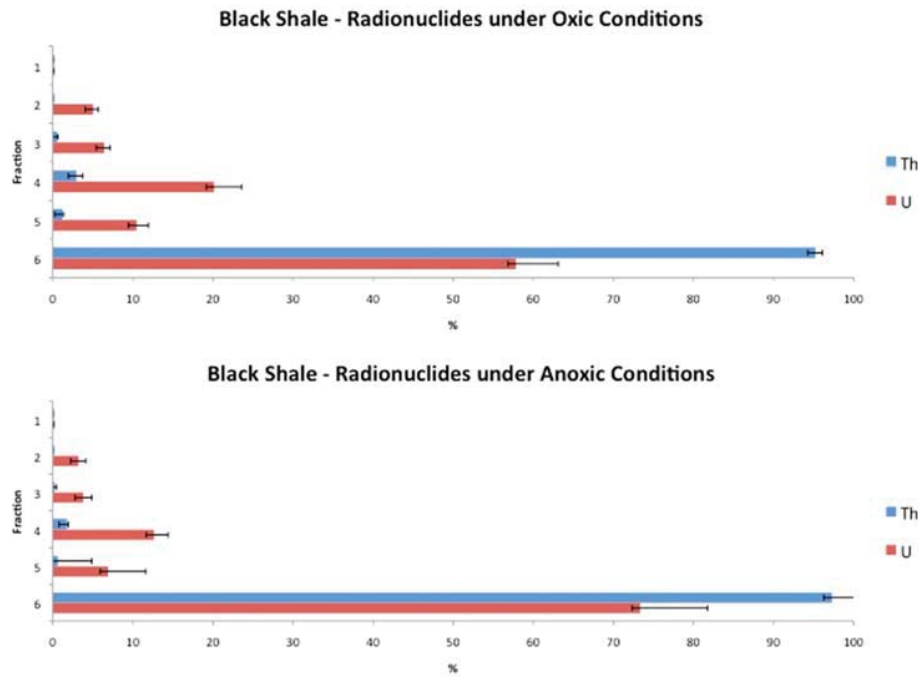


Figure 74 Sequential Extraction. Percentages of extraction for Radionuclides in Black Shale samples. Oxic and Anoxic conditions. Error bars calculated as 2 times the standard deviation of the three parallels.

4.4.3 Peat Moss samples

The distributions for Alum Shale and Black Shale presented many similarities; for Peat Moss, clear differences can be observed between the conditions, see Figure 23.

Iron, sulfur and aluminum have larger percentages of extraction in Step 6. Calcium presented a larger extraction percentage in Step 3 under anoxic conditions, 57% while it showed 36% under oxic conditions. However in Step 2, the pattern was reversed. Manganese and calcium seem to have similar behaviors.

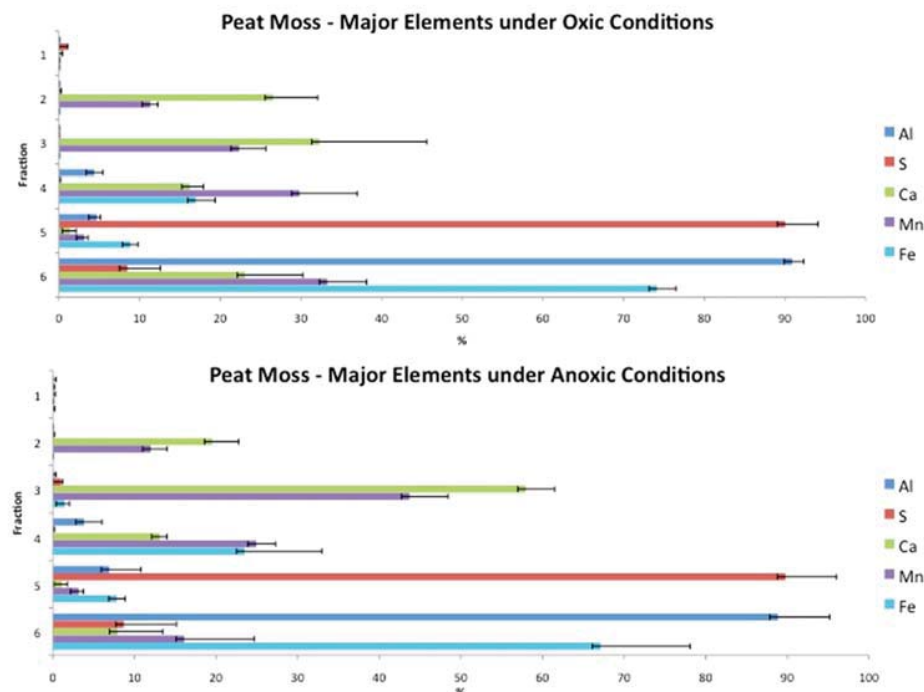


Figure 75 Sequential Extraction. Percentages of extraction for Major Elements in Peat Moss samples. Oxic and Anoxic conditions. Error bars calculated as 2 times the standard deviation of the three parallels.

For Trace Elements, Zn and Cu have different distributions under oxic and anoxic conditions see Figure 24. Zinc had an extraction percentage of 49% under oxic conditions in Step 6, while it had a 32% under anoxic. Over 85% of the total Cu was extracted in Step 6 under anoxic conditions while approximately 20% was extracted under oxic conditions, suggesting that Cu is less resilient under oxic conditions than under anoxic ones.

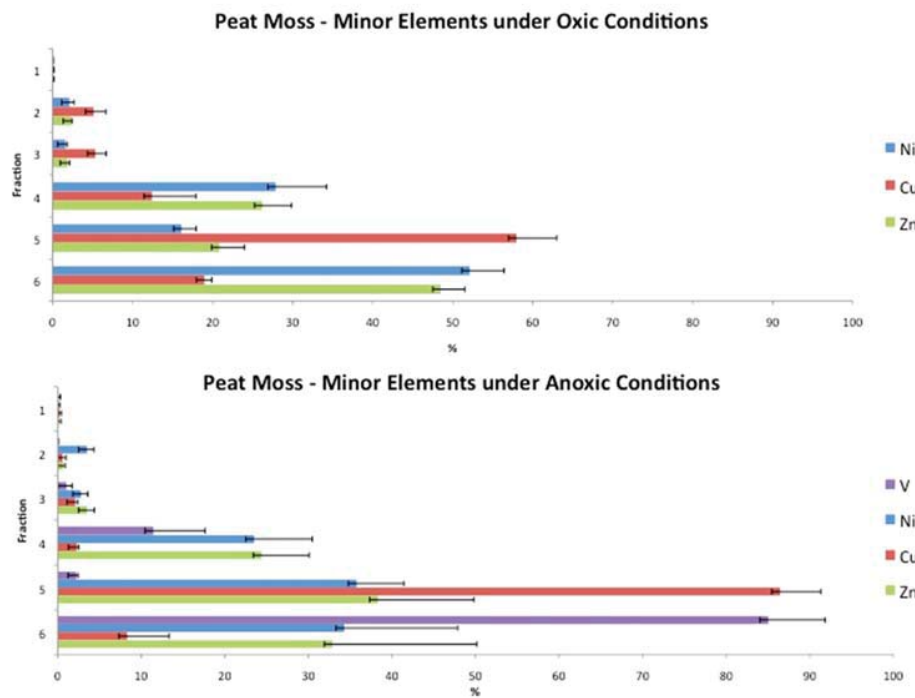


Figure 76 Sequential Extraction. Percentages of extraction for Minor Elements in Peat Moss samples. Oxic and Anoxic conditions. Error bars calculated as 2 times the standard deviation of the three parallels. Vanadium was not analyzed under oxic conditions for Peat Moss.

In Figure 25, chromium and tin had the highest percentages of extractions for the anoxic set with over 90%, followed by As and Mo.

Arsenic had a relatively high extraction percentage (70%) under oxic conditions in the acid step followed by Mo and Co.

For both conditions, molybdenum has a visible extraction percentage in the first step. This percentage is higher for the anoxic set, suggesting that the mobility is higher for element under anaerobic conditions.

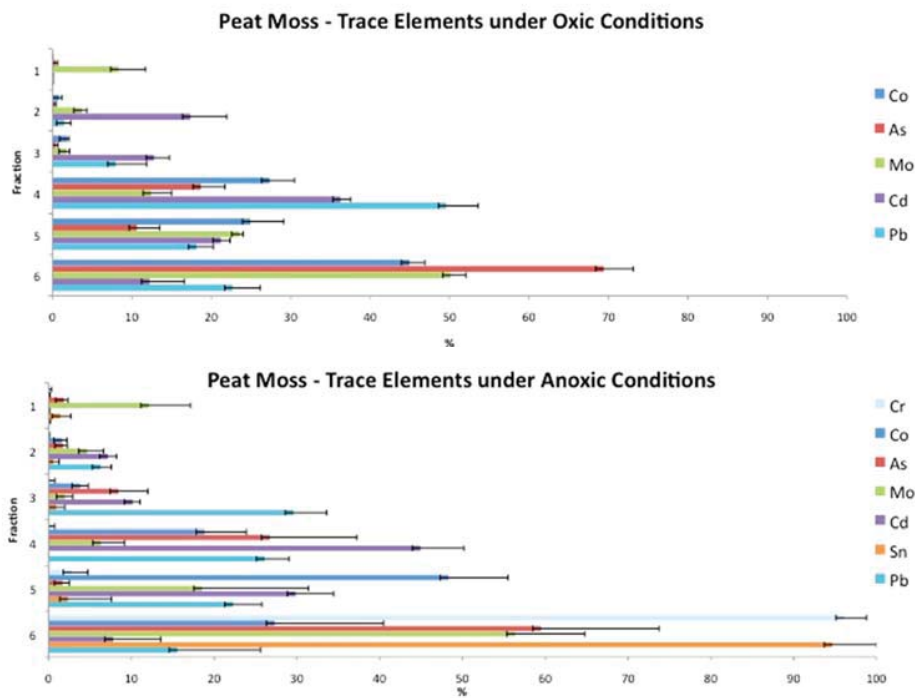


Figure 77 Sequential Extraction. Percentages of extraction for Trace Elements in Peat Moss samples. Oxic and Anoxic conditions. Error bars calculated as 2 times the standard deviation of the three parallels. Chromium and tin were not analyzed under oxic conditions.

Figure 26, illustrates that the extraction distributions for radionuclides present visible differences. Thorium, which showed a low mobility for the first 5 steps in Alum Shale and Black Shale, is present in Step 3 for the anoxic set, becoming a part of the bioavailable fraction for this data set.

Uranium also shows an evident difference in concentration for Step 1. The percentage of extraction is visibly higher under anoxic conditions than for oxic ones. In general, the bioavailable fraction under anaerobic conditions seems to have higher percentages of extraction than the ones for the oxic set. However, the error bars for this distribution are larger than the ones for the aerobic distribution.

The differences between oxic and anoxic conditions for Peat Moss seem to have more differences than the ones for the other two materials. By looking at the Eh values presented in Table 4, it is evident that the redox

potentials differ more for this material as well; this fact may be an important factor for these results.

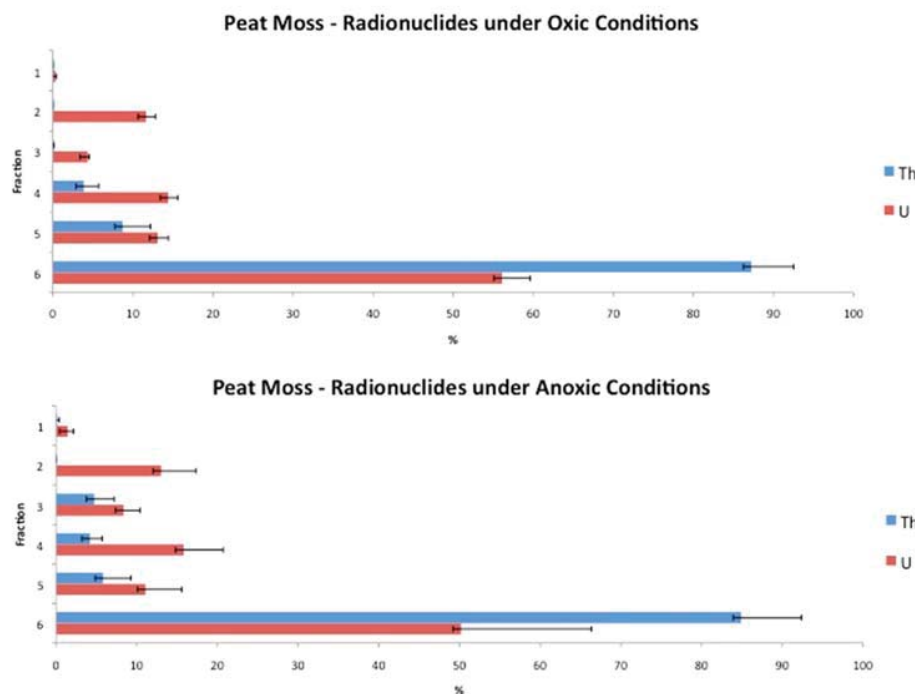


Figure 78 Sequential Extraction. Percentages of extraction for Radionuclides in Peat Moss samples. Oxic and Anoxic conditions. Error bars calculated as 2 times the standard deviation of the three parallels.

In Table 11, extraction percentages under aerobic and anaerobic conditions are presented. These values are based on the total concentration analysis performed on the samples. For Peat Moss, values for vanadium, chromium and tin are missing for the oxic set (marked in yellow).

In Table 11, the extraction percentages for Alum Shale are very similar under the two conditions. For Black Shale, higher concentrations were achieved under anoxic conditions. However, the largest concentrations were observed for Step 6. This observation suggests that though, elements may be more mobile under anoxic condition, strong oxidizing agents are needed for mobilizing the majority of the metals.

On the other hand, for Peat Moss it is possible to observe that higher extraction percentages were achieved under aerobic conditions for uranium. This observation suggests that even though uranium proved to be more mobile under anoxic conditions, the concentration of the mobilized fraction is still less for anoxic conditions than for oxic ones.

Table 32. Extraction percentages of elements under oxic and anoxic conditions compared to total concentration of extraction. Missing values are shown in yellow for V, Cr and Sn for the oxic date set in Peat Moss.

Material	V		Cr		Mn		Co		Ni	
	Oxic %	Anoxic %	Oxic %	Anoxic %	Oxic %	Anoxic %	Oxic %	Anoxic %	Oxic %	Anoxic %
Alum Shale	6	6	6	5	53	51	47	46	44	44
Black Shale	1	3	3	7	55	68	38	56	50	60
Peat Moss		8		14	54	51	63	54	63	51

Table 11. (Continued) Extraction percentages of elements under oxic and anoxic conditions compared to total concentration of extraction. Missing values are shown in yellow for V, Cr and Sn for the oxic date set in Peat Moss.

Material	Cu		Zn		As		Mo		Cd	
	Oxic %	Anoxic %								
Alum Shale	43	43	46	49	48	57	31	30	48	52
Black Shale	34	47	43	54	28	50	24	48	44	58
Peat Moss	63	61	64	47	65	51	50	33	73	68

Table 11. (Continued) Extraction percentages of elements under oxic and anoxic conditions compared to total concentration of extraction. Missing values are shown in yellow for V, Cr and Sn for the oxic date set in Peat Moss.

Material	Sn		Pb		U	
	Oxic %	Anoxic %	Oxic %	Anoxic %	Oxic %	Anoxic %
Alum Shale	3	3	45	46	43	42
Black Shale	2	2	41	55	30	52
Peat Moss		4	56	46	46	29

4.4.4 Statistical Analysis: Principal Component Analysis, Paired t-test and ANOVA

Principal Component Analysis was conducted on the sequential extraction results in order to identify general trends on the data and possible correlation of elements in the different materials and conditions.

Results obtained for principal component values are summarized in Table 12 and 13. In Table 12, shows that PC1 explains the 63.6% of the variation of the data set and PC2, 15.1%, together these components are accounted for the 78.7% of the total variation of the complete data set.

Table 33 Principal components with the variation proportion and the cumulative values of the variation they explain of the complete data set.

Principal Component	Proportion %	Cumulative %
PC1	63.6	63.6
PC2	15.1	78.7
PC3	8.5	87.2

Principal component values are listed in Table 13, it illustrates a positive correlation between all variables and PC1. Manganese and calcium have the strongest negative correlation to PC2, while for the rest of the variables PC2 show a near to neutral value except for Mo and S, which present relatively high positive correlation to this component.

Table 34 Principal components 1 and 2 values for the variables for the complete data set.

Variable	PC1	PC2
Al	0.27	-0.07
S	0.26	0.31
Ca	0.09	-0.58
Mn	0.12	-0.60
Fe	0.27	-0.13
Co	0.28	0.08
Ni	0.29	-0.11
Cu	0.28	0.15
Zn	0.30	-0.06
As	0.29	0.10
Mo	0.2	0.25
Cd	0.25	0.13
Pb	0.29	-0.13
Th	0.25	0.06
U	0.27	-0.01

In Figure 27, Score Plots and Loading Plots for the sample are presented. The largest variation for all samples can be explained by PC1. Black Shale and Alum Shale samples reach higher values for this component than the Peat Moss samples.

The Score Plot by material shows that there are samples from the 3 materials sharing properties. The first PC may refer to the concentration of elements in the sample, since Alum Shale and Black Shale are expected to contain a higher amount of metals than the Peat Moss samples. The Score Plot by condition shows that samples under different conditions share properties as well, suggesting that the condition is not the dominant factor for the distribution of the samples along the score plot. On the other hand, in the score plot by step of the sequential extraction process, a more evident pattern can be observed.

Samples from Step 1, both conditions, share properties. This pattern can be observed for all steps, although the rest of the steps seem to be also associated with each other. Step 5 and 6 show the highest score values of all samples. However a greater distance can be observed among these samples, this suggests that other factors, such as material and condition, cannot be ignored when analyzing these patterns.

Score Plots offer information about the samples on a data set and Loading Plots give information about the possible correlation of the variables (Shaw, 2003). The Loading Plot for the complete data set is presented in Figure 27 as well. The majority of the elements have the largest variation on PC1. The Major Elements Ca and Mn, have the largest variation on PC2, from these observations it can be infer that the PC2 may explain the leachability pattern of specific elements in the sample. In this case, for manganese and calcium, these elements appear to be closely correlated.

Uranium, aluminum, zinc, lead, nickel and iron are also closely correlated to each other. Thorium, cadmium, cooper, arsenic and cobalt seem to form another cluster in the graph and thus, are closely correlated. Molybdenum and sulfur are closely correlated to each other, while they show a weak positive correlation with Mn and Ca.

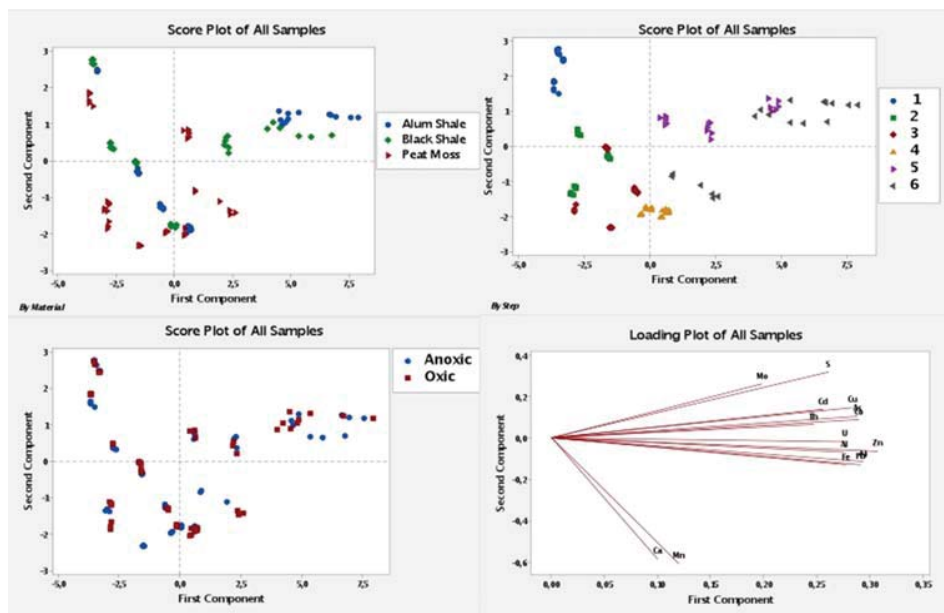


Figure 79 PCA analysis for the complete data set. Score Plots by material, by condition and by step of the sequential extraction process and its correspondent Loading Plot are shown.

By comparing the loading plot to the score plot by step, it is possible to observe the majority of the elements have high concentrations in Step 5 and 6. For Ca and Mn, however, the highest concentrations are in Step 3 and 4, which is consistent with the sequential extraction protocol (Skipperud, 2013), (Salbu, 2000), (Tessier, 1979). Fraction 3 and 4 are related to carbonates and pH sensitive amorphous Fe and Mn oxides and hydroxides, from which the Mn are more likely to be leached out in these steps.

Step 1,2 and 3 seem to contain low for the majority of the elements. However these fractions constitute the bioavailable fraction and will be subjected to independent analysis.

For the analysis in Alum Shale, all the variables were taken in consideration, since there are no missing values in this data set. Table 14, displays proportion values for PC1 and 2, where PC1 explains 72.4% of the total variation of the data set and PC2, 16.8%. Together they are accounted for 89.2% of the total variation of the data set. Table 15, displays the values

for PC1 and PC2 for the variables and it is possible to observe a positive correlation between all the variables and PC1. On the other hand, the majority of the variables have negative correlation to PC2. Calcium and manganese have a strong positive correlation to PC2 and Mo, a relatively strong negative one. This may suggest that PC2 is related to the leachability of these specific elements.

Table 35 Principal components with the variation proportion and the cumulative values of the variation they explain for Alum Shale.

Principal Component	Proportion %	Cumulative%
PC1	72.4	72.4
PC2	16.8	89.2
PC3	7.7	96.9

Table 36. Principal components 1 and 2 values for the variables for Alum Shale.

Variable	PC1	PC2
Al	0.26	0.07
S	0.24	-0.18
Ca	0.07	0.49
V	0.25	-0.05
Cr	0.24	-0.15
Mn	0.06	0.54
Fe	0.25	0.12
Co	0.25	-0.10
Ni	0.23	0.26
Cu	0.25	-0.06
Zn	0.25	0.18
As	0.27	-0.08
Mo	0.18	-0.37
Cd	0.25	-0.01
Sn	0.22	-0.15
Pb	0.26	0.14
Th	0.23	-0.15
U	0.25	0.16

In Figure 28, the Score Plot and the Loading Plot for Alum Shale are displayed. In the Score Plot, both conditions, anoxic and oxic, are closely related to each other in every step. This suggests these samples share similar properties. However, Step 6 shows a different pattern, it shows more dispersion of the samples. By observing the distances between steps, it is possible to recognize that Step 2,3 and 4 have more similarities among each other than with the rest of the steps.

In the Loading Plot, two distinctive trends are observable, Ca and Mn and the rest of the variables. Also Mo and Mn-Ca are with respect to each other

almost at a 90-degree angle, this suggests that there is very little correlation between these variables. Uranium seems to be closely correlated to Al, Fe, Pb, Zn and Ni while Th to S, Sn and Cr. By observing these graphs together, it is evident that Mn and Ca are correlated with steps 2,3 and 4 and have the highest concentrations in the 4th step. Step 1 presents vey low concentrations of all the studied elements. While Step 5 and 6 contain the highest concentrations of all analytes except for Ca and Mn. This observation is consistent with the percentages of the sequential extraction experiment.

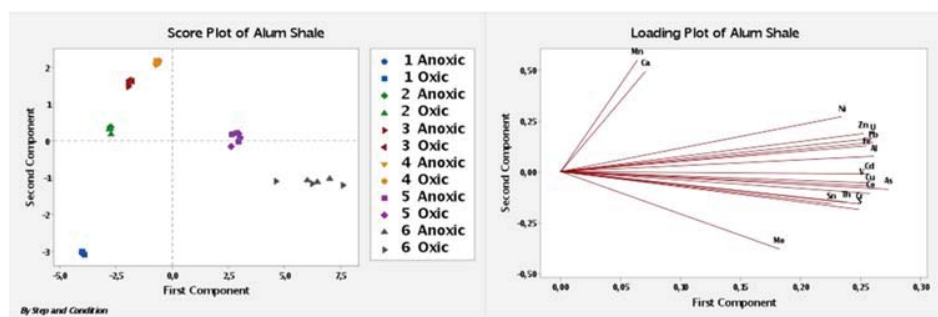


Figure 80 PCA analysis for Alum Shale. Score plot by step of the sequential extraction process and loading plot are shown.

For Black Shale, all variables were included in the analysis. In Table 16, PC1 explains 68.1% of the total variation of the data set and together with PC2, are accounted for the 83% of variation. In Table 17, PCA values for the studied variables are displayed, PC1 present positive values for all the variables while PC2, have negative values for V, Cr, As, Mo, Sn, Th and U.

Table 37 Principal components with the variation proportion and the cumulative values of the variation they explain for Black Shale.

Principal Component	Proportion	Cumulative
PC1	68.1	68.1
PC2	15	83.1
PC3	11.9	95

Table 38 Principal components 1 and 2 values for the variables for Alum Shale.

Variable	PC1	PC2
Al	0.27	0.01
S	0.23	0.07
Ca	0.14	0.15
V	0.25	-0.24
Cr	0.24	-0.30
Mn	0.17	0.19
Fe	0.24	0.22
Co	0.26	0.14
Ni	0.23	0.32
Cu	0.24	0.13
Zn	0.25	0.25
As	0.24	-0.30
Mo	0.20	-0.40
Cd	0.22	0.24
Sn	0.18	-0.25
Pb	0.26	0.15
Th	0.24	-0.30
U	0.26	-0.10

Figure 29, displays the Score Plot and Loading Plot for the Black Shale data set. In the Score Plot, all samples within the same step share properties in spite its condition. In Step 6, however, the data is more spread over PC1 than in PC2. Step 6 has relatively high values for PC1, which are higher for the anoxic condition. In the Loading Plot, all the elements have positive values for PC1 and follow the same direction on the plot. Uranium is positively correlated to all elements; same observation is true for Th.

By comparing these graphs, it is possible to infer that the majority of the elements have larger concentrations in Step 6, except for Ca and Mn, which

have highest concentrations in Step 5. Step 1 and 2 seem to have small concentrations of all elements, while Step 3 and 4 have concentrations close to the mean value. These patterns can be confirmed by the observations made in the sequential extraction experiments.

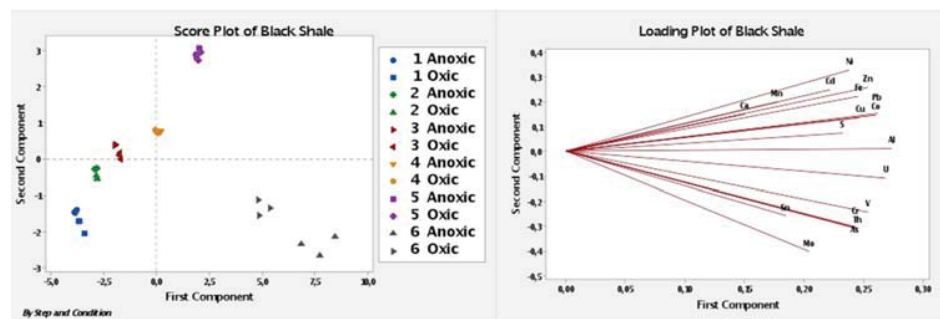


Figure 81 PCA analysis for Black Shale. Score plot by step of the sequential extraction process and loading plot are show.

Three variables, V, Cr and Sn, were excluded from the Peat Moss data set due to missing data. The missing data represented 50% of the data for these variables.

Table 18, illustrates that PC1 explains 61.4 % of the variation in the sample, while PC2, 17%. Together these components are accounted for the 78.4% of the variation of the data set. In Table 19, PCA values for each variable are presented; all variables are positively correlated to PC1. The lowest values for this component are for Ca, Mn and Cd. These elements also feature relatively high negative values for PC2. This suggests that Ca, Mn and Cd may follow a different trend than the rest of the elements.

Table 39 Principal components with the variation proportion and the cumulative values of the variation they explain for Peat Moss.

Principal Component	Proportion %	Cumulative %
PC1	61.4	61.4
PC2	17	78.4
PC3	13	91.4

Table 40 Principal components 1 and 2 values for the variables for Alum Shale.

Variable	PC1	PC2
Al	0.31	0.12
S	0.20	0.36
Ca	0.06	-0.55
Mn	0.16	-0.51
Fe	0.30	0.03
Co	0.31	0.05
Ni	0.31	-0.04
Cu	0.22	0.14
Zn	0.32	-0.03
As	0.28	-0.02
Mo	0.26	0.26
Cd	0.15	-0.30
Pb	0.25	-0.27
Th	0.26	0.11
U	0.27	-0.01

In Figure 30, three clusters of data can be observed: Step 1, Steps 2,3,4 and Steps 5,6. This suggests that the clustered steps have similar properties.

Step 6 in oxic conditions show the highest values for PC1 suggesting that the concentration of elements in these samples may be the highest of all samples. In general, Peat Moss shows fewer similarities between the oxic and the anoxic stops, these differences can be also observed in Section 4 for Peat Moss.

The Loading Plot illustrates that Major Elements Ca, Mn and S seem to follow a different pattern of leachability than the rest of the elements. However, Mn seems to be very little correlated to S. Calcium, being at approximately 90 degrees in respect to sulfur, suggests little to no correlation between these elements. Uranium, arsenic, nickel, zinc and iron appear to be strongly correlated. In general Th, Al, Co, Fe, U, As, Zn and Ni appear to be correlated to each other. By comparing the Score Plot and the Loading Plot, the majority of metals and radionuclides seem to be associated with Step 5 and 6, suggesting that they are irreversibly bound species or species that are incorporated into the crystallographic structure of the minerals. While Major Elements Ca and Mn are associated to steps 2, 3 and 4, suggesting that the later are sensitive to pH changes. Step 1 seems to have very little concentrations of all elements. Thus, stronger contributors to the bioavailable fraction are Step 2 and 3.

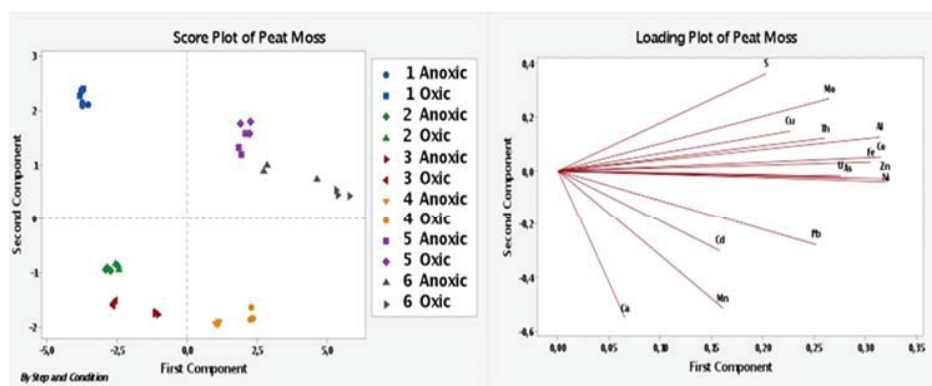


Figure 82 PCA analysis for Peat Moss. Score plot by step of the sequential extraction process and loading plot are show.

From the Principal Component Analysis done for each material, it is possible to observe that oxic and anoxic steps for Alum Shale and Black Shale follow similar patterns in the score plots and by the results for the sequential extraction experiments.

These results may have a relation to the Eh values reported in the sample characterization section. The Eh values for Alum Shale and Black Shale under oxic and anoxic conditions are similar; this suggests that in spite of the efforts made to keep the materials under anoxic conditions, this goal may not have been achieved.

On the other hand, principal component analysis and extracted concentrations data show visible differences between oxic and anoxic conditions for Peat Moss samples. This observation is consistent with the Eh values for these samples presented in the sample characterization section, which shows a value of -3 mV for oxic samples and a -115 mV for anoxic set.

However the relevance of these differences needs to be statistically proved, thus principal component analysis (complete data set and analysis shown in Appendix B) and inferential statistics were applied to the steps 1, 2 and 3. In Figure 31, Score Plot by condition and material and Loading Plot for bioavailable fractions are displayed.

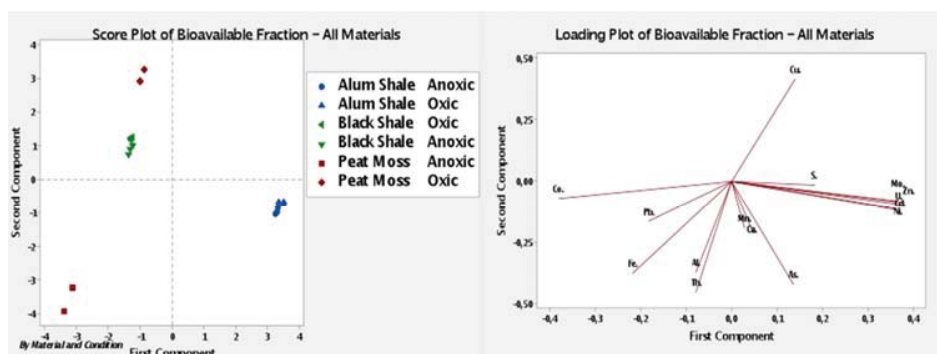


Figure 83 PCA analysis for Bioavailable Fraction of all materials. Score plot by material and corresponding loading plot are shown. Score Plot shows differences in each material under different conditions.

This Score Plot shows that samples from Alum Shale and Black Shale have similar properties under the two different conditions. On the other hand, Peat Moss shows that samples treated under anoxic conditions do not share properties with the ones under oxic conditions. These observations are similar to the ones done for the complete data set.

In the Loading Plot, it is possible to observe that U, Mo, Zn, Cd and Ni are closely correlated and are present in higher concentrations in Alum Shale than in the rest of the materials. For Black Shale and Peat Moss under oxic conditions, they show concentrations near mean value. Uranium and Thorium, being at approximately 90 degrees, have little to no correlation for the bioavailable fraction. Major elements Ca and Mn show a positive strong correlation to arsenic.

Aluminum and Thorium seem to be strongly correlated in this fraction. Molybdenum, zinc, uranium, cadmium and nickel seem to have a negative correlation to iron, lead and cobalt.

The association in soil between the two redox sensitive elements, arsenic and uranium, also visible in the loading plot for Peat Moss, have also been observed by Schöner et al. (2009) and Zayre et al. (2006).

The concentrations from steps 1,2 and 3 are of particular interest since together, they represent the bioavailable fraction. Inferential statistics can be applied to the calculated values for PC1, PC2 and so on. As said before, the data transformations that the method does on the original data set, changes the mathematical values not the properties of this original data set. See Appendix B.

For the bioavailable fraction, inferential statistics were applied on the transformed score values for PC1. This was done in order to test if the bioavailable fractions of the materials present statistically significant differences under the two different conditions.

In Figure 32, the boxplot illustrates the trends of PC1 under different conditions in the materials. While it is evident that the greatest difference

between oxic and anoxic conditions is for Peat Moss, paired t-test analysis is needed to verify the statistical significance of these differences.

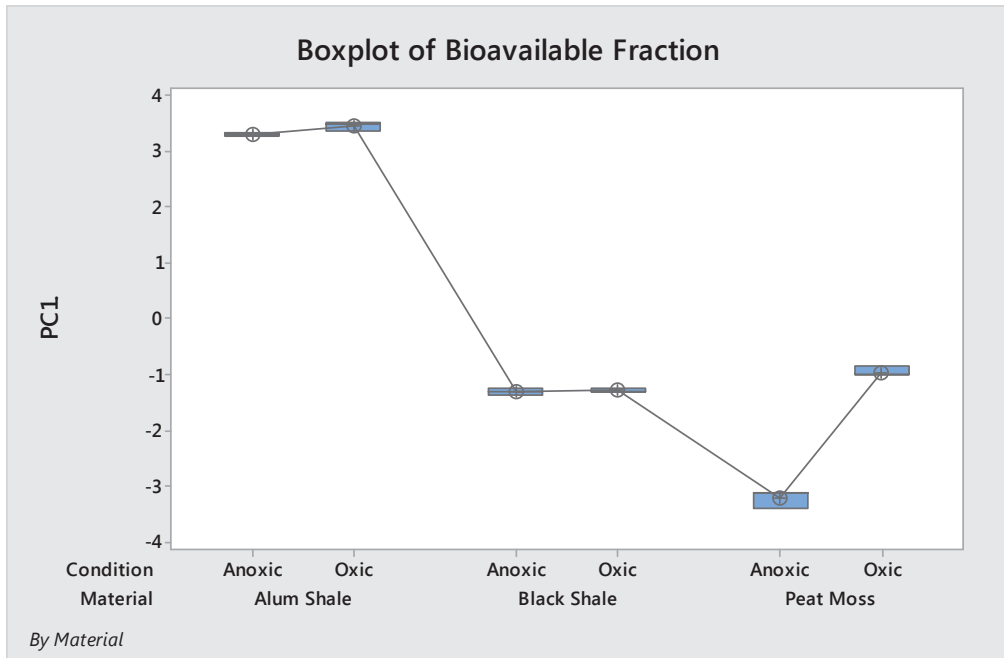


Figure 84 Boxplot of PC1 for the Bioavailable Fraction. Boxplot shows the differences between Alum Shale, Black Shale and Peat Moss under oxic and anoxic conditions. Boxplot shows mean, median, Q1, interquartile range, Q3 and connecting mean line.

Results from paired t-test (for the bioavailable fraction in each material) demonstrate, with a 95% of confidence interval, that only the differences between oxic and anoxic conditions for Peat Moss are statistically significant. In Table 20, the results for t-tests are summarized. For Johnson transformation and normality, see Appendix C.

Table 41 Summarized results for paired t-test.

Material	Hypothesis	Result
Alum Shale		The p-value of 0.122 indicated that there is insufficient statistical evidence to reject H_0 . Thus, it is established that $\mu_1 = \mu_2$.
Black Shale	$H_0: \mu_{\text{differences}} = \mu_1 - \mu_2$ $H_1: \mu_{\text{differences}} \neq \mu_1 - \mu_2$	The p-value of 0.606 indicated that there is insufficient statistical evidence to reject H_0 . Thus, it is established that $\mu_1 = \mu_2$
Peat Moss		The p-value of 0.001 indicated that there is very strong statistical evidence to reject H_0 . Thus, it is established that $\mu_1 \neq \mu_2$.

The results of the t-tests suggest that there is a relation between the Eh values of the samples before extractions as it was stated earlier.

The values of redox potential for alum shale and black shale showed similarities for both conditions, hence the similar results. Oxic alum shale Eh= 118 mV and Eh anoxic=110 mV and for Black Shale Oxic 65 mV and Eh anoxic= 32. For the peat moss, Eh values were much more different for the conditions, hence the significance on the differences.

ANOVA was done on transformed data for PC1; see Appendix F for Johnson data transformation. This analysis suggests with a 95% of confidence interval that there is statistically significant evidence to state that at least one of the mean values of the samples is different from the rest.

Tukey test was applied to the data after ANOVA analysis. The results suggest, with a 95% of confidence interval, that the mean differing from the rest is Alum Shale. Table 21, summarizes these results.

Table 42. Summarized results for Tukey test.

Comparison	Hypothesis	Result
Alum Shale-Black Shale		The p-value of 0.003 indicated that there is very strong statistical evidence to reject H_0 . Thus, it is established that $\mu_1 \neq \mu_2$.
Alum Shale- Peat Moss	$H_0: \mu \text{ differences} = \mu_1 - \mu_2$ $H_1: \mu \text{ differences} \neq \mu_1 - \mu_2$	The p-value of 0.001 indicated that there is very strong statistical evidence to reject H_0 . Thus, it is established that $\mu_1 \neq \mu_2$.
Black Shale- Peat Moss		The p-value of 0.838 indicated that there is insufficient statistical evidence to reject H_0 . Thus, it is established that $\mu_1 = \mu_2$.

4.5 Experiment two: Leaching experiments on thin-section for weathering process analysis

Prior to leaching experiment, the thin-section sample was characterized using a combination of micro-analytical techniques: Digital Autoradiography, ESEM-EDX, micro-XRD and micro-XRF and LA ICP-MS.

After treatment, the leaching solutions were analyzed with ICP-MS for elemental concentrations after different leaching times. The thin-section was analyzed with electron microscopy after leaching time of 10 days and 22 days as the characterization analysis after treatment. In the present section, the results of these experiments are shown.

4.5.1 Sample characterization: Before treatment

4.5.1.1 Digital Autoradiography

The radiograph, see Figure 33, shows the presence of radiation distributed along the sample (darker areas), however two distinctive areas are visible, Area 1 and area 2. A heterogeneous distribution of dark zones in the radiograph is illustrated in the figure, this observation is consistent with studied heterogeneities in environmental samples from non-contaminated zones (Lind, 2006).

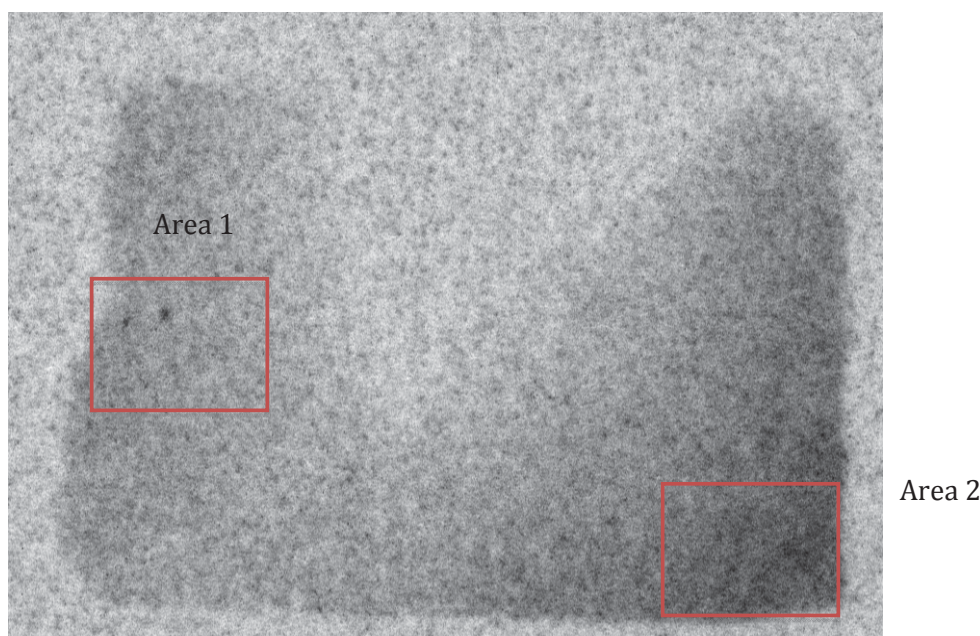


Figure 85 Radiograph for thin-section sample showing two areas of interest: Area 1 and Area 2.

4.5.1.2 Environmental Electron Microscopy EDX-ESEM

Area 1 was scanned for general mapping in order to locate the darker spots shown in Figure 33. The collected sum spectrum showed a variety of metals such as iron, aluminum and nickel. However, uranium and thorium were not identified. This analysis can be consulted in Appendix D.

A possible explanation for it is that radioactivity may arise from radionuclides other than uranium, for example 226-Ra. This elemental has a higher specific activity than the ones for Th and U. Which is why even though Digital Autoradiography may detect its energy, its mass may be

below the detection limit of ESEM-EDX, which is approximately 0.1 mass %.

Area 2 is of particular interest since the Laser Ablation ICP-MS analysis was performed here as well. Figure 34 shows an image of the area showing LA ICP-MS profiles using the BEI mode and one using SEI mode of the EDX-ESEM.

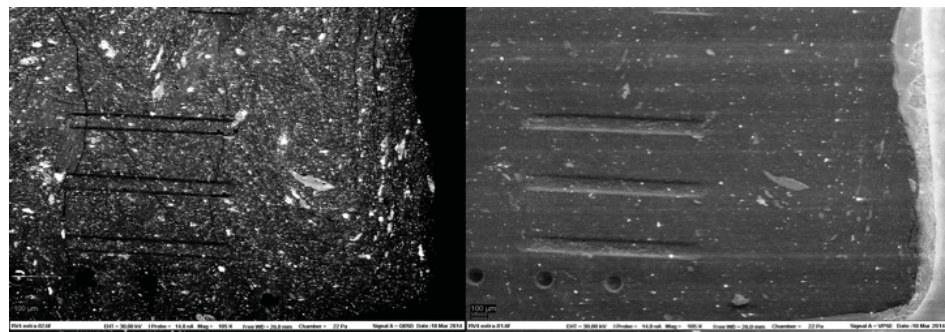


Figure 86 Electron Microscope Image using BEI mode of Area 2, magnification 105 X. (left). Electron Microscope Image using SEI mode of Area 2 (right). Magnification 105 X. Profiles for LA ICP-MS are visible.

A general scan mapping and a sum spectrum were collected from this zone. In Figure 35, it is possible to observe the general scan mapping image and in Figure 36, its correspondent sum spectrum. The spectrum shows a variety of elements present in the scanned area. This area was also analyzed using point-to-point scanning, see Figures 37 and 38.

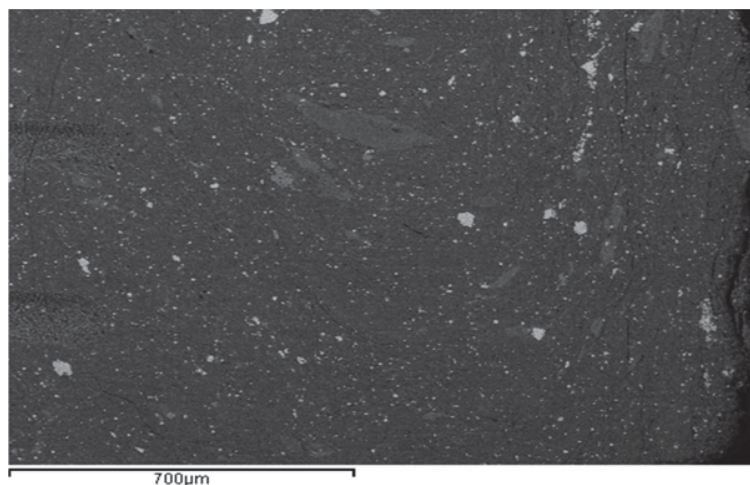


Figure 87 Electron microscope general scan mapping image of Area 2, using BEI mode.

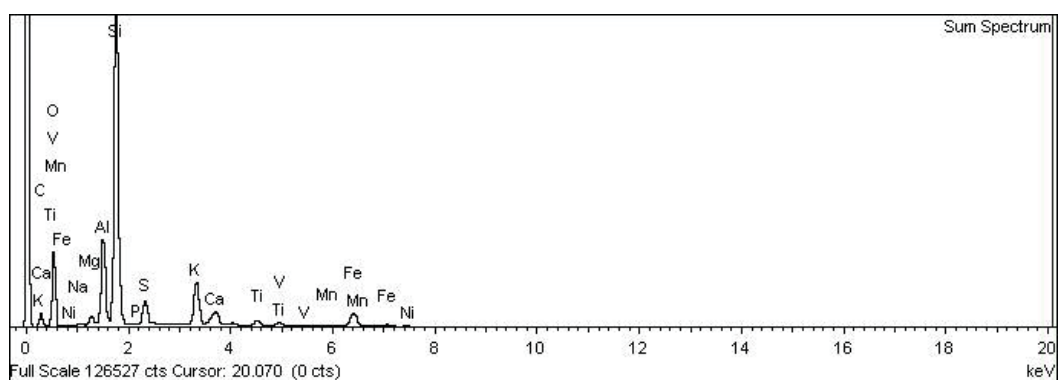


Figure 88 Electron microscope sum spectrum of Area 2, corresponding to Figure 35.

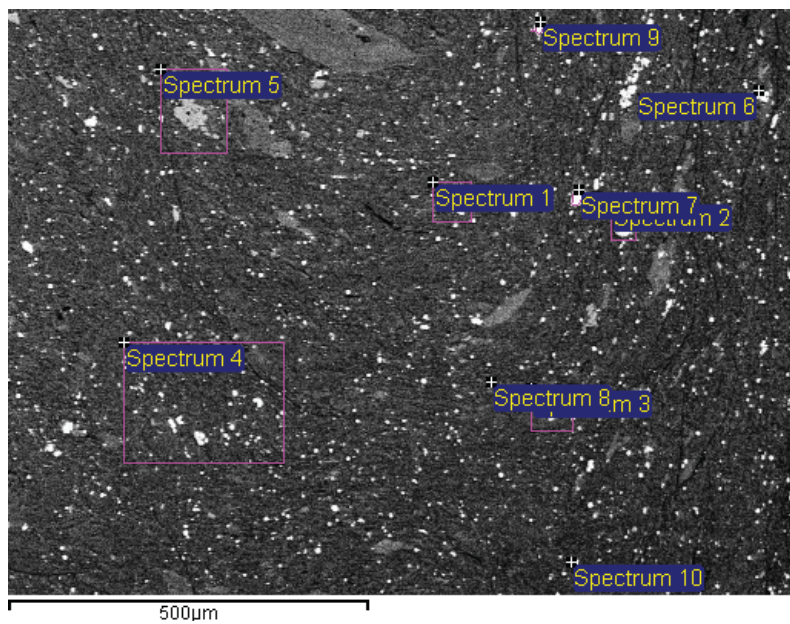


Figure 89 Electron microscope image of area 2 using BEI mode. The figure shows the position of the point spectra performed on the zone.

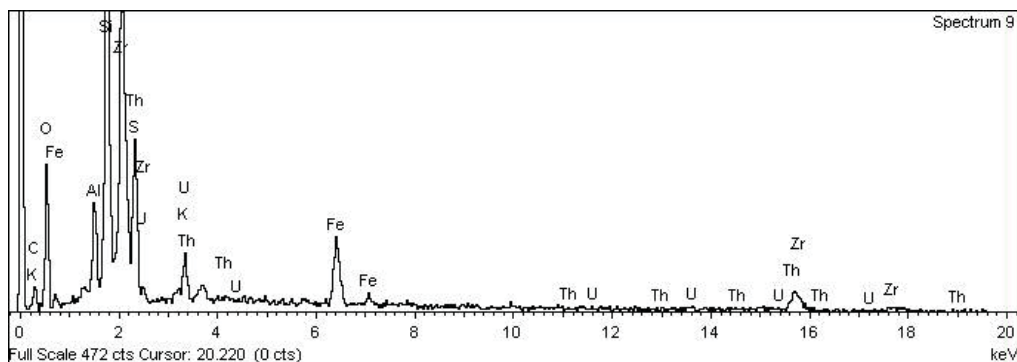


Figure 90 Spectrum corresponding to Spectrum 9 position in Figure 37. This spectrum shows the presence of uranium, thorium and zirconium in the sample.

Figure 38, displays a variety of metals in the sample, this information can complement the XRD analysis, for example Fe and S peaks may indicate the presence of pyrite in the material.

In order to confirm the presence of radioactive elements, U and Th, a new point-to-point analysis was performed in the area, see Appendix A. This analysis confirmed the presence of uranium in the sample. Th was not identified in this analysis; this may be due to the small size of the particle containing Th.

A magnification on the area was done in order to locate the particle containing the uranium. In Figure 39, the image of this area is presented with the location of the particle (Spectrum 9) and in Figure 40, its corresponding spectrum.

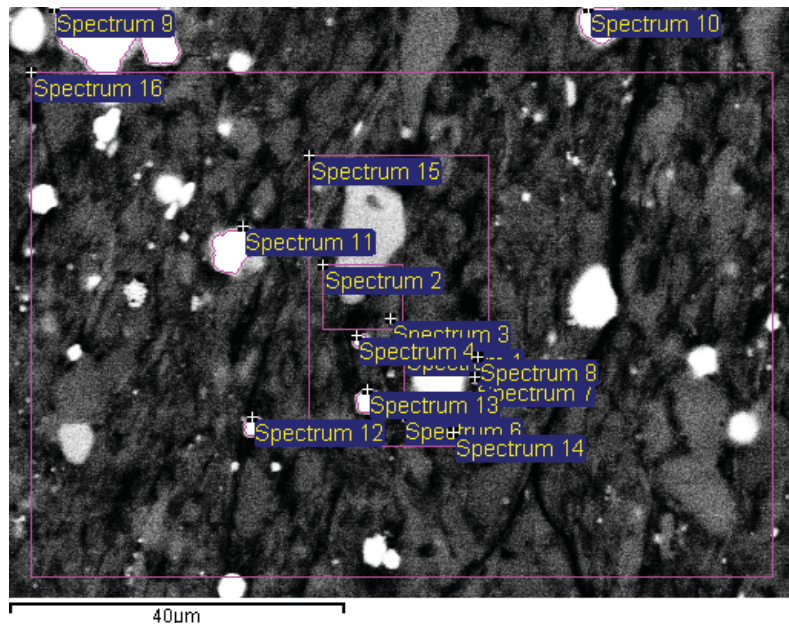


Figure 91 Electron microscope image of area 2, using BEI mode. The image shows the position of different point spectra performed on the sample.

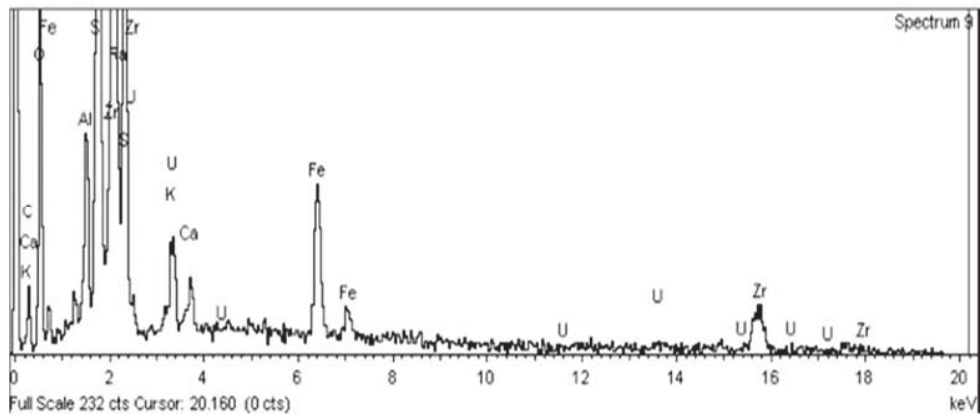


Figure 92 Spectrum corresponding to Spectrum 9 position in Figure 55. This spectrum shows the presence of uranium in the sample.

In Figure 40, the spectrum confirms the presence of uranium along with zirconium and a variety of elements.

The electron microscope images together with the corresponding spectra can confirm the observations made on the LA ICP-MS profiles regarding the heterogeneous distribution of the material.

4.5.1.3 Micro X-ray Diffraction and Micro X-ray Fluorescence

Micro-analytical techniques – micro-XRD and micro-XRF – were used for sample characterization at a micro scale.

As mentioned before, small holes (milimetric scale) were drilled on the PMMA surface of the thin-section to test the material for possible interferences. These interferences were not detected, which suggests that this procedure does not improve the analysis; moreover, in the section of characterization of the sample post-treatment will be discussed that these drillings may be interfering with the accuracy of the method.

In Figure 41, the results for the micro-XRD are shown. There are no visible peaks in this graph, but rather the presence of an amorphous background is illustrated.

No minerals could be identified by this technique; one of the possible reasons for it may be that the thin-section does not provide enough material to be detected by the instrument.

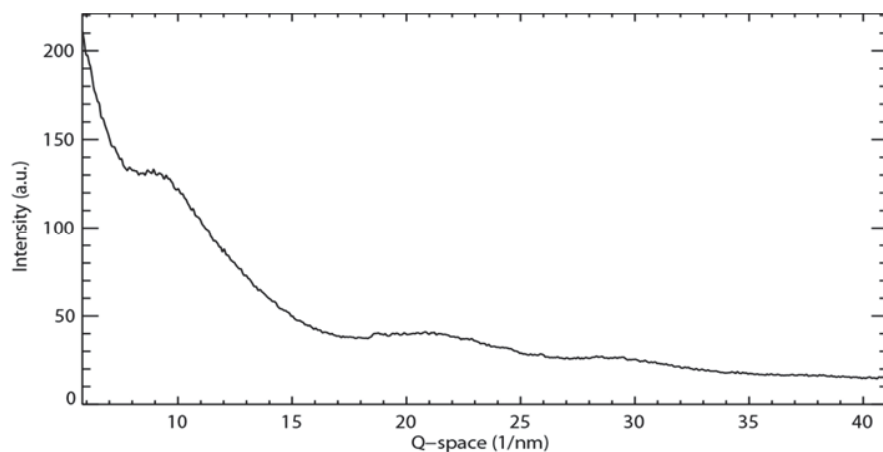


Figure 93 Micro-XRD. Diffractogram of the thin-section sample. The graph shows no mineral phases detected but rather an amorphous background.

The results for the Micro-XRF analysis are presented in Figure 42. The elements detected by this technique were K K-edge, Ca K-edge, Ti K-edge and V K-edge.

These results are consistent with the ones observed for the analysis of the leaching Solutions and the XRD data, see Appendix A, that shows the presence of mineral phases containing these elements.

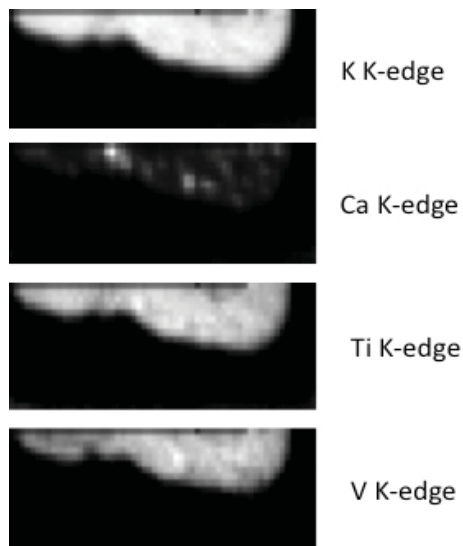


Figure 94 Micro X-ray Flourescence analysis. The image shows the presence of K K-edge , Ca K-edge. Ti K-edge and V K-edge in the thin-section sample.

4.5.1.4 Laser Ablation Inductive Coupled Plasma Mass Spectrometry LA ICP-MS

The thin-section sample was characterized with LA ICP-MS before treatment. In Figure 43, is an electron microscope image that shows the location of the analyzed sites, three craters and three lines.

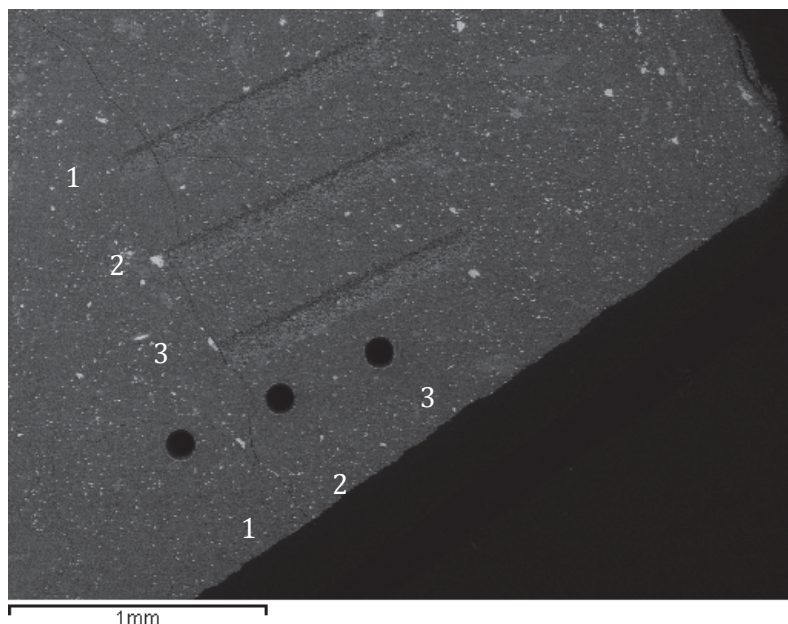


Figure 95. Electron Microscope ESEM image showing the location of the analyzed sites with LA ICP-MS, image taken in BEI mode. The circles represent the craters and the horizontal marks, the lines. From Left to right: Crater 1 corresponding to Depth Profile 1, Crater 2 corresponding to Depth Profile 2 and Crater 3 corresponding to Depth Profile 3 and top to bottom, Line 1 corresponding to Surface Profile 1, Line 2 corresponding to Surface Profile 2 and Line 3 corresponding to Surface Profile 3.

The LA ICP-MS profiles are a powerful tool to identify associations among the elements in a micro-scale; this can provide information about how the mineral phases present in the sample are conformed.

The aim of performing two different kind of analysis, Depth and Surface, is to identify the differences between distribution of elements in the surface and in deeper layers of the material.

Depth Profiles are created by a repeated laser pulse in the sample spot over a period of time; these profiles offer an overview of the distribution of elements through the material, thus the peaks found at time 20 second

represent the surface of the material while peaks at 100 represents deeper layers of the material.

Surface Profiles are created by a repeated laser along the surface of the material creating the shape of a line. These profiles offer an overview of the surface distribution of elements in the sample.

For this analysis, the y-axis corresponds to a logarithmic transformation of the normalized counts. Usually, a high peak on LA ICP-MS profiles refers to a high concentration, that assumption cannot be done for Figure 34 and 35 since a logarithmic transformation is used. However, associations and distributions of the elements can be observed.

In Figure 44, the similar distributions for Al, U, V, Pb, Mg and Fe are possible to observe by the overlapping of the profile lines. The elevated peaks randomly distributed along the x-axis suggest that elements in the material follow a heterogeneous distribution.

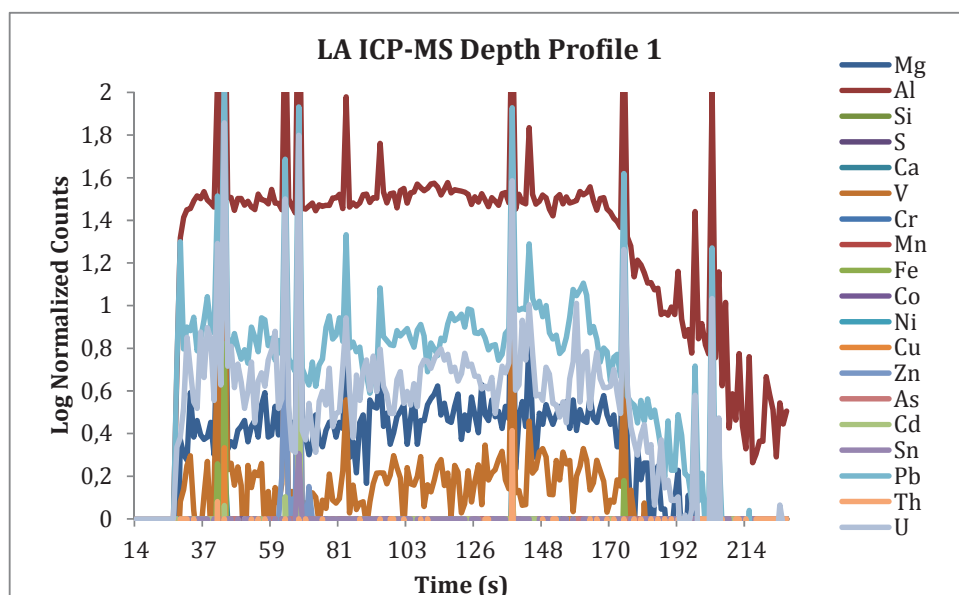


Figure 96. LA ICP-MS Depth Profile 1. General profile for all elements is displayed. The y-axis, refers to a logarithmic transformation of the normalized counts of these values.

Figure 45 displays the general profiles for all elements found in Surface Profile 1. It is possible to observe similar distributions for Al, Si, V, Fe, Pb, Th and U. However, calcium, magnesium and manganese have a distinctive

different distribution. These observations are consistent with the diffractograms shown in Appendix A, that shows Titanomagnetite and Muscovite as identified mineral phases.

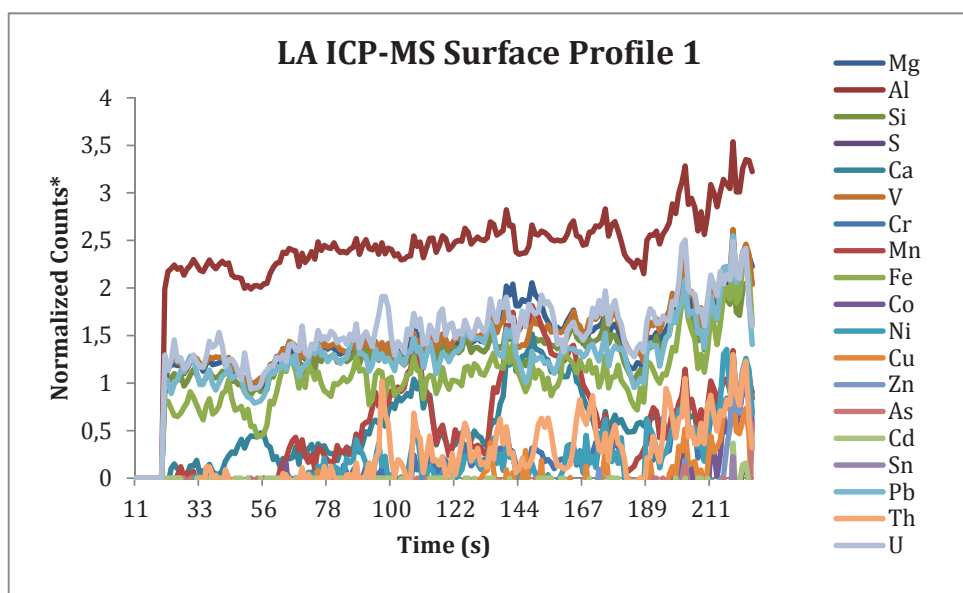


Figure 97. LA ICP-MS Surface Profile 1. General profile for all elements is displayed. The y-axis, Normalized Counts* refers to a logarithmic transformation of these values.

In general, profiles for the three Depth Profiles and the three Surface Profiles show aluminum as the most abundant element by, in some cases, orders of magnitude compared to the rest of the elements. Profiles indicate that the abundance of elements decreases as Al>> V> Pb> Mg> U> Si> Fe> Mn> Ca> Th> Ni> Cr> Zn> Co> Cu> As> Cd> S> Sn. This pattern is similar for all element profiles, both Depth and Surface.

The heterogeneous distributions observed with LA ICP-MS are consistent with the analysis done with electron microscopy and with literature for imaging techniques (B. Salbu, 2005) (Lind ,2012) (Lind, 2006).

4.5.2 Leaching Solutions Analysis

Extracts from the leaching experiments were collected after 5 different leaching times: 1 hour, 24 hours, 72 hours (3 days), 168 hours (7 days) , and 528 hours (22 days). These extracts were analyzed with ICP-MS for the same elements as experiment one: Al, Ca, V, Cr, Mn, Fe, Co, Ni, Cu, Zn, As, Mo, Cd, Sn, Pb, Th and U, except sulfur since the leaching agent was a pH 2 sulfuric acid solution. In this section the terms “Major Elements”, “Minor Elements”, “Trace Elements” are used with respect to the concentrations found in the leaching solutions and not in the material itself, although some elements may fall into the same classification.

The results of the analysis for Major and Minor Elements are shown in Figure 46. Calcium and manganese concentrations decrease with time in contrast to Al and Fe, which present increasing concentrations over time. This suggests that Ca and Mn may be found in association with carbonates, which are dissolved in acidifying conditions. Other metals that are found in association with carbonates are Zn, Cd and Ni (Tessier, 1979). Fifty percent of the total extracted Ca was leached out after 1 hour, see Figure 47, and over 50% of Mn was leached out within the same time. For Al and Fe, this percentage was increasing over time and after 22 days of leaching time reached 41.98% for Fe and 43.48% for Al, suggesting that contact time is a decisive factor for the mobilization of these elements, this phenomena was also observed by Helmers (2013). The elements corresponding to these groups represent the elements with the higher mobility of all the studied elements.

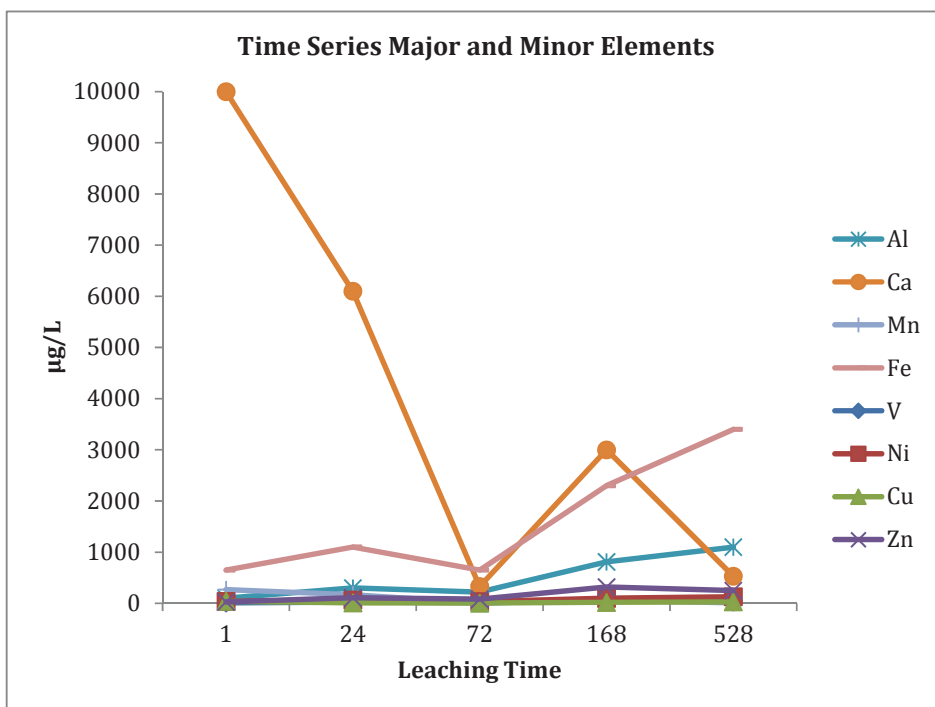


Figure 98 Leaching Experiment. Time Series for Major Elements Al, S, Mn and Fe and Minor Elements V, Ni, Cu and Zn against leaching time in hours

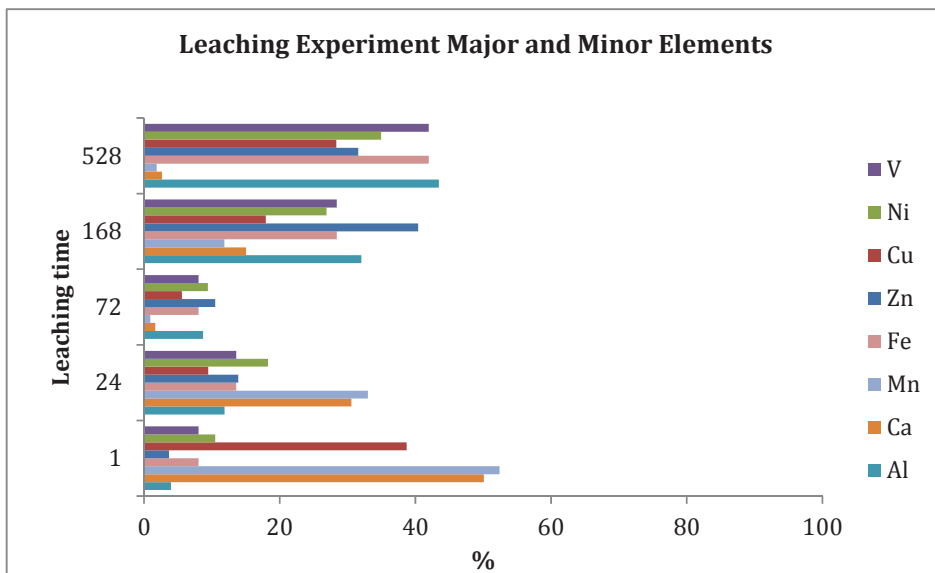


Figure 99 Leaching Experiment. Leaching percentage for Major Elements Al, S, Mn and Fe and Minor Elements V, Ni, Cu and Zn against leaching time in hours.

In these figures, it is possible to observe that Cu, which has a concentration of $41 \mu\text{g/L}$ after 1 hour leaching time and represents 37.82% of the total

extracted; the rest of the Minor Elements have an increasing concentration with leaching time, as it was seen for Al and Fe. Zinc reaches a relatively high concentration, 320 µg/L, which represents 40.40% of the extracted total. This may suggest that Zn is a metal sensitive to changes in pH and may be found in relatively mobile species, this observation is consistent with the work of Fjermestad (2013).

In Figure 48 and 49, the results of leaching experiment for Trace Elements and Radionuclides are displayed. It is possible to observe that the leaching profiles of these elements are similar and a clear distinction of which of these elements are more sensitive to pH changes. The most sensitive of these elements is Pb, followed by Mo and As, these are also the elements among the Trace Elements that are more likely to leach out into water during weathering processes. However, the similarity of the patterns suggests that the contact time is an important factor as it was seen for Major Elements. The most resilient element to mobilization is Sn, which had 0.28 µg/L as its highest concentration during leaching time; however this concentration was observed after 1 hour of leaching time, suggesting that even though Sn is resilient to mobilization, it does occur relatively fast. This phenomenon was also observed by Fjermstad (2013).

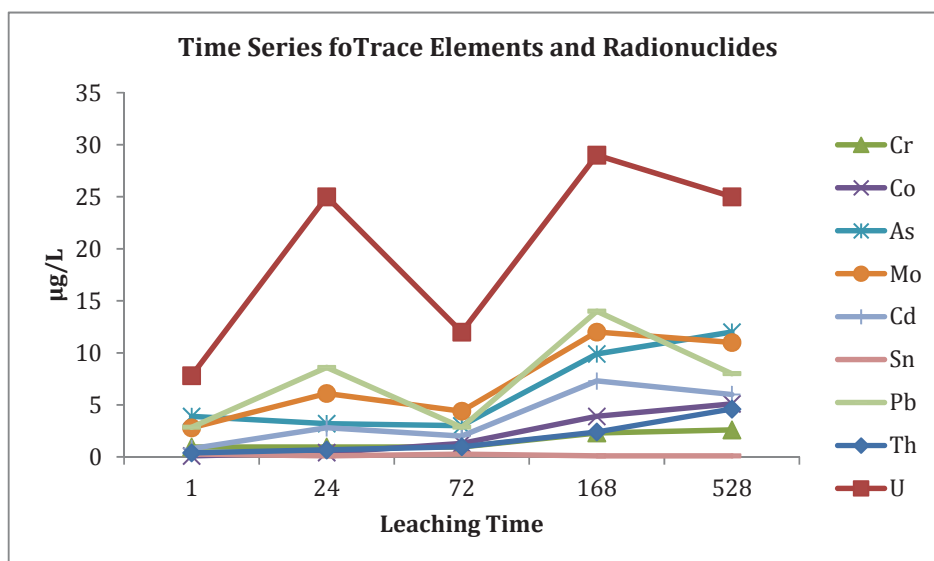


Figure 100 Leaching Experiment. Time Series for Trace Elements Pb, Sn, Cd, Mo, As, Co and Cr and Radionuclides Th and U concentrations in leaching solution. Leaching time in hours.

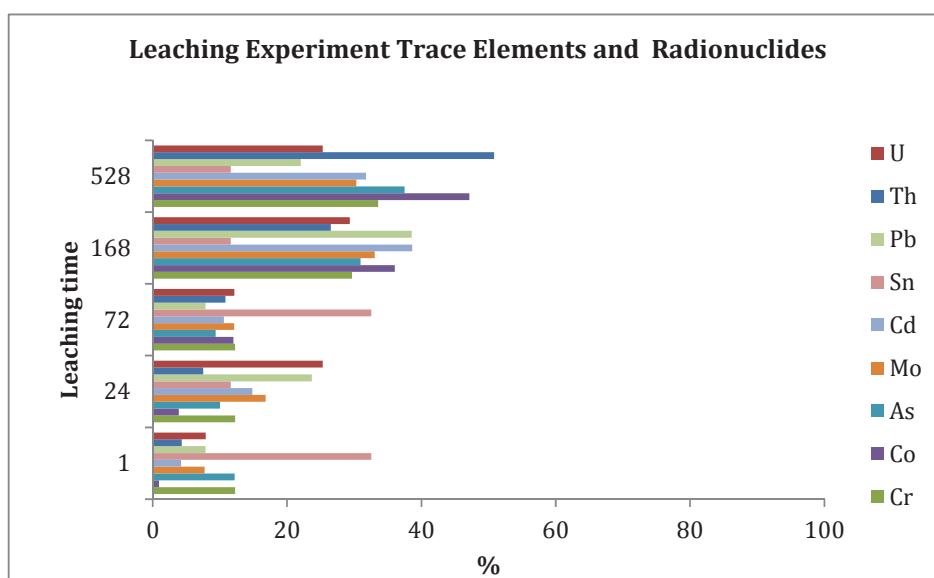


Figure 101 Leaching Experiment. Leaching percentage for Trace Elements Pb, Sn, Cd, Mo, As, Co and Cr and Radionuclides U and Th against leaching time in hours.

Regarding Radionuclides, it is evident that U has a higher potential for mobility than Th, which reaches 4.6 µg/L as its highest concentration after 22 days of leaching time. On the other hand, U reaches 29 µg/L after 7 days of leaching time. It is also possible to observe that the concentration of U decreases between 7 days and 3 days of leaching time and increases again after 22 days of leaching time in comparison to Th, which does not present such changes. This may suggest that U is more sensitive to pH changes than Th, this phenomena was also observed by Helmers (2013), Fjermstad (2013) and Regnesprug et al. (2009).

4.5.3 Sample characterization: After treatment with EDX-ESEM

Characterization of the sample after treatment was intended to be done with µ-XRF and X-ray detector on the ESEM; however these instruments malfunctioned and it was not possible to perform these analysis. The characterization presented in the next section was done using the imaging section of the EDX-ESEM.

The sample was analyzed with electron microscopy after 10 days and 22 days of leaching time. This characterization focuses in Area 2 of the thin-

section, specifically where the radionuclides were located during the characterization before the treatment. In Figure 50, an element mapping and the sum spectra for Area 2 done in the sample before treatment is shown.

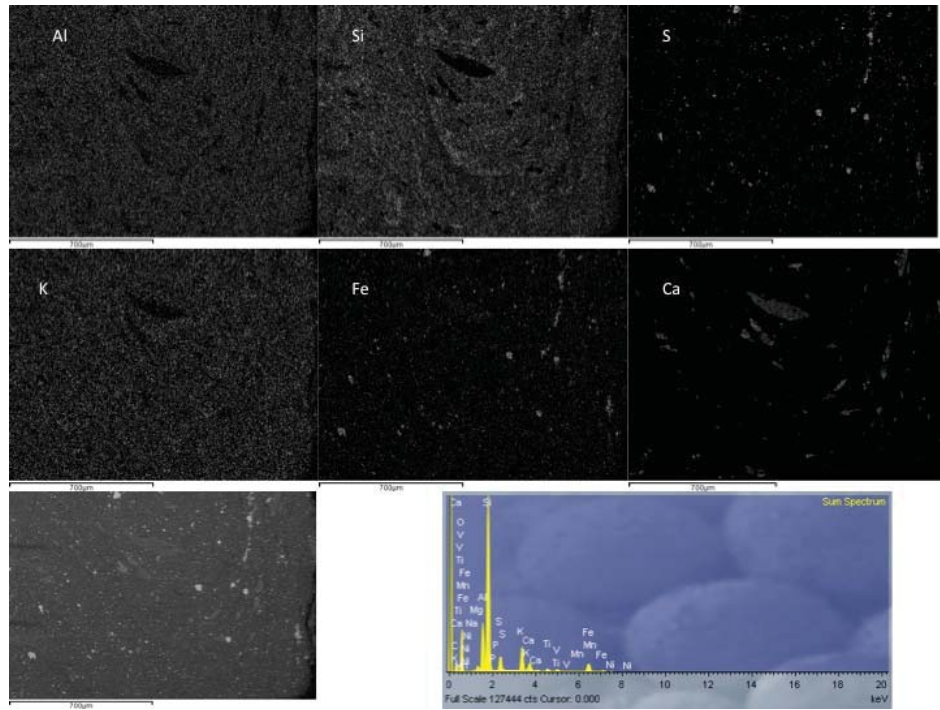


Figure 102 Elemental mapping and sum spectra for site of interest in Area 2. Image shows the elemental mapping for Al, Si, S, K, Fe, Ca. The bottom left image BEI mode image from the same area as the elemental map. Intensity on bright areas reflect on the intensity of energy given by the element in question.

Figure 51 displays and image of the zone of interest after 10 days of leaching time on the left side and after 22 days on the right one.

Both electron images show less light colored zones than the images for the initial characterization. Clear signs of weathering have appeared in the material as “cracks” colored in black along the thin-section, see Figures 68.

Figure 51 confirms what can be observed in the analysis of the leaching solution for Major Elements: The majority of calcium has been extracted by the leaching solution. In Figure 50 in the sum spectrum of calcium, it is possible to see the heterogeneous distribution of this element in the sample and in Figure 50, it is evident that black color fills the space

occupied by calcium before characterization. This suggests that mineral phases related to this element have also been efficiently removed by the leaching solution. However, there is presence of calcium and manganese after 3 days of leaching time but in relatively low concentrations.

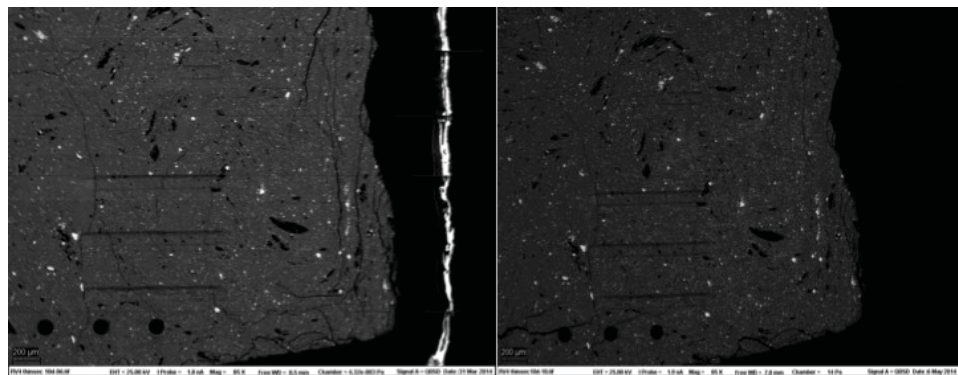


Figure 103 After treatment characterization. Electron Image after 10 days of leaching time BEI mode, magnification 85x (left) and Electron Image after 22 days of leaching time BEI mode, magnification 85x (right). Weathering signs are visible as black "cracks" on the material.

Figure 52, displays an image of the particle containing uranium after 10 days of leaching time (left) and an image after 22 days. The image of this particle before treatment can be observed in Figure 51, position of Spectrum 9. It is possible to observe that the edge of the particle after 10 days of leaching time is rounder than before treatment and after 22 days, the shape of the particle has changed again. This suggests that contact time has a direct influence on weathering processes.

In general, the light colored zones in the 10-day characterization image are more abundant than in the 22-day one. This suggests the dissolution of heavy materials in the sample, this observation is consistent with the increasing concentration of metals and radionuclides in the solution over time.

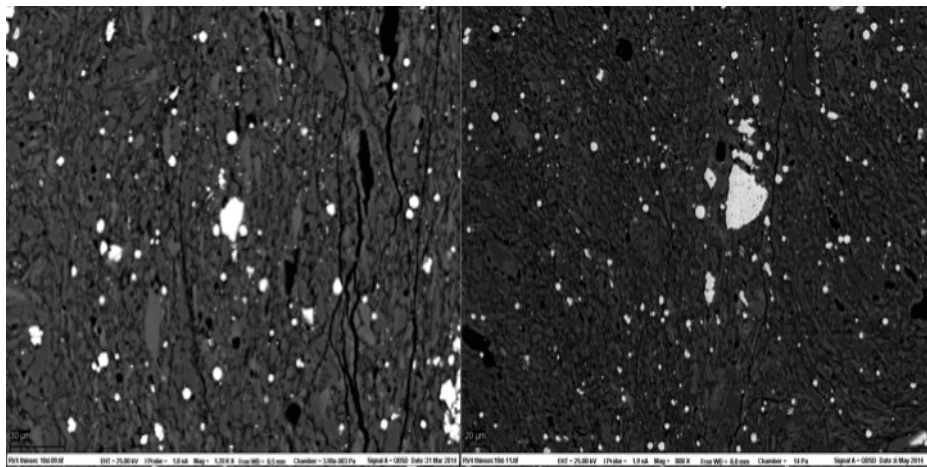


Figure 104 Electron Image after 10 days of leaching time BEI mode, magnification 1200x (right) and Electron Image after 22 days of leaching time BEI mode, magnification 800x. Weathering signs are visible as black “cracks” on the material.

It is important to mention that after 10 days of leaching, the thin-section showed signs of weathering without the use of any instrument. The material began to “peel off” from the PMMA surface. This may have had a direct influence of the concentration of elements in the leachate after this signs appeared, since a larger amount of material was in contact with the leaching solution.

This observation is consistent with the fact that increasing weathering signs were observed in the sample without the use of an instrument. The peeling of the material from the Plexiglass surface was especially evident in zones near the drilled holes in the surface. As, it was said before, PMMA did not provide interferences for the micro-analytical techniques used in these study. Thus, more accurate values of elemental concentrations in the leaching solutions may be achieved by avoiding this particular feature in the sample preparation process.

5 Conclusions

The results of the present work have characterized the potential mobility of redox sensitive metals, radionuclides and other elements in Alum Shale, Black Shale and Peat Moss collected at Gran Hadeland in Norway. Alum and Black shales were selected according to its uranium content in order to study “the worst case scenario” of environmental impact. Peat Moss was characterized as a representative sample from the deposition area extracted from 9.2 to 10 m of depth, corresponding to a silty-clay material.

The Sequential Extraction process was tested for efficiently demonstrating differences between aerobic and anaerobic extractions performed on environmental samples. Redox sensitive metals and uranium presented a different behavior under different conditions in Peat Moss and similar behaviors for Alum Shale and Black Shale.

Results for Alum and Black Shale demonstrated that there are no statistically significant differences between oxic and anoxic conditions for the extracted concentrations of uranium in the bioavailable fraction. However, the similarities in the redox potential suggest that anoxic conditions were not achieved for the experiment.

Uranium presented higher extraction percentages under anoxic conditions (22%) for the bioavailable fraction than under oxic conditions (16%). Paired t-test on Bioavailable Fraction for Peat Moss demonstrates statistically significant differences for the concentrations of uranium extracted in this fraction. However, 45% of the total concentration of extracted uranium in the sample was mobilized under oxic conditions, while a 28% was mobilized under anoxic conditions. These results suggest that uranium may be found in more stable forms under anoxic conditions than in oxic ones. This supports the main hypothesis of the present work. However, since the percentage of extraction presented the opposite behavior, this observation should be considered during risk assessment studies.

The distribution of elements on the loading plots for the sequential extraction procedure, illustrates the different behavior of elements in sedimentary rocks, like Alum and Black Shales and Peat Moss material. This observation suggests that different binding mechanisms of elements play an important role for these materials. Incorporation of elements into the mineral lattice of the shales along with chemical sorption may be the dominant mechanisms for Alum Shale and Black Shale, while for Peat Moss may be dominated by adsorption and desorption mechanisms.

The combined method for studying weathering process was tested for efficiently describing this process. Micro-analytical techniques – micro-XRD, micro-XRF and LA ICP-MS – proved effective to demonstrate the heterogeneous elemental distribution of Alum Shale.

Digital Autoradiography proved to be very useful for recognizing distributions of radiation in a solid sample; the fact that localized radiation was visible with this technique but not with electron microscope imaging EDX-ESEM, illustrates the importance of combining methods for a wider understanding of these phenomena.

Leaching experiment on the thin-section sample combined with general elemental mapping with EDX-ESEM, demonstrates the dissolution of mineral phases related to calcium. Having a second analytical technique confirm the results of obtained by another, may increase the scientific accuracy for this kind of studies.

The weathering processes to which materials are exposed in Gran area, may mobilize redox sensitive metals and radionuclides, especially uranium. This mobilization may add important amounts of these elements to the natural inventory and may promote reaching toxic levels. Weathering processes can impact the environment in a negative way; therefore these findings emphasize the need for improving our understanding of these phenomena.

References

- Agency for Toxic Substances and Disease Registry. (2013). *Toxicological Profile for Uranium*. U.S. Department of Health and Human Services.
- AMAP Secretariat . (2002). *AMAP Assessment 2002: Radioactivity in the Arctic* .
- Appelo C.A.J., P. D. (2005). *Geochemistry, groundwater and pollution*. (2nd Edition ed.). (C. Press, Ed.)
- Armienta M.A., V. G. (2012). Geochemical processes and mobilization of toxic metals and metalloids in an As-rich base metal waste pile in Zimapán, Central Mexico. *Applied Geochemistry* , 2225-2237.
- Betti M., A. d. (2004). Results of the European Commission MARINA II study: part I—general information and effects of discharges by the nuclear industry. *Journal of Environmental Radioactivity* .
- Björlykke, K. (1974). Geochemical and mineralogical influence of Ordovician Island Arcs on epicontinental clastic sedimentation. A study of Lower Palaeozoic sedimentation in the Oslo Region, Norway . *Sedimentology* , 21, 251-272.
- Brown, C. E. (1998). *Applied Multivariate Statistics in Geohydrology and Related Sciences*. Berlin Heidelberg: Springer.
- Chopin Gregory, J.-O. L. (2002). *Radiochemistry and Nuclear Chemistry*. Sweden: Butterworth-Heinemann.
- Clemens, S. (2006). Toxic metal accumulation, responses to exposure and mechanisms of tolerance in plants. *Biochimie* , 1707-1709.
- Craw, D. (2005). Potential anthropogenic mobilisation of mercury and arsenic from soils on mineralised rocks, Northland, New Zealand. *Journal of Environmental Management* , 74.
- Donald, C. D. (1998). *Environmental Toxicology and Chemistry*. New York: Oxford University Press.
- Dutrow, B. L. (2012). *X-ray Powder Diffraction (XRD)*. *Geochemical Instrumentation and Analysis*. Retrieved 2014 йил 10-April from <http://serc.carleton.edu/>: http://serc.carleton.edu/research_education/geochemsheets/techniques/XRD.html
- Duyusen E Güven, G. A. (2011). Comparison of Acid Digestion Techniques To Determine Heavy Metals In Sediment And Soil Samples . *Gazi University Journal of Science* , 29-34.

Effekter og miljørisiko knyttet til inngrep i områder med sulfidrike mineraler (2012). Project NORWAT between NPRA and Norwegian University of Life Sciences.

Fallon Stuart, M. M. (2011). *Measuring Elemental Ratios in Coral by LA-ICP-MS*.

Filgueiras A.V., I. L. (2002). Chemical sequential extraction for metal partitioning in environmental solid samples.

Fjermstad, H. (2013). *Mobilitet av Uran og Andre Metall i Bergartar i Ny Vegtrasé på Gran Hadeland*. Norwegian University of Life Sciences, Department of Environmental Sciences, Ås.

Garrett, R. G. (2000). Natural Sources of Metals to the Environment. *Human and Ecological Risk Assessment: An International Journal*, 6 (6), 945-963.

Giammar, D. (2001). *Geochemistry of uranium at mineral-water interfaces: Rates of sorption-desorption and dissolution-precipitation reactions*. California Institute of Technology , Pasadena, California.

Goulet, R. R. (2012). Uranium . In R. R. Goulet, *Homeostasis and Toxicological Effects of Non-essential Metals*. (Vol. 31 B, pp. 391-420).

Grosell, M. (2012). Copper. In A. P. Chris M. Wood, *Homeostasis and Toxicological Effects of Essential Metals*. (Vol. 31A, pp. 53-61). San Diego: Elsevier.

Helmers, T. A. (2013). *The Mobility of Uranium in U-containing Bedrock as a Function of pH: Implications for Tunnel Construction*. Norwegian University of Life Sciences, Department of Environmental Sciences, Ås.

Håvard Gautneb, O. M. (2009). *A compilation of previously published geochemical data on the lower Cambro-Silurian sedimentary sequence, including alum shales in the Oslo region*. Geological Survey of Norway, Trondheim.

Kassaye Yetneberk A. , L. S. (2012). Trace element mobility and transfer to vegetation within the Ethiopian Rift Valley lake areas . *Journal of Environmental Monitoring* , 14, 2698-2709.

Lind O.C., W. D. (2013). Micro-analytical characterisation of radioactive heterogeneities in samples from Central Asian TENORM sites. *Journal of Environmental Radioactivity* .

Lind, O. C. (2006). *Characterisation of radioactive particles in the environment using advanced techniques*. Norwegian University of Life Sciences, Ås.

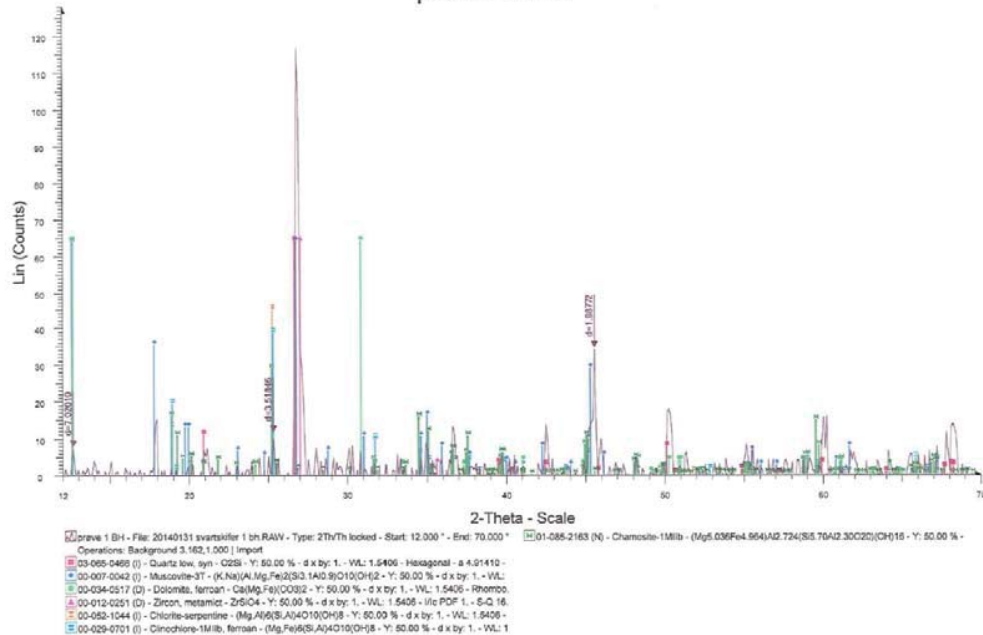
Milestone Microwave Digestion Systems. (2008). *Ultraclave The Next Generation Microwave Digestion System*. Retrieved 2014 йил 5-May from Milestonesci: <http://www.milestonesci.com/files/UC-Brochure.pdf>

- Mrdakovic P. J., S. B. (2010). Radionuclides and heavy metals bioavailability in a Norwegian area rich in naturally occurring radioactive materials. *Third European IRPA Congress*, (pp. 2589-2596). Helsinki.
- Muth, J. E. (2006). *Basic Statistics and Pharmaceutical Statistical Applications* (2nd. Edition ed.). Florida: Chapman and Hall/CRC.
- Nordstrom, D. K. (2009). Acid rock drainage and climate change. *Journal of Geochemical Exploration*, 100, 97-104.
- Ping, Z. G. (2005). Extraction of Oxidized and Reduced Forms of Uranium from Contaminated Soils: Effects of Carbonate Concentration and pH. *Enviermental Sciences and Technology*, 39 (12), 4435-4440.
- Regensprug, S. e. (2010). Speciation of naturally-accumulated uranium in an organic-rich soil of an alpine region (Switzerland). *Gerochimica et Cosmochimica Acta* , 74, 2082-2098.
- Schöner, A. e. (2009). Gerochemistry of natural wetlands in former uranium milling sites (eastern Germany) and implications for uranium retention. . *Chemie der Erde Geochemistry* , 69, 91-107.
- Salbu, B. (2013). Environmental Pollutants and ecological effects: Speciation of Elements. *Material for FMI 310 Ecotoxicology at UMB*.
- Salbu, B. (2000). Speciation of Radionuclides in the Environment . In *Encyclopedia of Analytical Chemistry* . John Wiley & Sons Ltd, Chichester .
- Salbu B., O. L. (2005). Radioactive particles released from various nuclear sources. *Radioprotection* , 27-32.
- Salbu, B. (2012). The Quality of Analytical Data. *Scientific writing - communicating analytical results*. Ås: Norwegian University of Life Sciences.
- Semeniuk V., S. C. (1997). A geomorphic approach to global classifcation for natural inland wetlands and rationalization of the system used by the Ramsar Convention- a discussion. *Wetlands Ecology and management* , 145-158.
- Shackley, M. S. (211). Chapter 2. An Introduction to X-Ray Fluorescence (XRF) Analysis in Archaeology . In *X-Ray Fluorescence Spectrometry (XRF) in Geoarcheology* (pp. 7-40). Springer.
- Shaw, P. J. (2003). *Multivariate Statistics for the Environmental Sciences*. Great Britain: Hodder Arnold .
- Skipperud, G. S. (2013). Environmental impact assessment of radionuclide and metal contamination at the former U sites Taboshar and Digmai, Tajikistan . (Elsevier, Ed.) *Journal of Environmental Radioactivity* , 50-62.
- Skipperud, L. S. (2013 January). Forslag til prøvetaking, områder og tidsplan. *Planlegging av prøvetaking ved Rv.4 Gran* . ÅS, Norway.

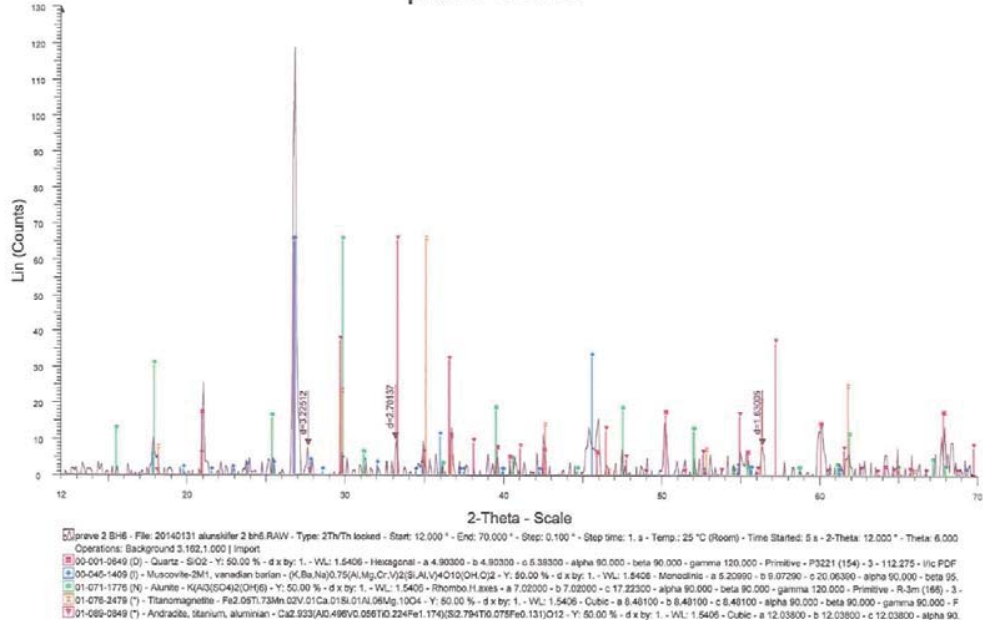
- Skipperud, D. O. (2004). Plutonium isotope ratios in the Yenisey and Ob estuaries. *Applied Radiation and Isotopes*, 589-593.
- Skipperud, L., Mrdakovic Popic, J., & Salbu, B. (2010). Radionuclides and heavy metals levels in environmental samples from thorium rich Fen area in Norway . *Third European IRPA Congress* . Helsinki .
- Smethurst Mark A., A. V. (2008). Testing the performance of a recent radon-hazard evaluation in the municipality of Gran, easter Norway. *Geological Survey of Norway Special Publication*, 11.
- Statens Vegvesen . (2013 26-April). Ingeniørgeologisk lengdeprofil. Gran border - Jaren.
- Tempelton Douglas M. , F. A. (2000). Guidelines for terms related to chemical speciation and fractionation of elements. Definitions, Structural Aspects, and methodological approaches (IUPAC Recommdnations 2000). *Pure Applied Chemistry*, 72, 1453-1470.
- Tessier A., P. C. (1979). Sequential Extraction Procedure for the Speciation of Particulate Trace Metals . *Analytical Chemistry*, 51 (7).
- Tosaka. (2008 December). *Decay chain 4n, Thorium series*. Retrieved 2014 юил 8-May from Wikipedia:
[http://en.wikipedia.org/wiki/File:Decay_chain\(4n,Thorium_series\).PNG](http://en.wikipedia.org/wiki/File:Decay_chain(4n,Thorium_series).PNG)
- Tosaka. (2008 December). *Decay chain 4n+2, Uranium series*. Retrieved 2014 юил 8-May from Wikipedia:
[http://en.wikipedia.org/wiki/File:Decay_chain\(4n%2B2,_Uranium_series\).PNG](http://en.wikipedia.org/wiki/File:Decay_chain(4n%2B2,_Uranium_series).PNG)
- Tourtelot, H. A. (1979). Black Shales - Its depositon and diagenesis. *Clays and Clay Minerals*, 27 (5), 313-321.
- Vanloon W. G., D. J. (2010). *Environmental Chamistry. A Global Perspective*. (Second Edition ed.). (O. U. Press, Ed.) Oxford University Press.
- Wolf, R. E. (2013). *Introduction to ICP-MS* . Retrieved 2014 юил 10-April from <http://crustal.usgs.gov/laboratories/icpms/intro.html>
- Zawisza, R. S. (2012 1-2). Quantification in X-Ray Fluorescence Spectrometry. *X-Ray Spectroscopy* . (D. S. Sharma, Ed.)

Appedix A – XRD Analyses

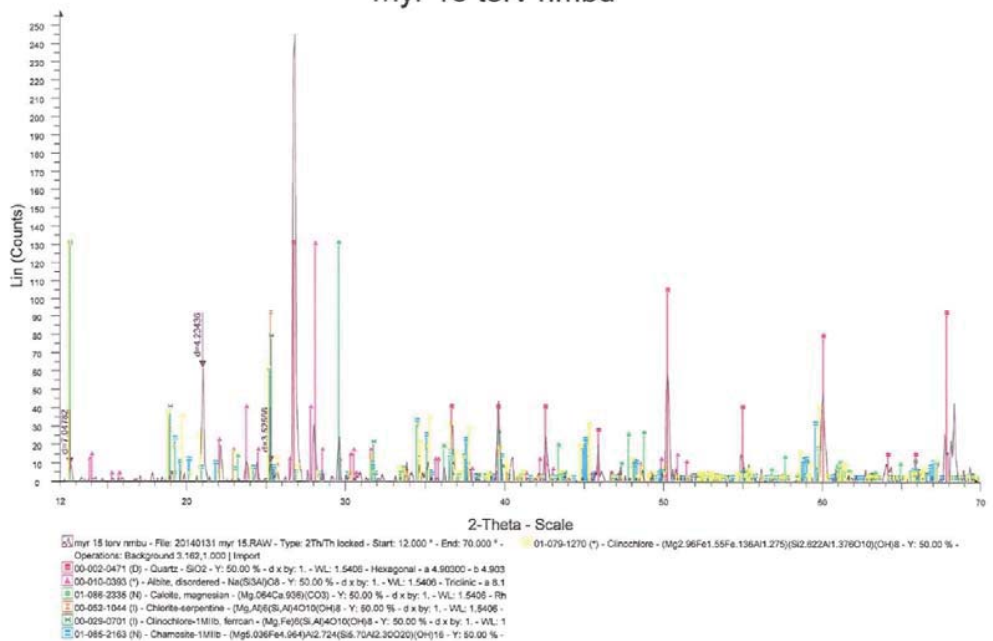
prøve 1 BH



prøve 2 BH6



myr 15 torv nmbu



Appendix B – Principal Component Analyses

Principal Component Analysis for Bioavailable Fractions.

PCA analysis for Bioavailable Fractions, all materials.

Table 43 Proportion of description of PC1, PC2 and PC3

Principal Component	Proportion	Cumulative
PC1	0,441	0,441
PC2	0,294	0,735
PC3	0,256	0,991

PCA analysis for Bioavailable Fraction in Alum Shale.

Table 44 Proportion of description of PC1, PC2 and PC3

Principal Component	Proportion	Cumulative
PC1	0,407	0,407
PC2	0,228	0,635
PC3	0,199	0,834
PC4	0,126	0,96

Score Plot and Loading Plot for Bioavailable Fraction Alum Shale

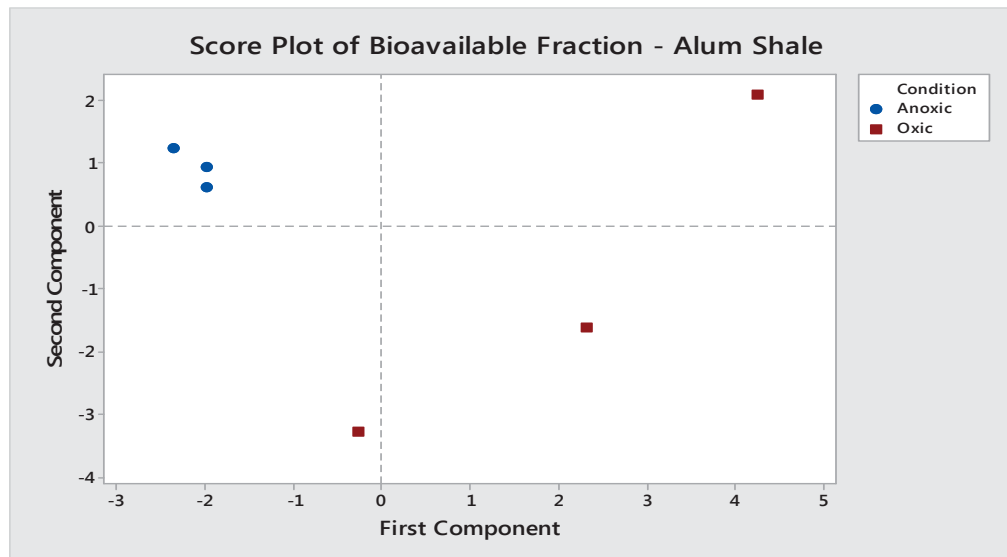


Figure 105 Score Plot for Bioavailable Fraction Alum Shale

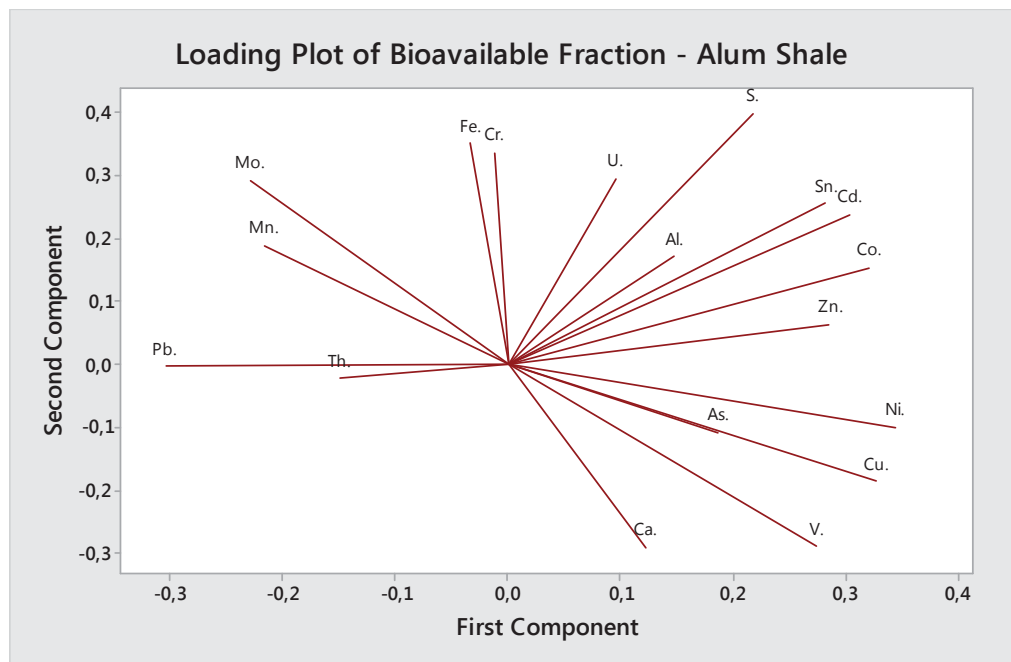


Figure 106. Loading Plot for Bioavailable Fraction Alum Shale

PCA analysis for Bioavailable Fraction in Black Shale

Table 45 Proportion of description of PC1, PC2 and PC3

Principal Component	Proportion	Cumulative
PC1	0,571	0,571
PC2	0,187	0,758
PC3	0,128	0,886
PC4	0,083	0,969

Score Plot and Loading Plot for Bioavailable Fraction Black Shale

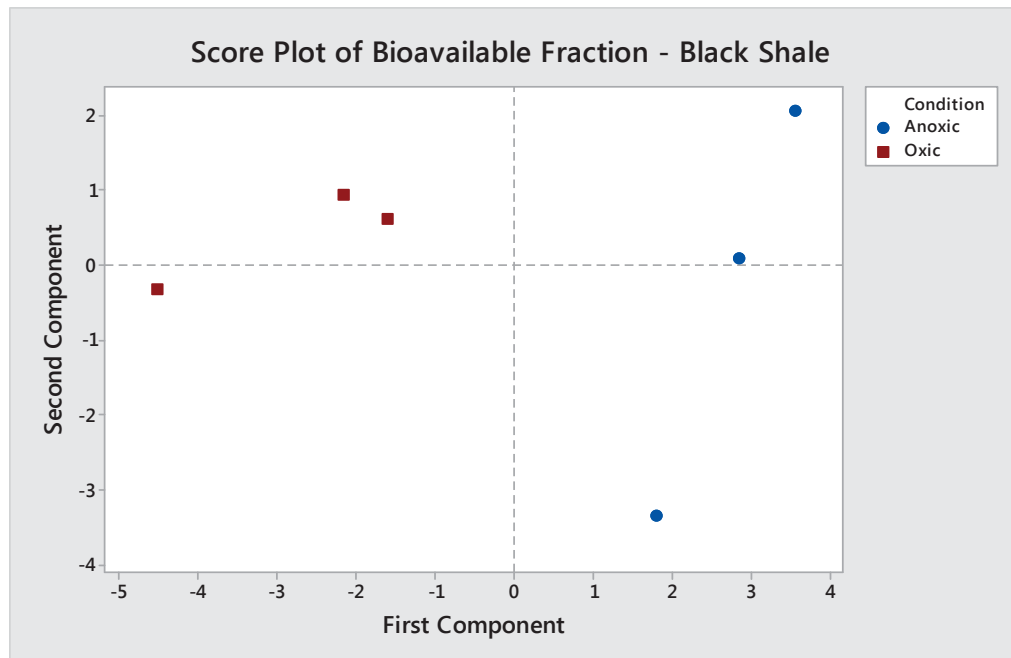


Figure 107 Score Plot for Bioavailable Fraction Black Shale.

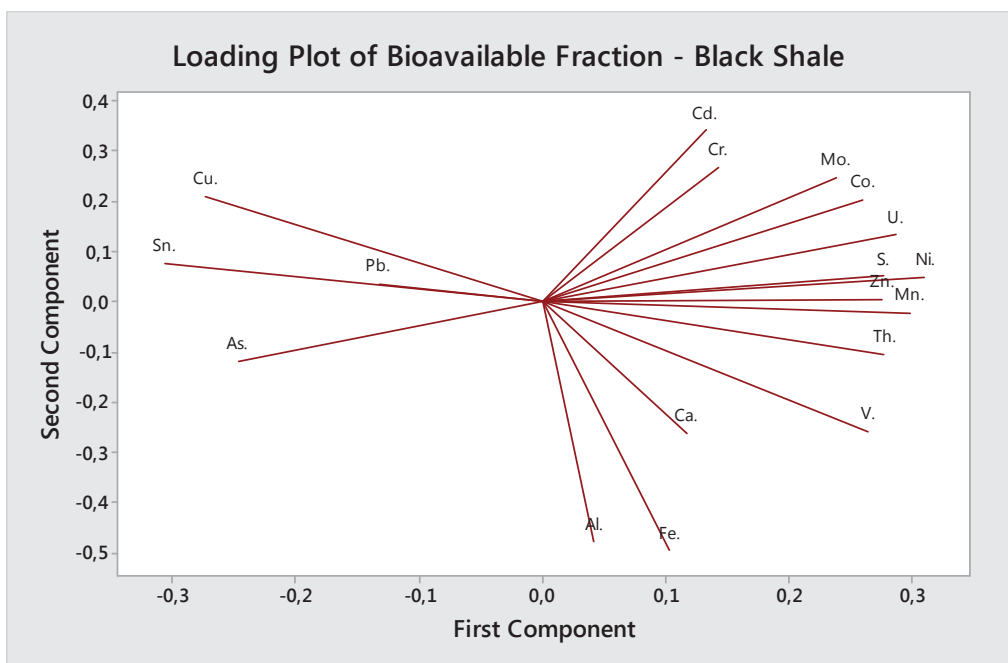


Figure 108and Loading Plot for Bioavailable Fraction Black Shale.

PCA analysis for Bioavailable Fraction in Peat Moss

Table 46 Proportion of description of PC1, PC2 and PC3

Principal Component	Proportion	Cumulative
PC1	0,891	0,891
PC2	0,063	0,954
PC3	0,026	0,98

Score Plot and Loading Plot for Bioavailable Fraction Peat Moss

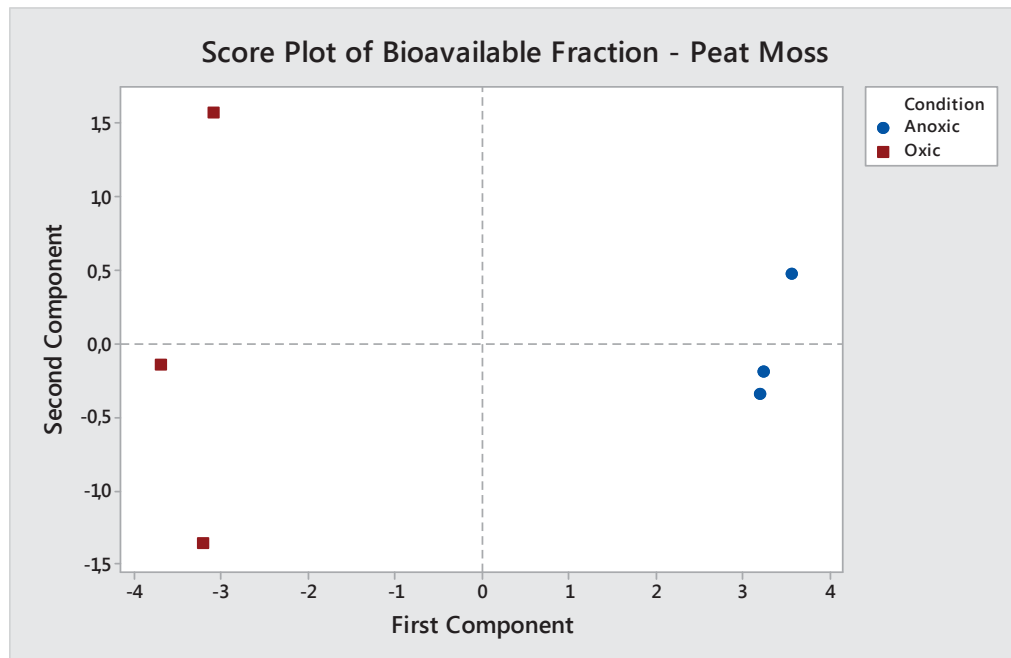


Figure 109. Score Plot Bioavailable Fraction Peat Moss

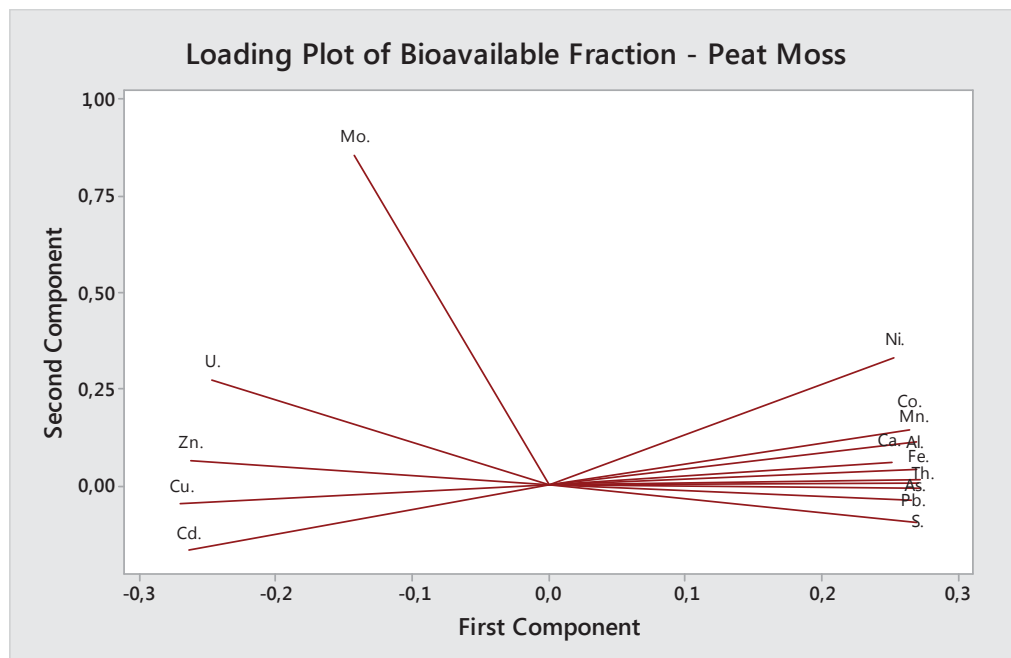


Figure 110 Loading Plot for Bioavailable Fraction Peat Moss

Appendix C

Johnson transformation for data normalization done in PC1

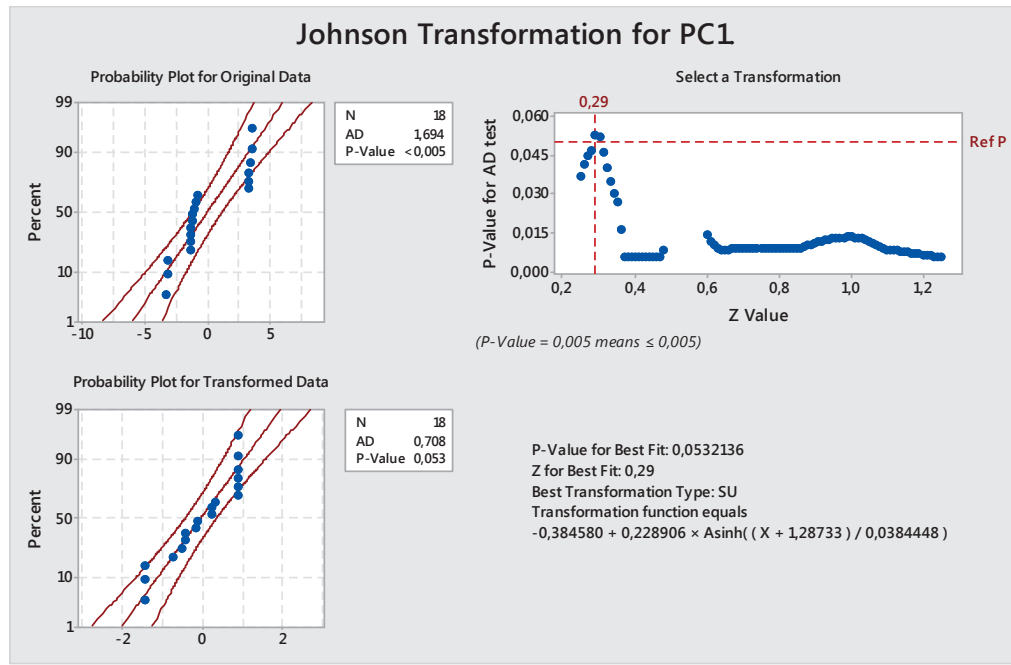


Figure 111. Johnson transformation done in PC1 from the bioavailable fractions in order to perform inferential statistics.

Appendix D

General Mapping and Sum Spectra for Sample Characterization of Thin-Section

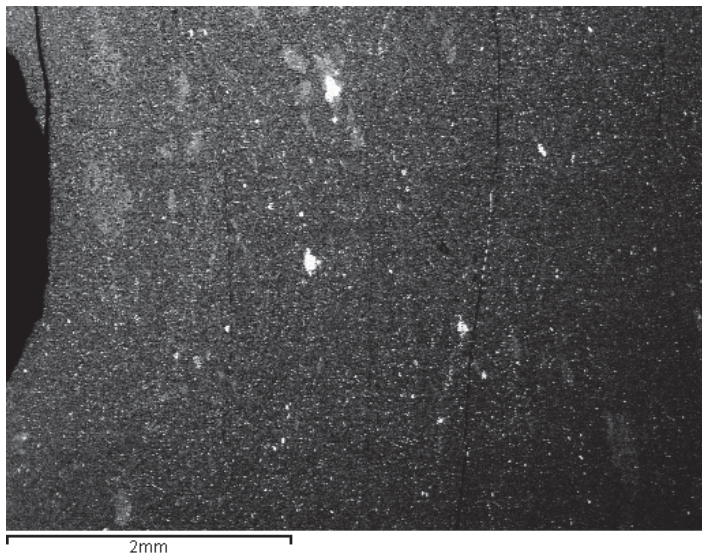


Figure 112. Electron microscope general scan mapping image of Area 1 using BEI mode.

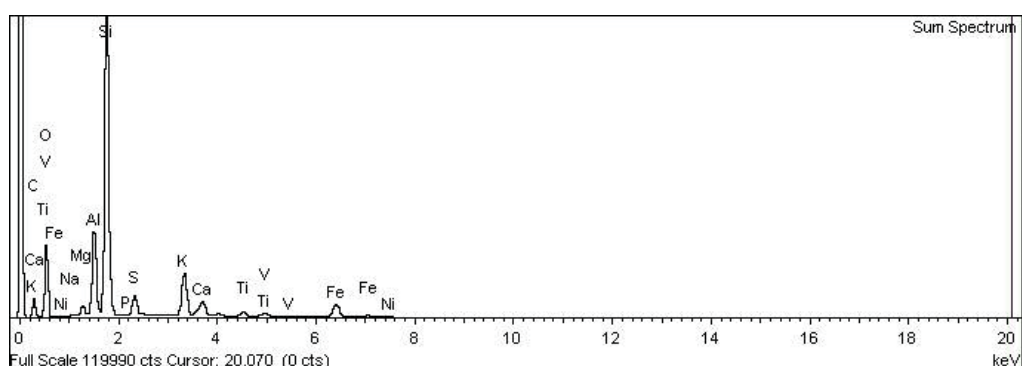


Figure 113. Sum spectrum of scan mapping for Area 1. Corresponding to Figure 45.

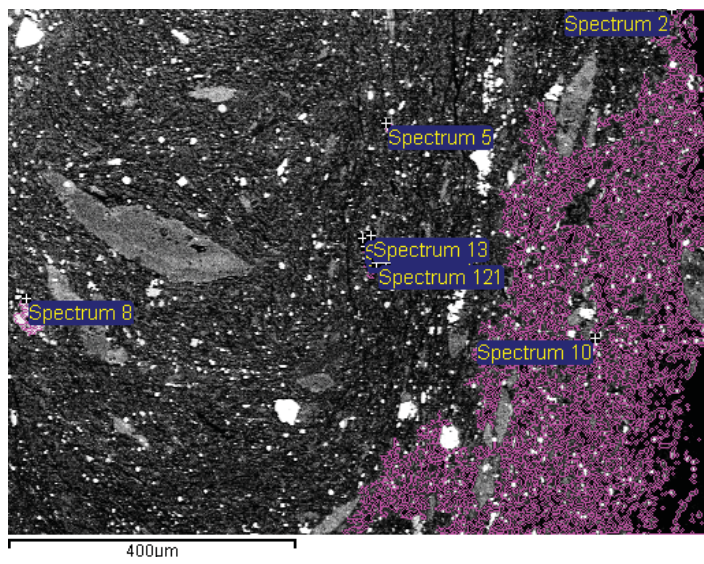


Figure 114. Electron microscope image of area 2, using BEI mode. Spectrum 13 corresponds to one spectra taken from the violet area (wizard selection of area based on a specific grey scale).

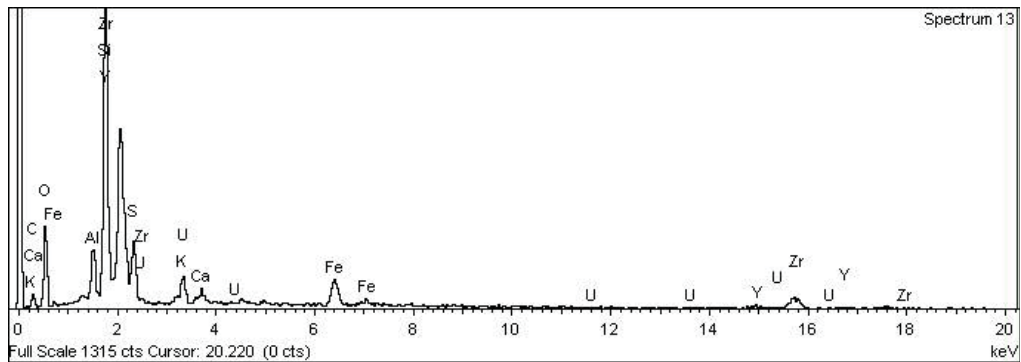


Figure 115. Spectrum corresponding to Spectrum 13 position in Figure 53. This spectrum shows the presence of uranium in the sample.



Norwegian University
of Life Sciences

Postboks 5003
NO-1432 Ås, Norway
+47 67 23 00 00
www.nmbu.no